EFFECT OF PROCESS PARAMETERS ON FRICTION STIR WELDING OF ALUMINIUM ALLOYS

A THESIS

Submitted by

SREENIVAS P

for the award of the degree of

DOCTOR OF PHILOSOPHY

MECHANICAL ENGINEERING DIVISION

SCHOOL OF ENGINEERING

COCHIN UNIVERSITY OF SCIENCE AND TECHNOLOGY, KOCHI

DECEMBER 2017

CERTIFICTE

This is to certify that the thesis entitled **EFFECT OF PROCESS PARAMETERS ON FRICTION STIR WELDING OF ALUMINIUM ALLOYS** submitted by **Sreenivas P** to the Cochin University of Science and Technology, Kochi for the award of the degree of Doctor of Philosophy is a bonafide record of research work carried out by him under my supervision and guidance at the Division of Mechanical Engineering, School of Engineering, Cochin University of Science and Technology. The contents of this thesis, in full or in parts, have not been submitted to any other University or Institute for the award of any degree or diploma. All the relevant corrections and modifications suggested by the audience during the pre-synopsis seminar and recommended by the Doctoral committee have been incorporated in this thesis.

Kochi-682022

Date

Dr P S Sreejith
Professor & Dean
Faculty of Engineering
Cochin University
of Science and Engineering
Research Guide

Dedicated to :-

My Guru

H H Swami Thuriya Chaithanaya

<u>DECLARATION</u>

I hereby declare that the work presented in the thesis entitled **EFFECT OF PROCESS PARAMETERS ON FRICTION STIR WELDING OF ALUMINIUM ALLOYS** is based on the research work carried out by me under the supervision and guidance of Dr. P S Sreejith for the award of degree of Doctor of Philosophy with Cochin University of Science and Technology. I further declare that the contents of this thesis, in full or in parts, have not been submitted to any other University or Institute for the award of any degree or diploma.

Kochi 682022   **Sreenivas. P**

Date   Research Scholar

ACKNOWLEDGEMENT

I am deeply indebted for the consistent support given by my wife Dr Archana R without whom I would not have been able to complete the research. I have deep sense of gratitude to my daughter Aparna and son Chandrasekhar who had been understanding and patient for the whole period of my research. Thanks are also due to my friends, brothers, and in-laws for their sincere well wishes and prayers.

I am truly grateful for the blessings, of my parents N K Parameswaran Achari and late P P Saraswathy Ammal, which had guided me through the difficult path.

No work will become fruitful without the blessing of the Almighty - the creator, preserver and destroyer of the universe who himself is knowledge, power and truth. I submit my work on the lotus feet of the God.

Sreenivas. P

ABSTRACT

KEY WORDS: Friction stir welding; AA 2219 alloy, AA 6082- T6 alloy; Process parameters; Taguchi analysis; Strengthening precipitates.

Friction stir welding (FSW) has become a favourite choice in the joining process of light weight metals. In FSW the material joining is taken place at the solid state. The process is carried out by inserting a rotating tool traversing along the faying surfaces of the material to be joined. It offers nearly defect free welds with minimized distortion and fine grain structure. However, the mechanism of welding and the process parametric combination for welds with consistent and reliable results are not clearly established. Even though FSW offers many advantages over the conventional welding processes, it is considered to be a slow process from a commercial point of view. Efforts to gather a suitable combination of parameters to produce good welds were mostly confined to lower linear speeds. There exists an ambiguity in the determination of the process parameters to produce reliable welds at higher welding speeds. Efforts to increase the welding speed resulted in defect generation because of insufficient heating during welding.

The reported efforts in the optimization of process parameters of Friction stir welding have not gone in to the details of microstructural changes with variations in the parameters. The single consumable in the FSW process is the tool. The reported studies for the optimization of parameters for obtaining better results often suggested complex shape features for the tool which obviously increases the process cost. Gathering a suitable combination of process parameters with simple tool geometry, hence would have contributed much to the research in the area of FSW process.

The thesis elucidates the experimental efforts to propose an optimum combination of parameters with simple tool geometry for FSW at higher linear speeds.

Two precipitation hardenable aluminium alloys were selected as the materials for study: AA 2219 and AA 6082- T6. Both are light weight and possess high strength to

weight ratio. AA 2219 alloy is popular in the aviation manufacturing and AA 6082-T6 is a pioneer material in the structural applications. For the precipitation hardened alloys the concentration and distribution of the strengthening precipitates is most influential for the strength of the alloys. Hence the distribution and dissolution of the strengthening particles under the influence of the process parameters are crucial in the study of friction stir welds.

Taguchi analysis which is very useful for the identification of the control factors to obtain optimum results for the process was used to design the experiments and further analysis. The effect of process parameters on the microstructural changes in the weld region and on the defect formation was also investigated. The experiments were conducted with, perhaps the highest welding speed reported, so far. Through the analysis, optimum combinations of the parameters were suggested for each material at a high speed friction stir window. An analytical model was proposed from the basic theory and parameters for suggesting the process parameters and tool parameters for various aluminium alloys. The computed results of the model were validated by comparing with the reported results.

The important contributions of this work are concluded as below:

- Optimum combination of process parameters was suggested for the FSW of aluminium alloys.

- The most influential parameter for the strength and quality of the weld was identified

- The weld microstructural characterisation was carried out through optical microscopy and scanning electron microscopy.

- The effect of process parameters on the dissolution and re precipitation of the strengthening particles of the alloys was examined.

- An analytical model was proposed to gather optimum combination of process parameters at higher welding speed for various aluminium alloys and the model was validated.

TABLE OF CONTENTS

Chapter - 1 : INTRODUCTION TO FRICTION STIR WELDING

Chapter - 2 : LITERATURE REVIEW

LIST OF TABLES

LIST OF FIGURES

List of figures continued.

List of figures continued.

ABBREVIATIONS

AS	Advancing Side
ASTM	American Society for Testing and Materials
BM	Base Metal
EDS	Energy Dispersive Spectroscopy
FSP	Friction Stir Processing
FSW	Friction Stir Welding
HAZ	Heat Affected Zone
NZ	Nugget Zone
PAZ	Pin Affected Zone
PZ	Pin driven Zone
RS	Retreating Side
SAZ	Shoulder Affected Zone
SC	Straight Cylindrical
SEM	Scanning Electron Microscopy
TC	Tapered Cylindrical
TEM	Transmission Electron Microscopy
THC	Threaded Cylindrical
TMAZ	Thermo Mechanically Affected Zone
TMM	Trinocular Metallurgical Microscope
TWI	The Welding Institute
UTM	Universal Testing Machine
UTS	Ultimate Tensile Strength
WBZ	Weld Bottom Zone

NOTATIONS

English Symbols

D	Tool pin profile
E_l	Energy per unit length
$(E_l)_{eff}$	Effective energy per unit length
F	Force
F_N	Axial force
h	Pin height
r_i	Pin radius
r_o	Shoulder radius
S	Tool traversal speed (Welding speed)
S/N	Signal to noise ratio
SN_L	Signal to noise ratio for 'Larger the better'
t	Base plate thickness
T_f	Tool torque
T_{fL}	Sliding torque
T_{fT}	Sticking torque
T_{max}	Maximum temperature
T_s	Solidous temperature
v	Welding velocity

Greek symbols

μ_f	Coefficient of friction
σ_y	Yield shear stress
$\tau_{contact}$	Contact shear stress
$\tau_{friction}$	Frictional shear stress
τ_{yield}	Yield shear stress
ω	Tool rotational speed

CHAPTER 1

INTRODUCTION TO FRICTION STIR WELDING

1.1   OVERVIEW

The metal joining process has exercised a continuous and pervasive influence in the manufacturing industry. Welding is the most ideal joining process which is suitable for manufacturing complex components from materials which are otherwise difficult for forming operations. The metal joining scenario has been dominated by fusion welding processes, which are cited to be easy for manoeuvring. But the complexity of the process, associated defects, and safety issues tempted for the search of other means abreast.

1.2   PRINCIPLE OF FRICTION STIR WELDING

Friction stir welding (FSW) has emerged as an alternative to the traditional fusion welding in the last decade. FSW was invented at The Welding Institute (TWI) [1]. FSW has become a favorite choice for the welding of non ferrous metals, especially high strength aluminium alloys. It is a solid state welding process where the metal joining takes places much below the melting point of the parent metals. Since there is no melting and casting of parent metal it offers nearly defect free welds with superior mechanical properties [2]. As there are no hazards of radiation or pollutants FSW is safe and environmental friendly. Since the operating temperature is less than the melting point of base metals, it eliminates the inherent defects of fusion welding processes such as shrinkage, distortion and sensitivity to cracking. FSW replaces riveting in many applications as the former offers greater fatigue strength, increased structural rigidity and better weight reduction [3]. It has become a favorite choice for the welding of non ferrous metals, especially for high strength aluminium alloys. FSW gained momentum in application as it was found effective and efficient in

joining highly alloyed 2XXX and 7XXX series of aluminium alloys for joining aerospace structures. These aluminium alloys are considered as non weldable in the context of fusion welding because of the flaws in microstructure upon solidification and proneness to porosity in the fusion zone. The adoptions of other methods are expensive as the formation of surface oxides is a major problem.

FSW contributes to the elimination of problems associated with the joining of dissimilar metals which are incompatible with respect to their physical characteristics like melting temperature, thermal conductivity, and thermal expansion coefficient.

FSW has been extended to a large variety of materials with varied joint configurations and thickness. Based on the joint configurations Friction stir lap welding, Friction stir spot welding (FSSW) have been developed. Recent developments in FSW witness commercialization of this novel technique in shipbuilding industry, high speed train manufacturing and aviation industry [4 - 6].

In FSW a rotating tool of complex geometry is inserted under an axial pressure and traversed along the faying surfaces of the base metal parts which are secured in position by adequate clamping on a backing plate [7]. The tool is cylindrical in shape and has a specially designed tip called as pin which is having a smaller diameter. The tool is subjected to high temperature and severe stresses, which affects its life cycle. Hence tool can be considered as the only consumable in FSW. The friction between the base metal and tool increases the temperature and generates metallic flow in the plastic state. The plasticized material is stirred and forged behind the trailing face of the pin, where the material is still in the solid state. With the contact of the solid part of the material, plasticized metal cools down, forming a solid phase bond between the work pieces. Metallic joint is achieved through viscoplastic deformation and consequent heat dissipation occurring much below the melting point of the base metal.

The tool geometry, process parameters and base material properties play a significant

role in heat transfer and material flow and thereby influence the weld properties [8].
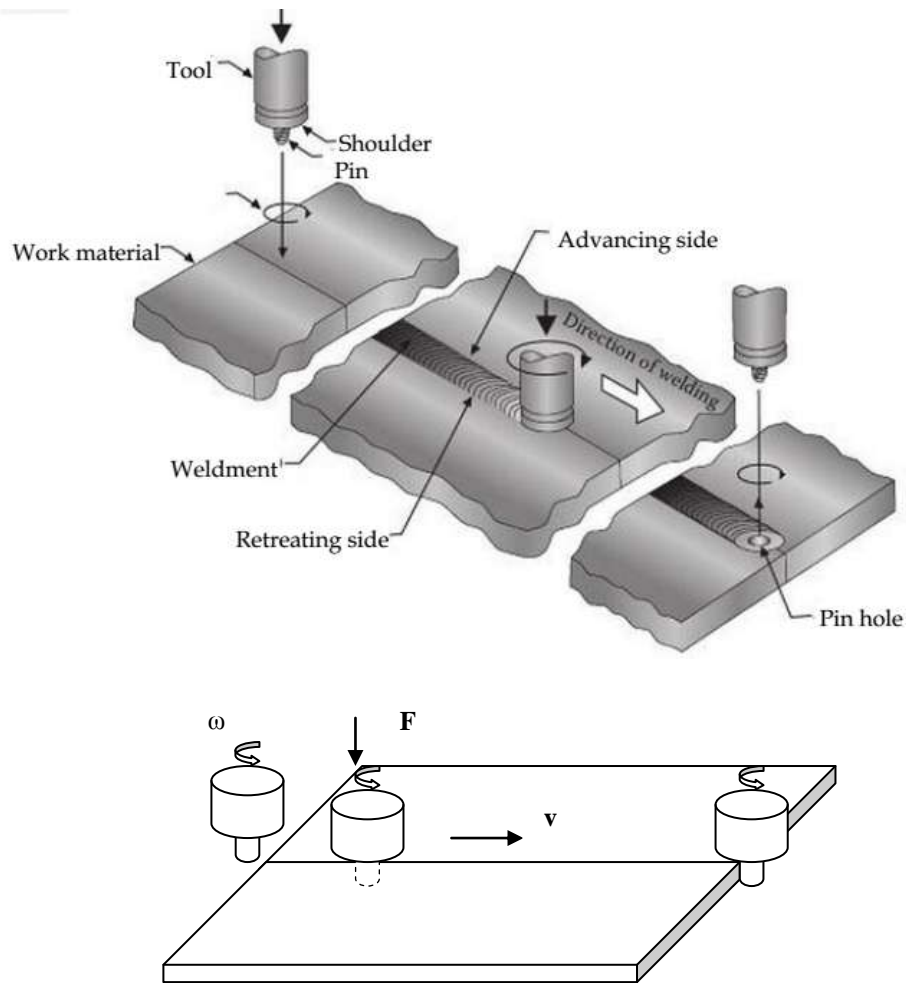
Fig. 1.1 : Schematic representation of FSW and the process parameters:
ω − Tool rotational velocity, F- Axial pressure, v- Welding velocity. [9]

Fig. 1.1 illustrates the principle of the FSW process and the primary process

parameters and Fig.1.2 illustrates the tool geometry, in general.
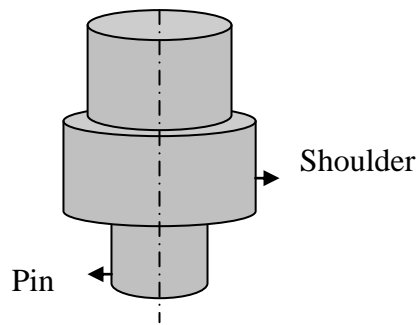
Fig. 1.2   FSW tool geometry.

1.3   MACROSCOPIC FEATURES OF FSW

The side of the weld where the direction of the tool rotation is same as the direction of the welding is known as the advancing side (AS) and the side of the weld where the direction of the tool rotation is opposite to the direction of the welding is known as the retreating side (RS) [10]. In case of FSW, the material and heat flow are more complex than the conventional fusion welding. The material and heat interaction bring about the meteorological changes in the parent metal. FSW results in dissolution, phase transformation, coarsening and, in some cases re precipitation of particles. Based on this, the weld region can be divided into four distinct macroscopic regions as shown in Fig. 1.3. Generally, they are known as unaffected base metal (BM), thermo mechanically affected zone (TMAZ), heat affected zone (HAZ) and weld nugget [11, 12].

Fig.1.3 : Macroscopic regions of friction stir weld.
1- Stir Zone (Nugget), 2 - Thermo-mechanically affected zone (TMAZ),
3 - Heat affected zone (HAZ) and 4 - Base metal (BM)

4

In the pin work material interface the material is subjected to plastic deformation and intense frictional heating which results in a fine recrystallized grain structure in the stir zone. This region is referred as weld nugget. [13 - 15]. The equi-axed grain structure is seemingly the result of dynamic recrystallisation. Hence it was also referred as dynamically recrystallized zone (DXZ) [16].

The region adjacent to the nugget zone (NZ) is referred as the (TMAZ). The microstructrure in TMAZ appears as deformed grains. The high temperature and deformation rotates the original grains [17 - 19]. The TMAZ- NZ boundary is where the recrystallisation commences. It is observed that the grains in TMAZ zones are larger than the grains in NZ.

The region beyond TMAZ which is subjected to thermal alterations is known as HAZ. As this region is not subjected to any plastic deformation, the original grain structure remains unaltered [20].

FSW operation proceeds through three phases which are described in terms of a time period, the relative position of the welding tool and the work piece. In the first phase the tool is inserted vertically into the joint line (plunge period). The rotating tool is then held in that position for a period sufficient to build up the heat (dwell phase). The velocity difference between the tool and the work piece and the resulting mechanical interaction generate heat by friction and plastic deformation of the metals. The heat generated is dissipated to the surrounding material causing material softening. After the dwell period, the rotating tool is moved along the joint line. Fig. 1.4 illustrates the progress of an FSW process.

Fig. 1.4. FSW in progress

1.4   PROCESS PARAMETERS OF FSW

In FSW, tool shoulder is the key component for heat generation and for containing the plasticized material in the weld zone. The pin mixes the material to forge thereby making a sound joint. The shoulder – pin action is driven by the speed and tool characteristics. Based on the above, the main process parameters in FSW are identified as follows [21 - 22],

- Rotational speed of the tool (N)

- Linear velocity of the tool (S)

- Tool shoulder surface geometry and dimensions

- Pin profile and dimensions

- Axial force (F)

The making of a sound joint with intended strength, efficiency, reliability and without any defects depends on the proper selection of these parameters. Reaching out to an optimum combination of parameters is cited to be cumbersome as an optimum combination of the parameters varies with materials. The effect of process parameters

on the weld quality and strength in FSW have been extensively studied by many researchers. These experimental studies or simulation analyses were concentrated on the optimum parametric combination for desirable results for welds, or figuring out the most influential parameter for obtaining good welds.

1.5 ADVANTAGES OF FSW

As the material joining is taken place at the solid phase, FSW is devoid of many problems associated with fusion welding processes. In FSW, the process temperature is much below the melting point of the metal and obviously the cooling rate is much lower than that in the case of fusion welding process. Hence, the microstructural changes are free from the complexity of grain growth and associated changes. As a result defects such as porosity, solidification cracking, liquation cracking and welding distortion do not arise during FSW. In general, FSW has been found to produce a low concentration of defects and is simple in operation with flexibility in the selection of parameters and materials. Advantages of FSW over the traditional welding techniques can be summarised as follows.

- FSW is a better choice for the welding 2xxx and 7xxx series of aluminium alloys which are otherwise difficult to weld using conventional welding methods.

- No shielding gas or filler wires are required which makes the process environment friendly.

- Low distortion of work piece, good dimensional stability and repeatability due to the absence of fusion removes much of thermal cyclic changes associated with solidification and cooling.

- The process eliminates problems related to edge preparation.

- FSW offers excellent metallurgical properties in the joint area.

- Even in thicker materials FSW can be accomplished in a single pass.

- It is safe since there is no ultraviolet or electromagnetic radiation, spatter, fumes or much noise.

- It offers better mechanical properties compared to other welding processes.

- The energy consumption is less than that of metal inert gas welding process.

- The process can be fully automated and hence quality does not rely on specialized welding skills.

1.6 LIMITATIONS OF FSW

In spite of the above advantages FSW is associated with certain defects, if it is not carried out properly. The material deformation and material transfer is dependent on a threshold value of temperature. Consistent and periodic transfer of material and consolidation of softened material is essential for a good weld condition. The selection of process parameters and the tool material is crucial in this context. In the circumstances of improper selection of process parameters, it may lead to defects in FSW. Apart from that FSW process sequence is unavoidably associated with certain disadvantages as listed below.

- The work piece should be well supported and clamped firmly in order to take the applied forces and to prevent the probe from pushing the work piece materials apart.

- Quality of FSW weld depends on the selection of weld parameters, which depends on base metal material, thickness and tool. The selection of weld parameters is a complex process.

- The presence of a hole at the end of the weld from where the probe was withdrawn affects the strength and appearance of the weld.

1.7 OBJECTIVES OF THE RESEARCH

FSW is a fast growing material joining technique especially in difficult to weld materials by other welding materials. However it is not commercialized adequately in response to the industrial demand. In spite of the operational simplicity, the prominent hurdle in the popularization of FSW is the difficulty in the proper selection of welding parameters. Each material requires different combination of parameters. A generic approach to select welding parameters is yet to be concluded.

Optimizations of welding parameters remain a hot issue among researchers for different welding conditions. The objective of the research is motivated from the fact that the welding speed of the FSW process is critical in deciding its acceptability and viability as an alternate material joining technique from the industrial point of view. Another aspect in this context is the demand for weight reduction in many applications such as automotive and aviation industries without sacrificing the strength sought for. Developments in material science are able to solve this issue by suggesting different materials especially aluminium alloys. Now the workability of these alloys forms the focus of research where FSW is one of the best introductory processes in manufacturing.

The objective of this work is to supplement the commercialisation of FSW by optimising the process parameters for FSW at high welding speeds. The microstructural characterisation of the welds with the selected parameters was carried out to consolidate a generic approach for the selection of process parameters for carrying out FSW with desired results.

……ഔ*ൟ……

CHAPTER 2

LITERATURE REVIEW

2.1 INTRODUCTION

The most investigated part in the analysis of FSW is is concentrated on the selection of welding parameters. Different materials and joint configurations reportedly demand different parametric combinations. Certain process characteristics determine the accurate thermomechanical bonding of FSW. They can be identified as heat generated, cooling rate, material flow in layers, degree of mixing and filling. Effects of the process parameters on these characteristics are crucial in deciding the strength and quality of the weld. Welding speed, tool rotational speed, axial force, tool geometry, tool tilt angle were identified as the most important parameters in FSW process. Optimized combinations of these parameters have been extensively suggested in various studies [23 - 26]. In most of the analysis of the FSW, the selection of the parameters was limited to rotational speed, transversal speed, tool geometry and axial force.

Weld quality and strength are influenced by the heat input or the highest process temperature and the material flow. In FSW stirred and softened material is subjected to extrusion by the tool pin rotational and traverse movements leading to formation of friction stir processing (FSP) zone. The formation of FSP zone is influenced by the material flow behaviour under the action of rotating tool. However, the material flow behaviour is predominantly influenced by the material properties such as yield strength, ductility and hardness of the base metal, tool design, and FSW process parameters.

The process temperature affects the grain size, dissolution, re-precipitation and distribution of strengthening precipitates which determine the tensile properties of the welds. The material flow in terms of stirring and filling is detrimental in defect formation. FSW joints are prone to defects like pin hole, tunnel defect, piping defect, kissing bond, zig- zag line and cracks, etc., due to improper flow of metal and insufficient consolidation of metal in the FSP (Friction processing zone or weld nugget) region [27]. Therefore, it can be concluded that the process parameters determine the temperature and material flow during the welding process whereby they affect the weld joint formation.

In heat treatable alloys, the static properties of the friction stir welded joints are dependent on the distribution of strengthening precipitates rather than the grain size [28]. The frictional heat and mechanical working of the plasticized material in the weld zone result in coarse and agglomerated precipitates in some areas and the distribution of few needle shaped precipitates in the weld nugget, which leads to considerable softening in contrast to the base metal. This decreases the hardness in FSW joints considerably and yields lower tensile strength than base metal [29].

2.2 HEAT GENERATED IN FSW

The heat generation in FSW is primarily from two sources; Friction between the tool and work piece surfaces and plastic deformation of the work material. The heat generated is conducted to the work piece, tool and support plates. The amount of heat conducted to the work piece determines the success of the metal joining, quality of the weld, weld micro structure and formation of defects. The amount of heat conducted to the tool dictates the tool life. The heat flux during the weld process must ensure a threshold value for the temperature which is enough to soften the material for the tool to process it adequately to achieve the joint. Temperature above this value is undesirable as it may lead to the melting of the base metal. The maximum temperature

required for the FSW process was estimated as 80 – 90% of the melting point of the base metal [30]. The direct and accurate measurement of this heat generation or temperature in FSW was found to be impossible due to the localisation of heat generation and the continuous tool action during FSW. However, experiments were performed to measure the maximum temperature using thermo couples inserted near the weld seam [31]. Reported results of experimental and numerical analyses revealed that 95 % of the heat generated during FSW flows to the work piece, indicating the high process efficiency of the FSW [32].

A set of analytical models were suggested for heat generation based on the tool torque and average power [33, 34]. These models considered only the heat generated through friction. These models were based either on the coloumb's friction or on the constant shear model.

Localised plastic deformation occurs in the bulk material also contributed to the heat generation during FSW process. The weld power input converted to plastic deformation energy in the bulk material was estimated to have a fraction converted to heat and the remaining stored in the microstructure [35]. The reported results of numerical simulations estimated the fraction of heat generated through plastic deformation as only 2 - 20 % of the total heat generated [35, 36]. Citing this conclusion, many researchers have ignored the heat generation by plastic deformation, in their mathematical models.

Heat generated during FSW is obviously affected by the selection of process parameters for a given material. Heat generation models for FSW have been developed for straight cylindrical [37], tapered cylindrical [38] and pin with eccentricity [39]. The variation of heat generation in terms of energy per unit length with pin eccentricity for the FSW of AA1050 - H12 and AA5754 - H2 are shown in Fig. 2.1.

For the equations developed for heat generation, torque and hence the rotational speed and axial force are the influential parameters for the heat generation. Increased rotational speeds and axial force increase the heat generation. These equations are independent of the welding speed. However it was experimentally proven that at increased welding speeds, heat generated reduces considerably as evident by the temperature values recorded. These observations are logical, as at increased welding speed, the tool has to process more material per unit time and the material ahead of the pin does not get enough time to get pre heated. The degree of softening of the base material decreases as the heat input decreases, which in turn increases the power consumption of the process. Fig. 2.2 illustrates the variation of power input and the specific weld energy (weld energy per unit length) with tool traversal speeds [40].
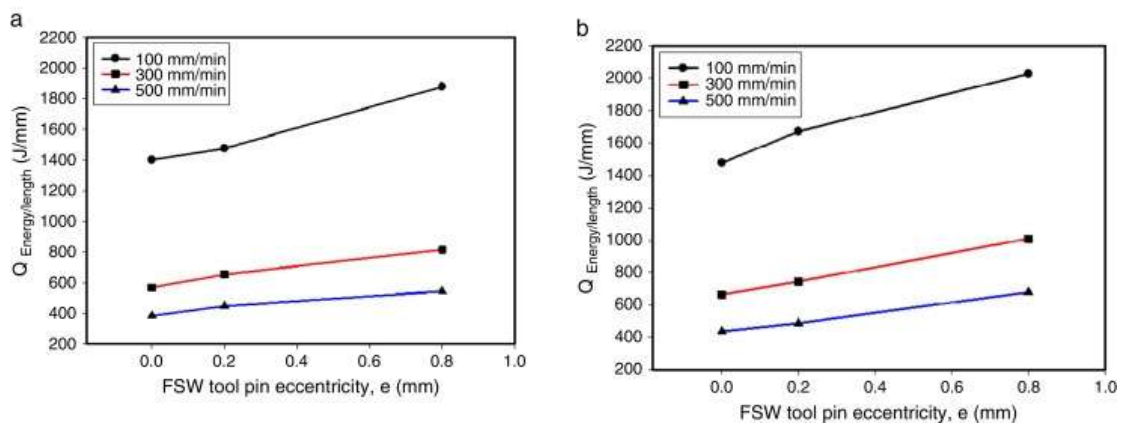
Fig. 2.1 : The variation of $Q_{Energy/length}$ with the tool pin eccentricity for (a) AA1050-H12 and (b) AA5754-H2. [39]
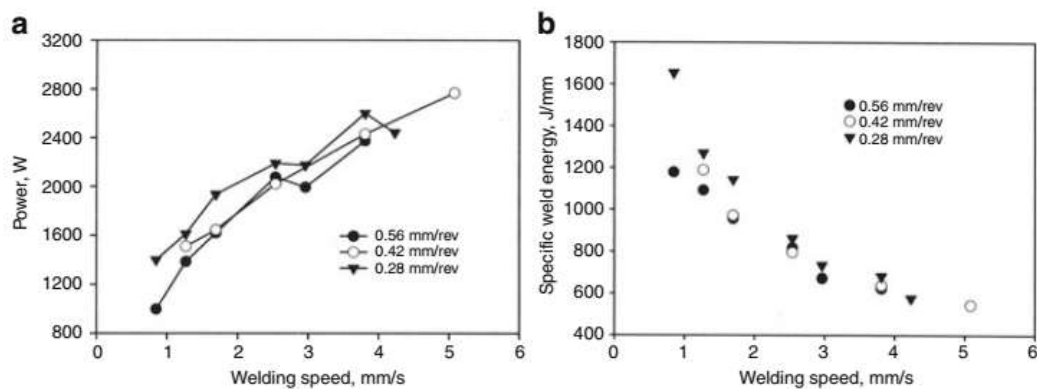
Fig. 2.2 Variation of (a) power consumption and (b) specific weld energy with tool traversal speeds [40]

2.3   MATERIAL FLOW IN FSW

In FSW the material flow under tool action plays an important role in determining the integrity of the weld joint. It may be concluded that the tool shoulder and the pin controls the material flow. The friction between the tool surfaces and the bulk material softens the base material in the immediate vicinity of the tool. The flow of the plasticized material is governed by the tool geometry (size and shape of the shoulder and the pin), rotational and linear speeds of the tool. The tool shoulder diameter and shape is critical, as its grip on the plasticized material organizes the material flow field [41]. The material flow happens in the sticking condition between the tool surfaces and the bulk material surfaces. Hence the heat generation, torque and the welding forces also play a key role in the material transfer.

The material flow pattern during FSW was experimentally investigated by many researchers. The material flow regime was established by using marker materials embedded in the work piece, where its movement after deformation was traced [42, 43], or by tracking the material deformation pattern using dissimilar metals for joining [44, 45].

The findings of different studies suggest that there is an unbalance in the material flow between the AS and RS. Material flows more from the advancing side to the retreating side. Material flow from the retreating side to the advancing side occurs in the tool shoulder region. The TMAZ region is under the influence of both the tool shoulder and the pin and the material extrusion is taken place only in the RS of the TMAZ [46]. This observation provides a plausible explanation for the influence of tool speeds on the material flow.

Material on the advancing side of a weld enters into a zone that rotates and advances with the profiled probe. This material was very highly deformed and sloughs off behind the pin to form arc-shaped features when viewed from above (i.e. down the tool axis). The lighter material came from the retreating side in front of the pin and was dragged around to the rear of the tool and filled in the gaps between the arcs of advancing side material. This material did not rotate around the pin and the lower level of deformation resulted in a larger grain size.

FSW is often viewed as an extrusion process. The material is extruded in layers in semi cylindrical patterns by the tool rotation. The periodic deposition of such layers appears as onion ring structure in the nugget zone [47] as shown in Fig. 2.3.
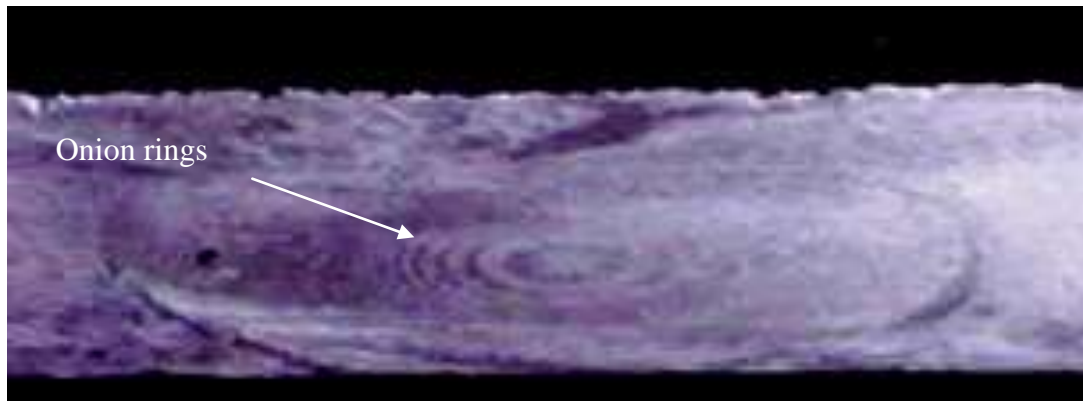
Fig. 2.3. Onion rings in FSW of AA 6082- T6 [48]

Material flow is remarkably influenced by the tool design and welding process parameters. Arbegast [49] observed a resemblance between the material flow in FSW and extrusion of aluminium alloys. With this approach the metal flow in FSW was explained in terms of five conventional metal working zones: (a) pre heat zone, (b) initial deformation zone, (c) extrusion zone, (d) forging zone, and (e) post heat or cooled down zone as shown in Fig. 2.4.b.

At the commencement of the tool plunging and rotation the area in front of the pin, which is the pre heated zone, temperature rises due to frictional heating and adiabatic heating of material deformation. The extension of pre heat depends on the tool speed and the material thermal properties. As the tool traverses material temperature increases, when it reaches beyond a critical value, and when the stress exceeds the critical flow stress material flow begins. This zone was identified as the initial deformation zone. The material in the deformation zone gets extruded between the pin and the bulk material in the pre heat zone. The material in this zone is directed upwards to the shoulder zone and downwards to the extrusion zone as shown in Fig. 2.4. (a). A small amount of material is trapped beneath the tool tip and follows a vortex flow pattern. In the extrusion zone the material flow follows a direction from the front to the rear with a fixed width. As the tool moves forward, the material flows in layer by layer leaving a cavity periodically. This cavity is continuously filled by the material from the forging zone which follows the extrusion zone, under the prevailing hydrostatic pressure conditions. The consolidation of the material for forging zone is the function of the tool shoulder under the applied axial force. Behind the forging zone the material is cooled under passive or forced cooling conditions, which is identified as the cooled down zone.

The above explained ideal material flow regime, clearly indicates that the material flow in FSW is influenced by the tool geometry, process parameters, and material thermal and mechanical properties. For a good weld condition defined by the non defective nature and adequate strength these parameters are needed to be selected appropriately. Any deviation from this combination of the parameters may result in an incomplete consolidation of the different process zones, which lead to ineffective stirring, material flow and inadequate filling of material. Such a condition will affect

the strength and integrity of the joints. Various reports observing the effect of process parameters on friction stir welding are included in the following sections.
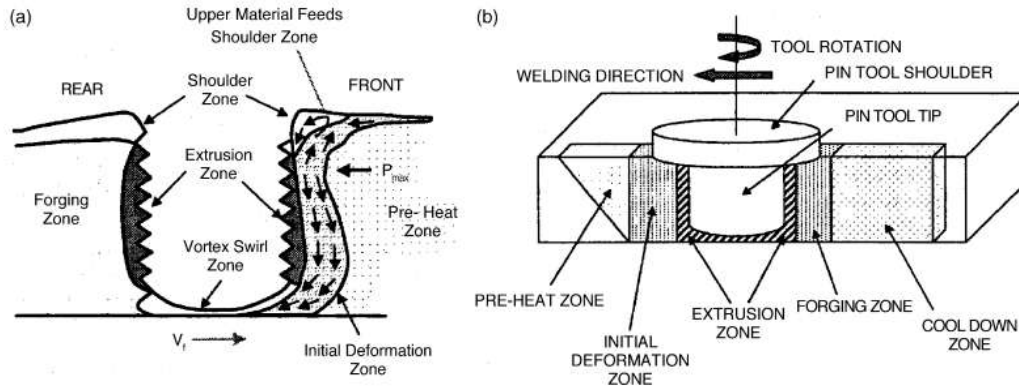
Fig. 2.4 (a) Metal flow pattern and (b) Metallurgical processing zones [49]

2.4 EFFECT OF TOOL ROTATIONAL SPEED

Variations in tool rotational speeds do not affect the weld appearance. Semicircular traces are discernable at all rotational speeds while weld surfaces appear smooth as rotational speed increases. However it was reported that if the rotational speed increases beyond a certain limit, material will be subjected to excess heat and this increases the melting and fluidity of material thereby increasing the turbulence. This condition was identified as a possible reason for cavity defect formation [50].
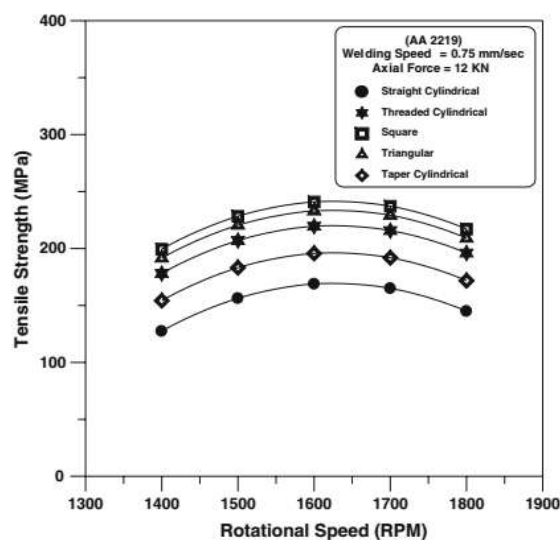
Fig. 2.5. Variation of tensile strength with tool rotational speed [51]

Another observation was about the effect of tool rotational speed in tensile strength of friction stir welds. Many researchers have reported that the tensile strength of the weld increases with tool rotational speed reaches a maximum value and then decreases with further increase in rotational speed as shown in Fig. 2.5 [51]. The tool rotation causes stirring and mixing of material which in turn increases the welding temperature. The temperature influences the grain growth and dissolution of precipitates. The intensity of grain growth and dissolution of second phase particles greatly affect the tensile properties. The heat input is, therefore, to attain an optimum value for the weld to have good tensile properties. At higher heat input, dissolution and grain growth were found to be more, degrading the tensile properties of the weld. On the other hand, at low tool rotational speeds, heat generation is inadequate to plasticize the material which results in the poor stirring and consolidation of the weld metal. At this condition, weld exhibits poor tensile properties [52, 53]. The weld strength increases with the increase in heat input per unit length of the weld up to a certain level. If the heat input is sufficient to assure the homogeneous distribution of the strengthening particles, the possibility of pore formation in the weld is reduced significantly and this enhances the weld strength [54, 55].

2.5   EFFECT OF TOOL TRAVERSAL SPEED

The reported analyses deal with low tool linear speeds to ensure adequate material joining [56, 57]. However these reports indicate that tool rotational speeds have significant effect on heat generation and material flow. As the speed increases, temperature decreases. The tensile strength exhibited significant variation at lower and higher welding speeds. At lower welding speeds, heat input increases due to increased tool action and friction. Higher heat input enhances grain growth and grain coarsening. Welds performed at lower welding speeds were reported to exhibit grains which contain many sub boundaries. The sub grain size increases with heat input. The

FSW is associated with severe mechanical deformation and complex thermal cycle. As the tool moves forward, the dynamically recrystallized grains statically grow during the cooling phase of the thermal cycle.

Larger the heat input, greater will be the cooling time which resulted in larger grains with a lower density of dislocations and sub boundaries [58]. For higher welding speed, the exposure of the material to elevated temperature gets shortened. This resulted in rapid cooling of the processed material producing finer grains at the FSP zone. Finer grains generally provide better tensile properties for the welds.

Generally it was observed that as welding speed increases the tensile strength of the weld increases reaching a maximum value and then decreases as shown in Fig. 2.6.
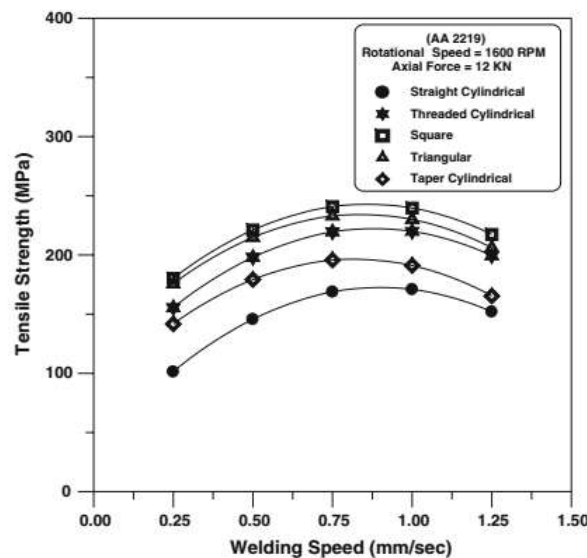
Fig. 2.6. Variation of tensile strength with welding speed [59]

2.6   EFFECT OF AXIAL FORCE

Axial force or down force affects the frictional force and hence the heat in put at the commencement of the welding process. Axial force keeps the shoulder in contact with the material. The axial force aggravates friction and keeps the softened and transferred material in the weld line. Increase in the downward force activates the plastic metal

flow [60]. Axial force at optimum temperature fills the weld cavity, pin driven and shoulder driven material and base material coalesced with each other. If the force is increased above a critical value the sub surface material flow is seemed to be increased. This resulted in the formation of flashes [61]. There is a limiting value for the axial force beyond which the tensile strength of the weld decreases as shown in Fig. 2.7 [62].
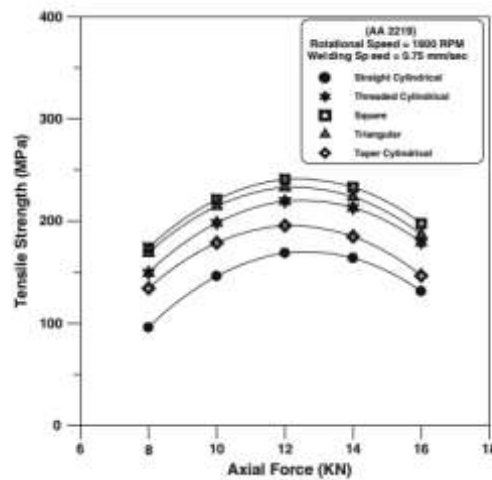
Fig. 2.7. Variation of tensile strength with axial force [62]

2.7   EFFECT OF TOOL GEOMETRY

A FSW tool has two basic functions: localized heating and material flow. The friction between the shoulder and the material provides the major part of heating. Shoulder is responsible for the trapping of material which is extruded upwards by the tool pin and pushing the softened material downwards, assuring the proper mixing of the softened material and the soundness of the joint. Material softening and mixing to form a sound joint are achieved by the action of shoulder and pin [63].

Studies revealed that the relative size (diameter) of the shoulder and the pin is critical. If the diameter of the shoulder is more than a critical value, heat generated will be more and the material flow from the pin part may not be appropriate [64].
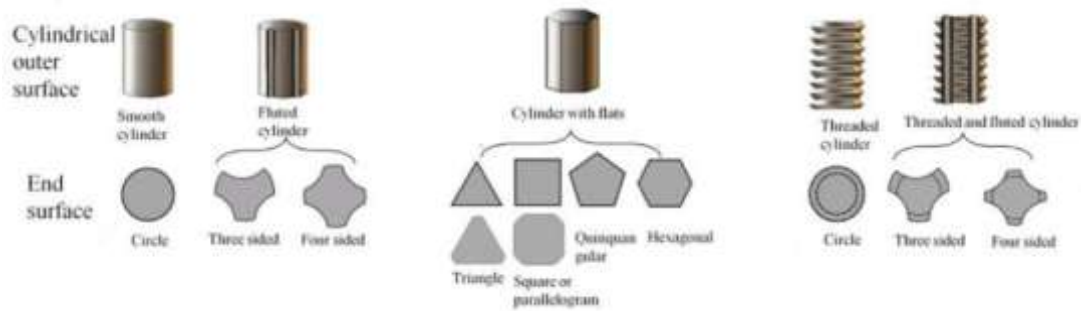
Fig.2.8. FSW tool pin profiles [65]

Pin geometry influences the material flow [65]. More over the pin geometry affects the grain size of the joint. It also influences the strain rate and dynamic recrystallisation of the stir zone. From the available literature, it is found that a cylindrical threaded pin, truncated cone and concave shoulder were widely used welding tool features. Non circular pin profiles with flat faces were reported to produce better results in terms of mechanical properties [58]. It was observed that the non circular pins allowed the plasticized material to pass around the probe. The relationship between the static volume and swept volume is a deciding factor for the flow of material from the leading edge to the trailing edge of the tool during welding, which in turn decides the weld quality. Moreover the pin with flat faces produces a pulsating stirring action which enhances the material consolidation at lower welding speeds [59].

2.8   EFFECT OF TOOL TILT ANGLE

Various studies reveal that a tilt in the tool towards trailing direction favors the weld joint. Tool tilt increases shoulder action, material stirring and mixing. But higher values of tilt angle retard the tool action. However, effect of tool tilt angle on the quality and strength of weld formation have not been studied in detail. Many researchers apparently used a tool tilt angle for best performance based on trial and error method. The effect of process parameters on the weld quality and strength is largely depends on the weld defect formation.

21

2.9   WELD DEFECTS

The metal joints formed by the FSW offer better surface quality and appearance than the conventional fusion welded joints. With appropriately selected process parameters, friction stir welded joints provides defect free joints with least distortion and smaller residual stresses [66]. However, the complexity in material flow and thermal cycle, associated with FSW results in the formation of defects such as kissing bond, tunnel defect, voids formation which affect the homogeneity and hence the weld strength.

Heat input necessary for plasticizing the material depends on the friction and degree of plastic deformation. If the heat input is not sufficient it affects the stirring and transportation of metal during welding. On the other hand excess heat input causes turbulence in material flow. In both the cases the tool action becomes ineffective to consolidate the softened material periodically. FSW requires softened material to pass around the pin and get consolidated periodically by the hydrostatic pressure. If the hydrostatic pressure is not adequate, or ineffective, defects are formed [67].

Insufficient heat input and metal transfer causes cavities in the welds known as wormhole defect. Wormhole defects occur for butt joint configuration. Insufficient pressure by the tool shoulder is the triggering factor for worm hole or tunnel defect. It is appeared as a cavity which runs along the weld under the weld surface [68]. Fig. 2.9 captures the macrostructure of a weld nugget with a worm hole defect [69].

Fig.2.9. Worm hole or tunnel defect [69]

Increased heat input as in the case of higher rotational speed and low welding speed, causes poor plasticization of material which leads to tunnel defects. The tunnel defect specifies locations in the weld, which are unfilled by the softened material [70]. Worm hole defects are caused by the excessive welding speed with lower rotational speed. At higher welding speed the tool shoulder becomes incapable to direct or push the plasticized material towards bottom of the stir zone and to maintain the constant depth of tool penetration. This condition leads to the formation of worm hole defect. Lack of consolidation of material may not form tunnel defects always, but they may appear as intermittent cavities known as voids (Fig. 2.10).
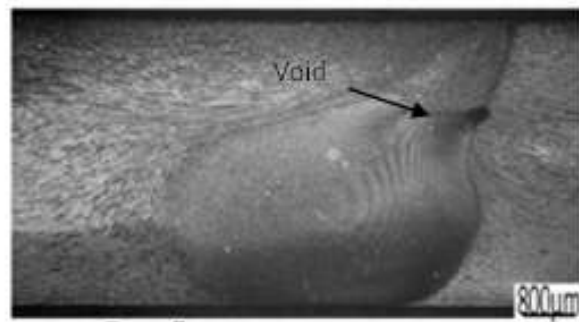
Fig. 2.10. Weld macrostructure showing voids.

In some cases the pin length may not be sufficient for a set of selected welding parameters. In such a situation a part of the joint layer may be left without adequate material consolidation. The imperfection, hence caused by the insufficient penetration of the tool is considered as lack of penetration defect (Fig. 2.11). Misalignment of the work piece in the butt joint configuration also leads to lack of penetration.
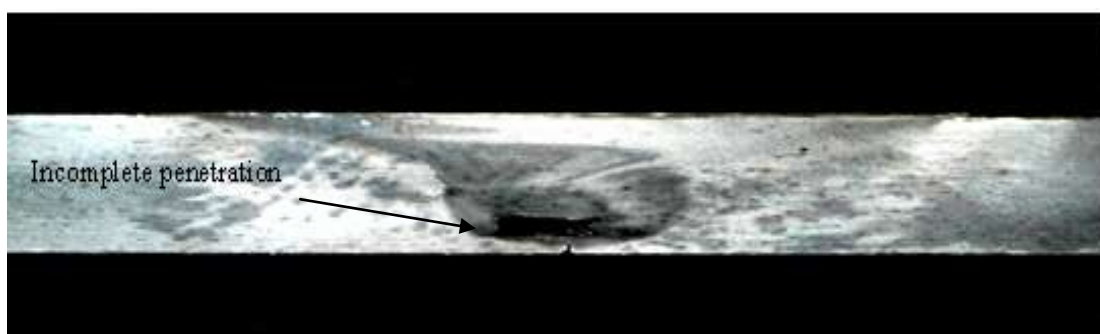
Fig. 2.11. Incomplete penetration

23

If the heat input is in excess, the vertical movement of the metal is retarded by the turbulence in material flow, resulting in smaller size cavities. These defects are known as pin hole defects. Excess heating associated with high plunge pressure causes the softened material to move up to form flashes. Flashes not only affect the appearance, but also reduce the weld strength [71]. It is well established that the tool geometry and welding parameters affect the material flow pattern.
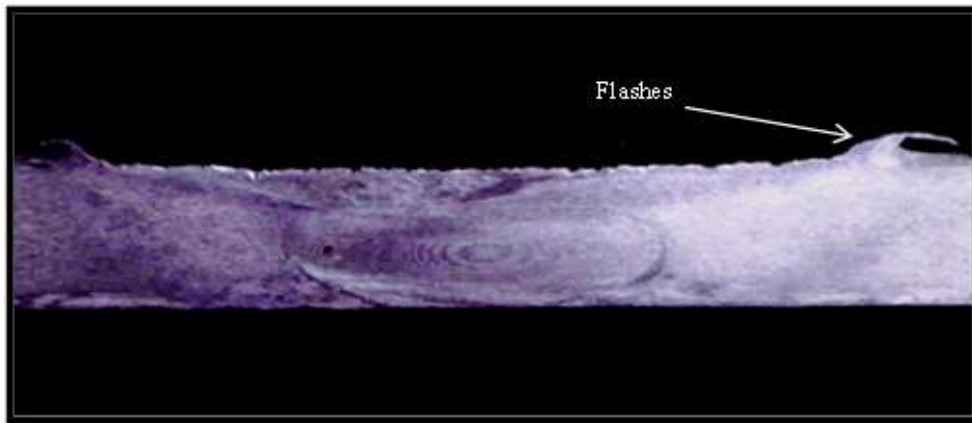
Fig.2.12. Flashes shown in weld macrostructure.

Another possible defect observed is the kissing bond. Kissing bond is formed at lower heat input during FSW. Lower heat input may not be sufficient to break up the oxide layer present in the parent metal, especially when the faying surfaces are not properly machined. In that case there is high possibility for the oxide layers on the initial butt surfaces to make bonds with oxide free surfaces in the root part of the weld. This flaw appears as a zig- zag line pattern in the weld zone [72]. Heterogeneity in the material flow leads to the formation of weld defects.
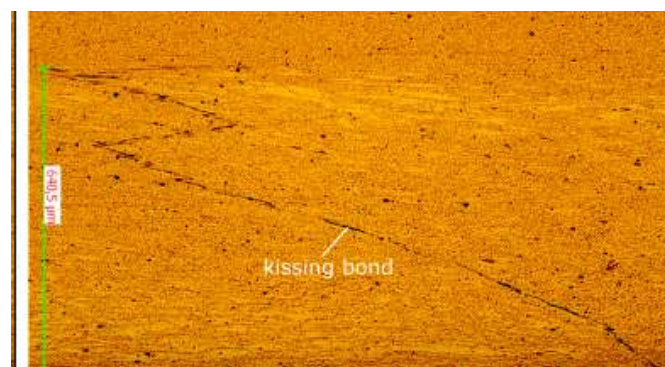
Fig.2.13. Kissing bond

Various reports suggested that tool geometry and welding parameters significantly affect the material flow and hence the defect formation. Scialpi [73] examined the effect of different shoulder geometries in the FSW of thin sheets of 6082 T6 alloys. He observed that defect free welds are generated for shoulders with fillet and cavity. Ramulu et al. [72] analysed the effect of tool speed, welding speed, plunge depth and shoulder diameter on internal defect formation during FSW of AA 6061 sheets. The study has suggested the range of parameters for defective and non defective welds as shown in Figs. 2.14 and 2.15.
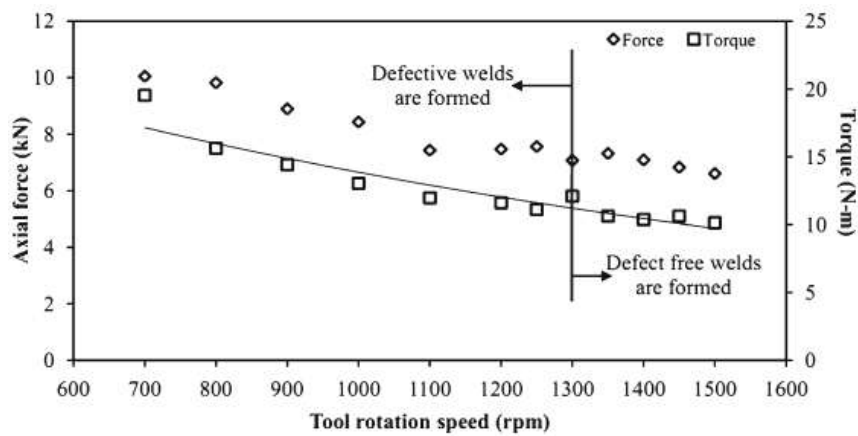
Fig. 2.14. Range of Tool speed, torque and axial force in defect formation [72]
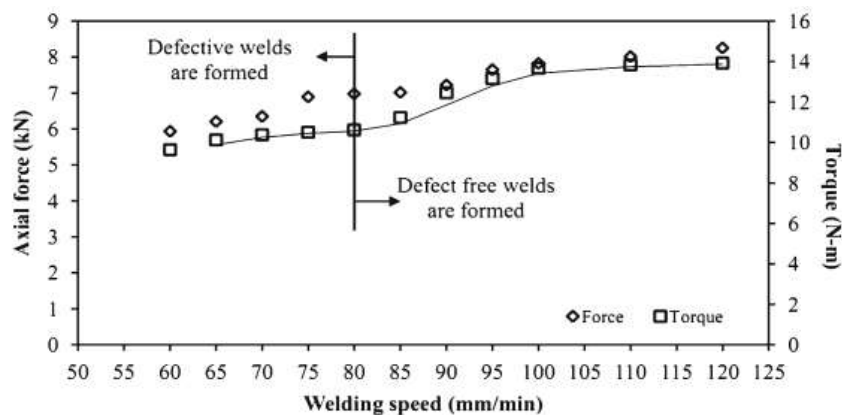
Fig.2.15. Range of welding speed, torque and axial force in defect formation [72]

2.10 OPTIMIZATION OF PROCESS PARAMETERS.

FSW has been extended to a large variety of materials with varied joint configurations and thicknesses. But productivity is still a matter of concern due to the lower welding speed. Efforts to identify an optimum combination of parameters which offers

welding at higher linear speeds with acceptable quality are not yet concluded. Reported efforts for the process optimization of FSW of aluminium alloys were done at lower welding speeds [58, 70]. Optimization techniques at higher speeds were found to be restricted by practical limitations as excessive welding speeds increase the risk of void creation [74]. Reghubabu et al. [75] examined the effect of tool rotational speed and welding speeds on mechanical and microstructural properties of friction stir welded 6082-T6 alloy. In the experiments the highest welding speed tested was 585mm/min and the welding speed corresponding to the optimum condition was 170mm/min. Patil et al. [76] investigated the effect of welding speed and tool pin profile on the weld quality of AA6082 - O aluminium alloy. The study used taper screw thread and tri- flute for pin profiles. They proposed a condition for high strength weld in terms of these parameters; however the maximum value of the welding speed was limited to 80 mm/min. Adamowski et al. [77] analysed the effect of welding speed and rotational speed on the FSW of 6082 - T6 alloy with a highest speed of 585mm/min and with a threaded pin tool.

In most of the analysis of the FSW, the selection of the parameters was limited to rotational speed, transversal speed, tool geometry and axial force. The role and effect of tool tilt angle were not clearly established. It was reported that as the tool tilt angle increases tensile strength and microhardness of the weld joint increases for dissimilar joint of aluminium and copper [78]. Researches on the FSW of dissimilar joints of aluminium and steel indicated that increase in tool tilt angle affects the tensile strength of welded joint [79]. Tool tilt angle of 1.5^0 or 2^0 was found to provide good results for aluminium welded joints [80, 11]. Certain studies stipulated that the surface defects can be eliminated with effective filling by tilting the tool for the FSW of aluminium alloys [81]. These reported results concluding the effect of tool tilt angle were also pertaining to lower welding speeds. Ana et al. [82] suggested an optimum condition

for FSW of 6082 - T6 alloy with good strength with a speed of 360mm/min. They have considered welding speed, tool rotating speed, axial force and tool tilt angle as the process parameters; nevertheless the effect of tool tilt on the weld strength was not established. Rodrigues et al. [83] proposed that friction stir welding at higher traverse speeds were strongly dependent on the base material characteristics and plate thickness. They have achieved good welds up to a speed of 350 mm/min for 6mm thick base metal. The process parameters included tool tilt angle; however its effect was not mentioned.

Arora et al. [84] carried out an extensive analysis of the process parameters on the tensile strength of the friction stir welded AA2219 - T87 alloy. The study focused on the effect of tool shoulder diameter, welding speed and axial force. They suggested that welding speed and shoulder diameter influence significantly the tensile strength. Coarsening and or dissolution of strengthening particles were revealed at the weld nugget. They achieved a reasonably good weld efficiency of 75% in terms of the tensile strength, but the welding speed was limited to 180mm/ min as the maximum value. But the effects of axial force on the weld strength have not been elaborated. Even though the micro structural changes have been elaborated using TEM and SEM studies, the micro structural changes and the weld quality were not correlated by incorporating the effect of process parameters.

Effect of tool pin geometry and tool speeds were studied in the report of experimental analysis conducted by Biswas et al [85]. It was proposed that tapered pin profile tools produced joints with superior mechanical properties. They have suggested a ratio for the tool rotational speed to the tool traversal speed for the better mechanical properties of commercial grade aluminum. They conducted the experiments with a maximum welding speed of 122 mm/min.

An optimal parameter window was suggested by Doude et al. [86] for the FSW of AA2219 - T87 alloy based on experiments. The defect free welds were produced around 100mm/min welding speed. They have conducted a thorough investigation in the microstructural changes of the FSW joints.

Yan et al. [87] examined the effect of rotational speed, translational speed, and axial force on tensile properties, nugget microstructure and nugget hardness. However, the study was largely focussed on the effect of rotational speed on the welding response variables. It was proposed that increase in rotational speed resulted in increased temperature, less torque and less flow stress, increased yield strength and hardness. The best combination of the strength and ductility corresponds to a rotational speed that does not cause melting. The welding temperature must be near to the solidous temperature for best results. The welding speed values were limited to a maximum of 250 mm/min. They observed that the effect of translational speed on the nugget properties is small. They surmised that at higher translational speeds, the slight increase in hardness is due to the shortening of time period for over ageing.

In the qualitative assessment study of FSW, Liu et al. [88] suggested that ultra sonic vibration enhanced FSW can eliminate tunnel defects. To facilitate the macro analysis, they have divided the nugget zone in to three regions; viz. shoulder affected zone (SAZ), pin affected zone (PAZ), and weld bottom zone (WBZ).

The converging point of these three sub zones act as the epicentre for the tunnel defect (Fig. 2.16). In case of a tunnel defect, a void may form at this point due to the insufficient material flow in the PAZ from the retreating side to the advancing side. In sufficient material transfer in the down ward direction in the SAZ also plays a crucial role in tunnel defect. In their work they supplied additional energy to enhance the material flow rather than identifying proper parametric combination. However, their

results and observations may be extended in the analysis of material flow in order to assure a defect free weld.
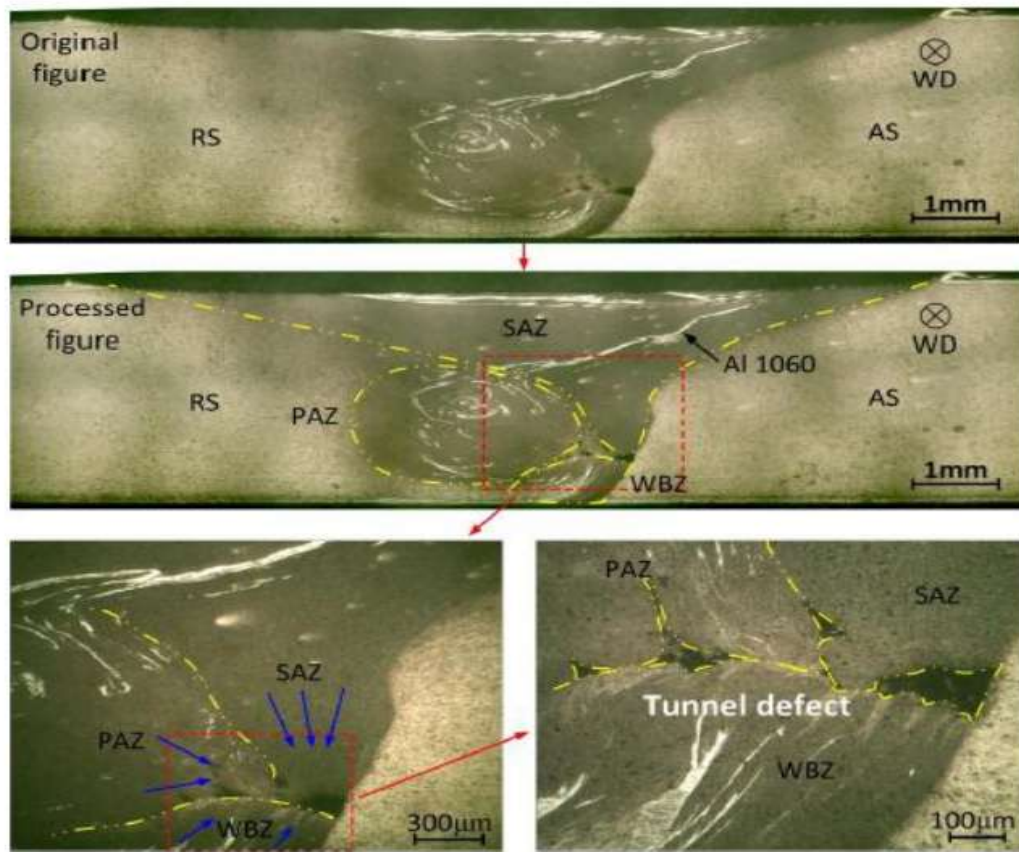
Fig. 2.16 Formation of tunnel defect in FSW [88]

Tunnel defect was reported to be caused by higher welding speed or insufficient axial force [89]. Both these conditions were identified by low heat input and insufficient material flow [90 - 92].

Ramachandran et al. [93] examined the effect of parameters on the FSW of dissimiliar joint involving AA 5082 and HAS steel. The study reported the formation of butt joints by varying the tool traversal speed, keeping other parameters as constant. They divulged that tool traversal velocity had significant effect on the weld strength by influencing the intermetallic compound layer formation. They were able to obtain a weld joint efficiency of 91% with a speed of 45 mm/min.

Dude et al. [94] suggested an optimal parameter window for the FSW of AA2219-T87 based on UTS, hardness and volumetric defect formation from their experimental analysis. The force acting was recorded using high speed data acquisition system. The report suggested that for the threaded tool used, voids near the crown is an indication rotational velocity above the optimal range and the voids appeared near the root proclaims the fall in rotational velocity below the optimal value.

Material flow regime determines the extent of bonding in FSW and the evolution of weld defects. As tool rotates and traverses the stirred material is to be deposited continuously without any void in between. Tongne et al. [95] observed the onion ring formation, a characteristic feature of material deposition as the result of periodic deposition of plasticized material in the weld progression. They quantified the extent of onion ring formation and predicted the characteristics of material deposition based on a steady state finite element model. They concluded that the formation of banded structure which appeared as onion rings related to the transient flow conditions which were influenced by the contact conditions between the base material and tool. The tool geometry had a great effect on the contact condition which in turn affects the weld quality. They suggested that the band formation sites depended on the strain rate gradient in the vicinity of the tool and the band formation pattern revealed the occurrence of defects, especially tunnel formation.

Role of tool shoulder geometry and features have been explored in various literatures. Tool shoulder is responsible for the major part of the heat generation, confinement of weld material in the weld seam and the periodic deposition of plasticized material. Majority of the weld defects are the results of poor material flow. Effect of shoulder features on the adequacy of material flow was experimentally studied by Trueba Jr. et al. [96]. They study explored the opportunities of employing additive manufacturing

in tool making by using Ti - 6Al - 4V tools with varying tool shoulder designs. The weld quality in each case was rigorously assessed through destructive and non destructive tests. The analysis was based on the material flow in welding. They claimed that shoulder with a raised spiral profile was capable of producing welds with best quality even in case of non ideal process conditions.

Only a few reports elaborate the parametric studies of FSW at welding speeds higher than 200 mm/min. The obvious reason for the lower or medium welding speed is that at higher speed the weld strength and quality are reduced considerably. The efforts to increase the welding speed without compromising the quality and strength continue to be a challenge. Trimble et al. [97] made a series of FSW to determine the effective combination of parameters to produce good quality welds at higher speeds. They conducted FSW with AA 2024 - T3 alloy and achieved good quality welds at a maximum speed of 355 mm/min. They recommended that tooling with scroll shoulder and triflute pin adequately stirred and transferred material to produce good quality welds at higher welding speeds.

Moshwan et al. [98] investigated the changes in the mechanical properties and microstructural evolution as the rotational speed changes using AA 5052 - O alloy. The weld forces were measured to estimate the variation in weld quality. Five different rotational speeds were used while the welding speed was kept as 120mm/min. It was revealed that dissolution of inter metallic phases during FSW lowered the weld strength. Variation of UTS, welding forces and micro hardness with rotational speeds were recorded to suggest the optimum rotational speed.

A few literature reports the effect of certain parameters which are otherwise not common in the investigations. Kumar et al. [99] examined the effect of variation of interposition of the joint with tool axis and the axial force on the tensile strength of

A - Zn - Mg alloy. They have conducted the experiments by continuously changing the axial load by gradually increasing the tool shoulder and base material interface, instead of applying different axial forces. Similarly the interface position of the joint with respect to the tool axis was changed continuously by keeping the tool traversal direction at an angle with the joint line. Material flow changes have been observed in the micrographs to find out a suitable axial force for making defect free weld joint. The variation of UTS with axial force showed a gradual increase, reaching a maximum value and then a decline. The variation in UTS was associated with the defect formation which in turn related to the pin driven and shoulder driven material flow. They suggested a safe range of tool deviation from the weld line for a frustum shaped pin.

The tool shoulder surface geometry is a key feature in the mechanical properties of FSW joints, as they influence the heat generation and the material flow. Scialpi et al. [73] evaluated the influence of shoulder geometry on the microstructural and mechanical properties of thin (1.5 mm) sheets of AA 6082 alloy joints. They used three types of tools with different shoulder features viz. scroll and fillet, cavity and fillet, and only fillet. The performance of these tools were analysed by micrographical examinations, microhardness, room temperature bending and tensile tests. By visual inspection they asserted that the crown and root quality would change with shoulder features. Through micrographical inspection changes in the nugget grain size was established for each tool. They proposed that the tool with fillet and cavity provided best results in terms of tensile strength and hardness for the other selected parameters.

Hariri et al. [100] proposed an optimum combination of tool rotational rate and welding speed focussing on the corrosion behaviour and mechanical properties of friction stir welded AA 5052 alloy. Potentio dynamic polarization, open circuit

potential monitoring, test of intergranular corrosion, weight loss, tensile test and microhardness tests were used to explore the effect of tool speeds. Welding speed and rotational speed were found to influence grain size by affecting the frictional heat in put and degree of deformation. Intergranular corrosion in the form of network attacks was found in NZ at 800 and 2500 rpm. Finer grain sizes were found to repel the corrosion activity. Extra fine grain structure was obtained at 400 rpm and 250 mm/min which were found to lessen the corrosive attack. They suggested optimum values for rotational speed and feed as 400 rpm and 250 mm/min for better mechanical properties and corrosion resistance.

FSW is generally devoid of residual stresses as the joining takes place at lower temperatures. However, for thicker sections and at high temperature process conditions friction stir welded sections show considerable residual stresses. A few reports were found to consider these issues. Gorgil et al. [101] presented their experimental analysis on the effect of tool shoulder features on the mechanical properties and residual stresses of friction stir welded AA 6082 - T6 alloy. They have used three types of tools with different shoulder features: a shoulder with scroll, a shoulder with a shallow cavity, and a flat shoulder for the welding of 1.5mm thick base plates. Tensile test with transverse and longitudinal specimen and fatigue tests were conducted to evaluate the mechanical properties and hole drilling method was used to analyse residual stress. Flat shoulder produced higher welding temperature which in turn caused the coarsening of grains in the NZ. Visual observation revealed that shoulder with scroll caused flash formation, where as flat shoulder and shoulder with cavity produces smooth weld surface with little flash. A key observation in their studies is that the shoulder geometry had little influence in the tensile strength as there was no much difference in the tensile strength for different shoulder geometries. Nevertheless, the fatigue properties were strongly affected by the shoulder geometries

with shoulder with scroll showed worse fatigue behaviour whereas flat and shoulder with cavity provided better fatigue properties with lower fatigue limit. Residual stress level was low for all joints, perhaps because of the uniqueness in FSW, but residual stress distributions were different for different shoulder geometries. They inferred that shoulder with scroll provided relatively better results when residual stress was concerned.

Ramulu et al. [72] proposed a criterion quantitatively for the formation of defect free welds from their experiments by performing FSW on 2.1 mm thick AA 6061 - T6 alloy. With a focus on the defect free weld formation they analysed effect of welding speed, tool rotational speed, axial force, and plunge depth and shoulder diameter on the FSW process. The study concluded that the shoulder diameters have little effect on the defect formation and higher welding speeds (80 - 120 mm/min) and higher rotational speeds (1300 - 1500 rpm) and increased plunge depth (1.85 – 2 mm) produced defect free welds. As a criterion for defect free weld formation they suggested that the change in axial force and torque with other parameters considered were high for defective welds and less in defect free welds.

Elangovan et al. [62] presented the friction stir processed (FSP)zone of AA 6061 aluminium alloy under various pin profiles and axial forces and the correlation of tensile properties of friction stir welds with FSP zone formation. They fabricated friction stir welds with five different pin profiles: straight cylindrical, tapered cylindrical, threaded cylindrical, triangular and square and three axial force levels: 6 kN, 7 kN and 8 kN. Macro structure of each weld was extensively analysed to understand the defect formation mechanism. They concluded that the square pin profile produced defect free welds with highest tensile strength and the variation in axial force had little effect in that case. On the other hand 7 kN axial force produced

34

defect free welds with superior tensile properties irrespective of the pin profile used. Interactive effect of axial force and the pin profile was concluded as the square pin profile with an axial force of 7 kN produced FSP region with finest grains which in turn cause high hardness and highest tensile properties. However it may be appropriate to notice that these results were produced with a tool rotational speed of 1200 rpm and a lower welding speed of 1.25 mm/sec.

Jayaraman et al. [102] analysed microstructural evolution of the weld zone of friction stir welded cast A 319 aluminium alloy and the corresponding tensile strength under varying process parameters. The welding was performed with different combinations of tool rotational speed, welding speed and axial force. The macrostructure revealed defect formation and the corresponding microstructure, modes and locations of tensile fracture were compiled to suggest the parametric combination for weld formation with zero defects and superior tensile strength. The precipitation and distribution of eutectic Si particles were found to be one of the decisive factors for the tensile strength. Accordingly, they suggested a combination of parameters at a tool rotational speed of 1200 rpm, welding speed of 40mm/min and 4 kN axial force for the formation of defect free weld with maximum tensile strength.

Rodrigues et al. [103] examined the effect of tool shoulder features on the microstructural and mechanical properties of 1mm sheets of AA 6016 - T4 alloy welds. Non defective welds were obtained using conical shoulder and scrolled shoulder tool where welding speeds were 180 mm/min and 320 mm/min. Tool rotational speeds 1800 rpm and 1120 rpm. As the welding temperature at higher rotational speed, welds produced were identified as hot and cold welds and they were distinguished by the appearance of the crown as shown in Fig. 2. 17. Conical shoulder tool produced hot welds with larger grain size and few coarsened precipitates. Larger

grain size in the report indicates slower cooling of the weld. Scrolled shoulder tool was reported to produce cold weld. Nuggets in that case were composed of grains smaller in size and many coarsened precipitates. This difference in microstructure was viewed to be the reason of reduction in hardness in case of cold welds. A reduction in elongation of 70% and 30% was observed for cold weld and hot weld respectively. They concluded that the tool shoulder geometry and welding parameters have significant impact on the material flow and mechanical properties of friction stir welds.
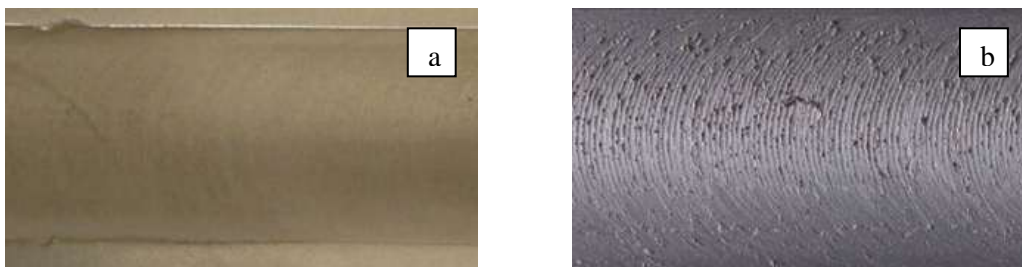
Fig. 2.17. Crown view of (a) Cold weld (b) Hot weld

Among the earlier reports, Patil and Soman [76] explained the effect of tool pin profile and welding speed on friction stir welded butt joints. They used triflute and taper cross section with threads pin profiles for butt welding AA 6082 - O alloy at a tool rotational speed of 1200 rpm, and welding speeds of 60 mm/min. 70 mm/min, 75 mm/min and 85 mm/min. It was proclaimed that the pin profile and welding speed significantly affect the tensile properties. They concluded that the taper and screw threaded pin profile produces superior quality weld than that of triflute pin irrespective of the welding speed. The highest ultimate and yield strength were reported for the welds produced by taper and screw threaded pin profile at a speed of 70 mm/min. For the triflute pin joint, UTS attains the maximum value for the welds fabricated at a speed of 60 mm/min. According to the report the authors were able to achieve a higher tensile strength value of 92.3% of the base metal value but at a very

low welding speed. It is significant to note that the shoulder and pin diameters of the tools were different. However the authors have not explored their significance and interactive effect.

Rodrigues et al. [104] reported a rare attempt to examine the feasibility of FSW of aluminium alloys at higher welding speeds. It was reported that the feasibility of FSW depends on the type alloy and thickness of the base metal apart from the general process parameters. They assessed the weldability of AA 6082 - T6 and AA 5083 - 111 alloys based on the defect formation analysis and mechanical strength characterisation. FSW of the alloys were performed for various tool geometry, welding speeds, rotating speeds, axial forces and tool tilt angle. The maximum speed tested was 350 mm/min for 6mm thick plates. By calculating the maximum energy consumed per unit length they suggested that FSW is less dependent on tool parameters and process parameters at high rotational speeds. Attaining the hot weld conditions, according to their analysis, was depending on the base material properties, which was more feasible for harder materials like 6082 alloys. Based on the maximum energy consumption and defect formation they proposed parameter window for good weld formation.

Barlas and Ozsarac [105] studied the effect of tool rotational speed, tool tilt angle and the direction of tool rotation on FSW of Al 5754 alloy using a threaded tool. Higher tool rotational speeds were tested in various trials. Best results were obtained for tool rotation of 1100 rpm, 2^0 tool tilt and counter clockwise rotation. With the support of the macrographs of the transverse sections of the welds, the authors revealed that the clockwise rotation of the right handed threaded tool in various trials with different parameters caused defects. The trials performed with tool rotation in counter clockwise direction produced non defective welds. They also suggested that shape of

weld nugget zone changes with the tool tilt angle and the direction of tool rotation. For clockwise rotation cavity defects occurred beneath the tool pin irrespective of other process parameters. For vertical tool application the defects were formed on both AS and RS whereas for 2^0 tool tilt the cavity was formed only in the RS. The authors concluded that insufficient heat input, stirring rate and axial force caused the defect formation in case of trials with clockwise rotation. They also opined that a slight increase in penetration depth with increase in tool rotational speed will favour the elimination of defects. Though it was not elaborated in their study, the macrograph clearly indicated the difference in material flow with the direction of tool rotation, where the location of defect formation was changed from interface to pin bottom as shown in Fig. 2.18. The direction of tool rotation with respect to the direction of thread advance will obviously have an effect on the material flow, the severity of which needs further investigation.
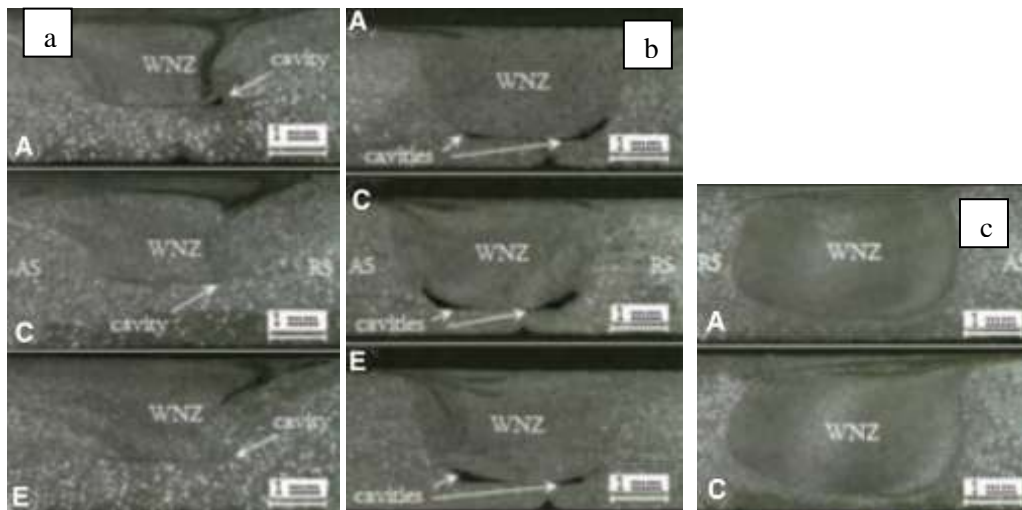
Fig 2.18 Material flow: (a)Tool rotation clockwise and tool tilt angle 2^0 (b) Tool rotation clockwise and tool tilt angle 0 (c). Tool rotation counter clockwise and tool tilt angle 2^0 [105].

Many studies summarized the effect of various parameters to the in-process thermal cycle experienced during FSW. Reynolds et al. [106] studied the relationship between welding parameters, hardness distribution and thermal history in FSW of Al 7050

alloy. Tool rotational speed, welding speed and axial load were selected as the parameters for the experimental trials while temperature- time history was recorded using FEM simulation. A series of welds were made with 7050 - T7451 alloy plates of 6.4 mm thickness and the highest welding speed tested was 5.1 mm/s. Weld power and welding speeds were chosen as the secondary parameters to rationalise the hardness variation in welds prior and after post weld treatment. They suggested that the rate of heating up and rate of cooling was dependent only on the weld speed and the weld temperature attained can reliably be correlated with the weld power rather than the primary process parameters. The study correlated the nugget hardness with peak temperature and the precipitation of M phase particles. Based on the thermal history and hardness distribution they deduced an optimum weld schedule which corresponds to a peak temperature value which is between the solution treatment temperature and the melting temperature and a higher welding speed.

The heterogeneity in microstructure of friction stir welded precipitation hardened aluminium alloys is crucial in deciding the corrosion properties as FSW influences the behaviour of strengthening precipitates. Rao et al. [107] studied the effect of tool pin profile on the evolution of weld nugget microstructure and pitting corrosion of AA 2219 alloy. A series of welds were made using tools with conical, square, triangle, pentagon and hexagon pin profiles. The performance of tools was assessed by measuring the temperature during welding, micro hardness survey, and microstructural changes including distribution of strengthening particles.

The study concluded that the shape of the weld nugget is dependant only on the shape and size of the tool pin, not on the welding parameters. More over the welds formed by the hexagonal pin exhibited equiaxed grain structure finer than other welds presumably by the dynamic recrystallisation. The second phase $CuAl_2$ particles were

more uniform and small in case of hexagonal pin, which was reported to be attributed to the higher degree of deformation owing to more number of flat faces in the hexagonal pin tool. The heat generation was found to be more for hexagonal pin tool which caused the disintegration and uniform distribution of eutectic network. Better dissolution of the precipitates were found in case of hexagonal pin which resulted in better corrosion properties of the weld nuggets better than the base metal due to the reduction in galvanic coupling. Hexagonal shape was the better option for tool pin profile for optimum combination of microstructure, hardness and corrosion properties.

Mishin et al. [108] precisely carried out the microstructural characterization of friction stir welds of 6082 commercial aluminium alloy using transmission electron microscopy (TEM) and scanning electron microscopy (SEM). They revealed that the weld nugget microstructure was characterized by large range of disorientations and resembled to a well recovered structure typical of hot deformed aluminium alloys. They suggested that TEM with suitable tilting can only reveal such characteristics for a particular region. However the process parameters used were not mentioned in the report.

The structural changes occurred during FSW by the heat input is paramount in deciding the weld performance. The metallurgical and structural transformations in weld joints are crucial and hence require close evaluation. Apart from the simulation studies some experimental studies put forward a realistic explanation in this extent. Cao et al. [80] conducted an experimental study to examine whether the maximum temperature reached the melting range and the possibility of occurrence of liquation. They have conducted FSW of AA2219 alloy as it has clear lower bound of melting temperature and as a bench mark to check the occurrence of liquation, gas metal arc welding (GMAW) of alloy was also performed. They spotted liquation from the

reaction of θ (Al2Cu) particles with surrounding aluminium matrix forming distinct composite like eutectic particles indicating outstretch to eutectic temperature. However in case of FSW, they ruled out the possibility of liquation as the nugget contains only θ particles, often larger in size, with no traces of eutectic particles. But they suggested that the θ particles underwent agglomeration and carried away by the stirred and transferred material throughout the weld. However no apparent correlation was evident between the extend of agglomeration of θ particles and the weld parameters.

Kamble et al. [109] studied the effect of pin geometry, tool rotational speed and welding speed on the mechanical and electrical properties of AA 6101 - T6 alloy joints made by FSW. They have used square and hexagonal profiled pin tools for weld joining. The maximum welding speed was limited to 120 mm/min. They concluded that the square pin provided better mechanical properties and microstructure. The welds made by using hexagonal pin tool exhibits traces of oxides and tunnel defects. In all the cases of weld joints the loss of conductivity was found to be negligible.

Singh et al. [110] discussed the effect of post weld heat treatment on the microstructure and mechanical properties of friction stir welded 7039 aluminium alloy. The experimental trials were conducted at a constant rotational speed of 635 rpm and welding speeds of 8 mm/min and 12 mm/min. For the selected parameters, they concluded that the tensile strength of the welds increases with the welding speed and the hardness decreases with increase in welding speed. It was observed that the post weld heat treatment lowered the ultimate tensile strength, yield strength while it improved the percentage elongation. The hardness of the as weld joint was reported to be decreased with welding speed except at the weld centre while the effect of welding speed was reversed for heat treated welds. But they have not discussed the cause of the difference in the properties of as welded and heat treated welds.

Cavaliere [111] studied the effect of process parameters on the tensile, fatigue and crack behaviour of various aluminium alloys from 2xxx, 3xxx, 5xxx, 6xxx and 7xxx series. The experimental campaign used threaded pin tools of different pin length and shoulder diameters. The parameters tested were rotating speed, weld speed, tool tilt, revolutionary pitch and axial force. The experimental data was used to create a database capable of generating a model to predict the weld quality under various parameters.

Prior studies in the FSW regime discussed the benefits of the process, optimum operating conditions based on the selection of process parameters and additionally the effect of the process parameters on the strength and quality of the weld joints. The results of these studies stipulated that process parameters determine the welding process temperature and the material flow during weld formation. However certain parameters, for example, the tool tilt angle have not been contemplated in these studies. Tool tilt angle, apparently has a significant effect on the material stirring during the FSW. The structural characterisation of the friction stir welds, especially for age hardened aluminium alloys is another aspect worth to be studied. Different experimental analyses have examined the structural changes of metal during FSW. However, the effect of tool parameters on structural changes of has not been adequately addressed. Most of the experimental analyses on the effect of process parameters in FSW are confined to lower welding speeds. Even though such studies are significant in understanding the FSW process, process mechanism at higher welding speeds is equally important, as it determines the acceptability of the FSW process as an alternate joining process.

……ॐ*ॐ……

CHAPTER 3

EFFECT OF APPLIED AXIAL FORCE ON FSW OF

AA 6082 - T6 ALUMINIUM ALLOYS

3.1   INTRODUCTION

In FSW, the frictional heat is highly localised around the shoulder and the pin and this causes the flow of plastic material. As the frictional heat flows away from the tool axis the heat intensity and the material flow gradually reduces confining the 'tool effect' to a relatively smaller volume. The material part exposed to the tool effect undergoes high strain rate and intense heat. The properties, viz. quality and strength of friction stir welds depend on the microstructural characteristics of various weld zones resulting from the heat dissipation and material deformation. Certain process characteristics determine the accurate thermo mechanical processing of FSW. They can be identified as heat generated, cooling rate, material flow in layers, degree of mixing and filling. Effects of the process parameters on these characteristics are crucial in deciding the strength and quality of the weld. Welding speed, tool rotational speed, axial force, tool geometry, tool tilt angle were identified as the most important welding parameters. Optimized combination of these parameters has been extensively derived in various studies [112 - 114]. Effect of the process parameters on the microstructural changes and weld quality is the focus of study for suggesting the optimum combination of parameters. In most of the studies on the FSW, the selections of process parameters were confined to rotational speed, traversal speed and tool geometry [115 - 120].

Biswas et al. [121] appraised the effect of process parameters on the mechanical properties of friction stir welds made of commercial grade aluminium. The study considered tool rotation, welding speed and pin geometry for their investigations. The

reported results of their study focussed on the degree of grain refinement in various weld zones. They recommended tools with pin of tapered cylindrical or trapezoid profile for the better performance of welds. They have suggested a ratio for welding speed to the tool rotational speed for better mechanical properties. Dude et al. [122] conducted a series of welding on AA2219 - T87 panels to optimize the process parameters by varying tool rotational speeds. The other parameters viz. tool speed and pin geometry were kept unaltered. The results suggested an optimum parametric window for welds with good mechanical properties without any volumetric defect. They emphasized a weld parameter regime with a trade off between the defect free conditions and better mechanical properties. Trueba et al. [123] deduced the effect of tool shoulder geometry on the defect formation and mechanical properties of friction stir welded aluminium 6061 - T6 alloy. They examined the welds with six different tool shoulder profiles and found that tool shoulder provided with a raised spiral design produced defect free welds with best mechanical properties.

In FSW, the tool is inserted by force acting along the tool axis in vertical direction. This force is referred as axial force with respect to the position of tool axis. The applied axial force can be directly measured in the FSW machines. The applied force plays a significant role in the weld quality and microstructural changes. However the effect of the axial force on the welds has not been detailed well.

Yan et al. [124] have studied the effects of tool rotational speed, welding speed and axial force on the mechanical and microstructural properties of friction stir welded AA 2524 - T351 aluminium alloys. They suggested that the interactive effect of the process parameters were to be regulated to obtain the peak temperature just below the melting point of the base metal. They indicated that the tool rotational speed had greater influence to achieve this condition. But the effect of axial force was limited to

44

the nature of interaction between the tool and metal interface interaction. Trimble et al. [125] proposed a combination of welding parameters for achieving sound and strong friction stir welds at higher speeds, through the post weld assessment and force monitoring. Their experimental investigation with AA 2024 - T3 was based on varying the rotational speeds and tool feed rates. However, they suggested tool geometry with scrolled shoulder and triflute profile for pin for achieving good results. Su et al. [126] described an economical method for measuring torque, axial force and traverse force to describe the process mechanism of FSW and optimisation of the process. Nevertheless the process parameters considered in their study to establish effects on the process was limited to low welding and rotational speeds.

It is seen that the aforementioned literature have not considered the effect of applied axial force on friction stir weld formation precisely. Here, in this report the experimental effort to gather the effect of tool axial force on FSW aluminium alloys is elaborated.

3.2   MATERIALS AND EXPERIMENTATION

The base metal used in the experiment was AA 6082 - T6 aluminium alloy. 6082 - T6 alloy comes under the category of Al - Mg - Si alloys and it is easily weldable. It is a precipitation hardened (heat treatable) alloy and a popular choice for structural applications. These alloys can easily be fusion welded. However, the proclivity for porosity formation and weld cracking is a serious concern in the fusion welding of such alloys. FSW circumvents the chances for the formation of such defects. But owing to the low melting point of the constituents formed during welding, higher welding temperature may lead to cracking defects. In FSW, the process parameters especially, tool speed and axial force determine the welding

temperature. Hence the effect of axial force is crucial in the formation of a defect free weld.

The mechanical properties of the base metal are summarized in Table 3.1. The base metal in as rolled condition and in the form of metallic plates of 6.2 mm thickness were cut in to 100 mm length and 50 mm wide rectangular pieces to make butt joints.

Table 3.1 Mechanical properties of base metal

UTS (MPa)	YS (MPa)	% Elongation(On 50mm GL)	Hardness, Hv, 02
300	245	9	110

The mating surfaces of the plates were machined by milling to make a perfect square butt. The plates were provided with adequate clamping with zero root gaps. The FSW tool was fabricated from H 13 tool steel and was oil hardened. The cylindrical pin was provided with right hand threads (Fig. 3.1). Simple tool shoulder with a flat face was provided. The shoulder diameter and pin diameter were fixed at 18 mm and 6 mm respectively.

Fig. 3.1. FSW tool.

The FSW was performed on a 11kV/440 V (AC) direct FSW machine shown in Fig.3.2. The technical details of the machine are given in the Table 3.2. The

experiment was carried out by varying the axial force, keeping the weld speed and tool rotational speed constant.

Fig. 3.2 Friction stir welding machine

Tool geometry, welding speed and rotational speed were selected based on the previous trials and reported studies, which produce good welds. The axial forces were selected based on preparatory experiments. It was revealed that below 1 kN weld joint didn't occur and above 5 kN tool shoulder pierced the parent metal. The process parameters are given in the Table 3.3.

Table 3.2 : Specifications of FSW machine

Spindle tapper	ISO 40
Spindle speed	2000 rpm
Spindle tilt angle	+- 5 deg
Z axis thrust force	30 kN
Z axis travel	300 mm
X axis travel	300 mm
Y axis travel	100 mm
Table to spindle nose (min./ max.)	100/ 400 mm
Weldable material	steel/ copper/ aluminium

Table 3.3 : Process parameters

Process and tool parameters	Value
Welding speed (mm/min)	110
Tool rotational speed (rpm)	1200
Axial force (kN)	2, 3, 4, 5
Tool shoulder diameter (mm)	18
Tool pin diameter (mm)	6

The weld samples were subjected to 100% destructive post weld examination. Three specimens were cut transverse to the weld seam from each sample, in a milling machine. Specimens were prepared in conformance with American Society for Testing and Materials (ASTM) standard E8 M - 04 for the tensile tests (Fig. 3.3). The average value of the tensile strength was considered for each sample.
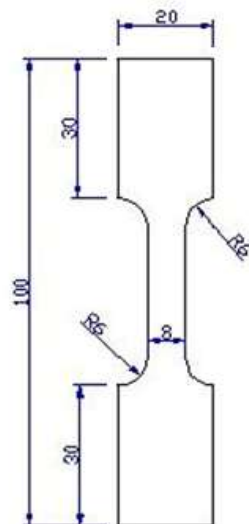
Fig. 3.3. Tensile test specimen.

Table 3.4 : Specifications of TMM

Model	DE-Wintor inverted TMM
Magnification	50X to 1000X
Eyepiece	Paired 15X and 10X
Power	12 volts 50 watts halogen lamp
Shaft	X – Y direction with 360 rotation
Polarization	With Polarizer Prism
Micro Scale	Attached with 0.01mm Occular scale.
Camera	3 M. Pixels camera

For micro structural analysis samples were cut transverse to the weld line. The specimens were ground, polished and etched with Keller's reagent. A Trinocular metallurgical microscope (TMM) was used to study the microstructure of the weld. Tables 3.4 and 3.5 detail the specifications of TMM and Universal testing machine (UTM).

Table 3.5 Technical details of UTM

Testing load range	5 T max.
Gear rotation speed (For gradual loading)	1.25. 1.5 & 2.5 mm /min
Software details	FIE make India
Make	Associated Scientific Engg. Works

The disparateness in mechanical properties was examined through hardness measurements across the transverse cross section of the weld. Measurements were taken by a Vicker's hardness tester at 0.5 kgf load with a dwell time of 10 sec. Readings were taken 1.5 mm below from nugget zone and at an interval of 1 mm. Table 3.6 shows the technical details of the hardness tester.

Table 3.6 Specifications of hardness tester.

Model	402 - MVD
Vickers scales	HV0.01, HV0.05, HV1 & HV2
Test loads	13 – 25- 50 – 100 – 200 – 300 – 500 – 1000 & 2000 gf
Load control	Automatic
Load duration	8 – 99 seconds
Resolution	0.1 µm
Measuring range	200 µm
Total magnification	400 x (for measurement) 100 x (for observation)
Power supply	110 – 222 V AC

3.3   RESULTS AND DISCUSSION

The effect of axial force on the mechanical properties and quality of the friction stir welds was analysed by measuring the tensile strength and examining the microstructure. The most predominant failure for a butt welded joint is the tensile failure. Hence the weld strength is represented by its tensile strength. The tensile strength of FSW of heat treatable alloys is affected by the coarsening of precipitates and voids creation due to flaws in material flow.

3.3.1 Tensile properties

The tensile specimen cut in the transverse orientation includes four microstructural zones viz. the base metal (BM), heat affected zone (HAZ), thermomechanically affected zone (TMAZ) and the nugget zone (NZ). The tensile strength survey of different weld coupons indicated that there was no considerable change in the tensile strength with the variation in axial force. The ultimate tensile strength (UTS) recorded

a maximum for the weld produced under an axial load of 4 kN. The UTS values and percentage elongation at the maximum load for each sample was compared as given in the Table 3.7. The variation of UTS with axial force recorded a gradual increase up to 4 kN and then decreased slightly as shown in Fig. 3.4.

Table 3.7 Ultimate tensile strength and percentage elongation

Weld No.	Axial load (kN)	UTS (kN/mm^2)	% Elongation
L1	2	0.167	7.929
L2	3	0.186	7.214
L3	4	0.21	14.321
L4	5	0.204	14.964

The mode and location of fracture varies with samples (Fig. 3.5). Out of the tensile test specimen prepared, the samples L1 and L2 using axial force 2 kN and 3 kN respectively, fail by brittle fracture and the fracture occurred at the joint line of weld whereas L3 and L4 subjected to axial forces of 4 kN and 5 kN failed through tensile fracture. More over the specimen prepared under 2 kN and 3 kN failed in the weld nugget and 4 and 5 kN failed in the TMAZ - HAZ inter face boundary.

The fracture locations reflect the weakest locations in the weld, and hence the mechanical properties of the weld joints. The local and heterogeneous deformations lead to fracture and it depends on the welding parameters. It was reported that during tensile tests the fracture of welds occurs at the interface of NZ and TMAZ, when the welds are free of voids and other defects. On the other hand, fracture occurs at the weld nuggets when defects exist in the welds [127].

51

Variation of UTS with axial force
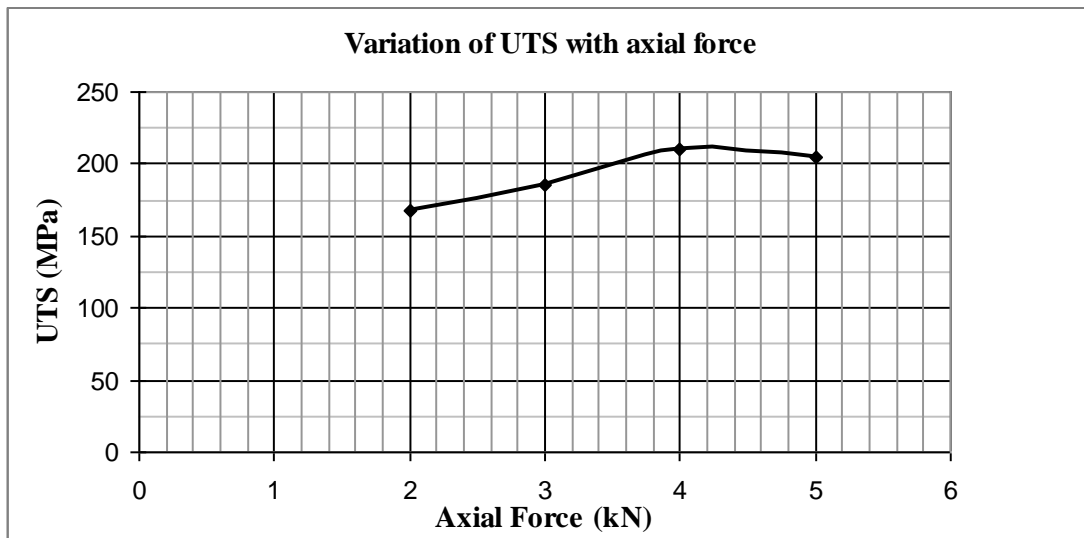
Fig. 3.4 Variation of UTS with axial load.

The defect formation might have contributed to the variation in the tensile properties and the fracture locations of the joints as depicted in Figs. 3.4 and 3.5. There is no significant and observable neck formation in tensile test specimen, in some cases, which is essential for tensile fracture.
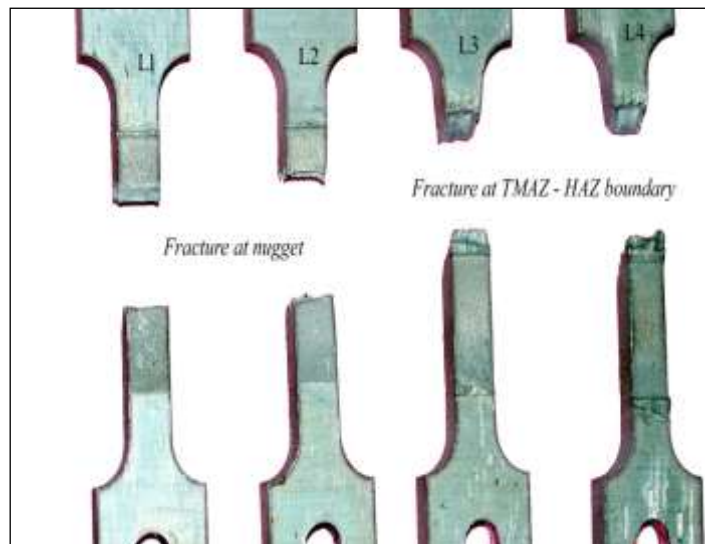
Fig. 3.5 Nature and position of fracture in tension tested sample

The stress strain curves for the base metal and the transverse weld samples are shown in Fig. 3.6.
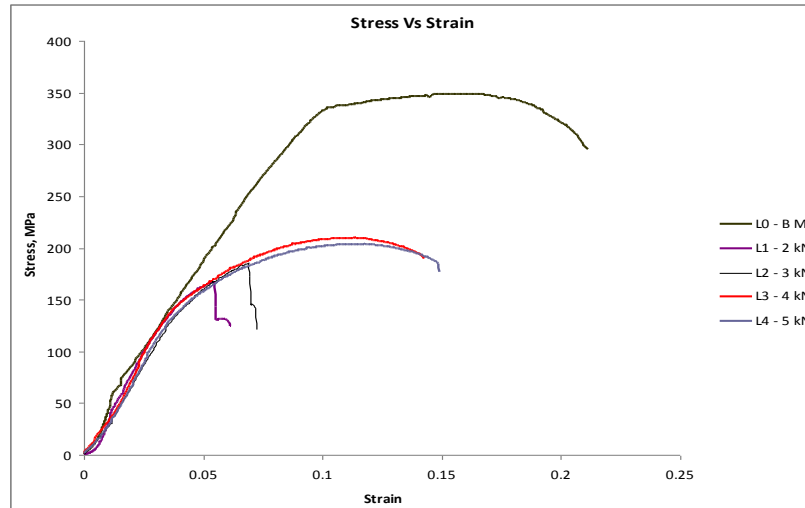
Fig. 3.6 : Stress strain curves for tensile specimen:
BM- Base metal; A – 2 kN; B – 3 kN; C- 4 kN; D- 5 kN.

Friction stir weld is akin to a heterogeneous composite with different material properties for different parts and their interfaces. When the weld is subjected to a tensile load stress and strain concentrations occur at the weakest part or location and the weld fractures at this location [128]. The stress strain curve in Fig. 3.6 indicates the mode of fracture of the welds. It may be concluded that the difference in modes of fracture was attributed to the presence of defects.

3.3.2 Macrostructure and microstructure of the welded joints

The macroscopic facets of the joints are shown in Fig. 3.7. The nugget regions of all the joints had basin shape which indicates adequate stirring and transfer of weld material by the tool action [2].
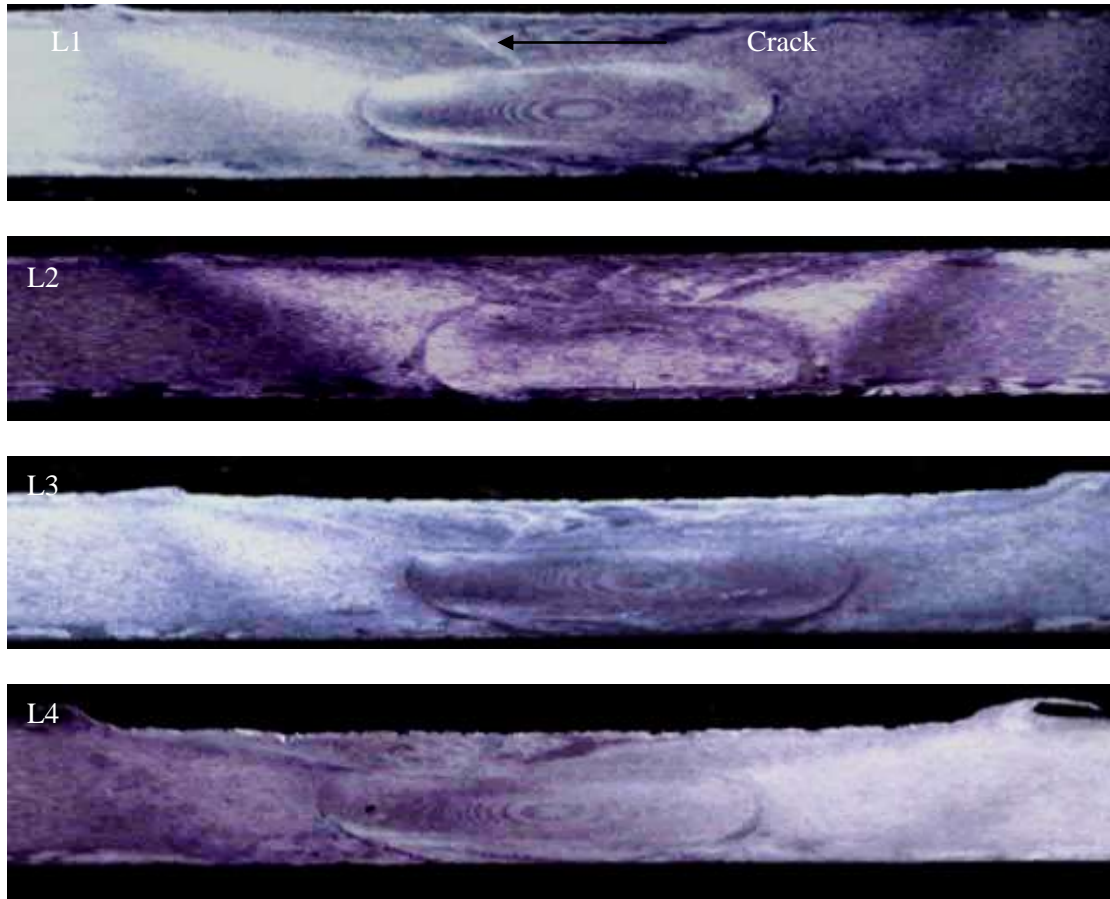
Fig. 3.7 :   Optical macrograph of different joints: L1- 2 kN, L2- 3 kN,
               L3- 4 kN, L4- 5 kN.

All the joints exhibited onion ring structure in the NZ except for L2 and the strength

of the formation was greater for 2, 4 and 5 kN joints. The FSW process can be thought

to be simply extruding material in layers through semi cylindrical paths in one

rotation of the tool and a cross-sectional view of such a set of semi cylindrical layers

appears as onion ring structure [129]. Hence it can be perceived that all the weld

joints especially under 2, 4 and 5 kN axial forces, for the given set of other

parameters, were formed with adequate material flow. The macrostructure of L3 and

L4 indicate that the material flow was more or less symmetrical when compared with

other joints and it has strengthened the mechanical properties of these joints.

AA 6082 has the highest strength among the 6000 series alloys. The presence of

larger amount magnesium controls the grain structure and hence the strength. The

microstructure of the parent alloy (Fig. 3.8) shows elongated grains of primary alpha aluminium with evenly distributed Mg_2Si particles in solid solution with aluminium.

Fig. 3.8. Microstructure of base material

The shoulder zones (Fig. 3.9) of all the welds appeared to be identical, finer grains with dissolution of the Mg_2Si particles and recrystallisation by the frictional heat generated and intense stirring. It can be observed that the variation in axial force does not have much effect on the heat generation at the shoulder zone, for a constant tool shoulder diameter.
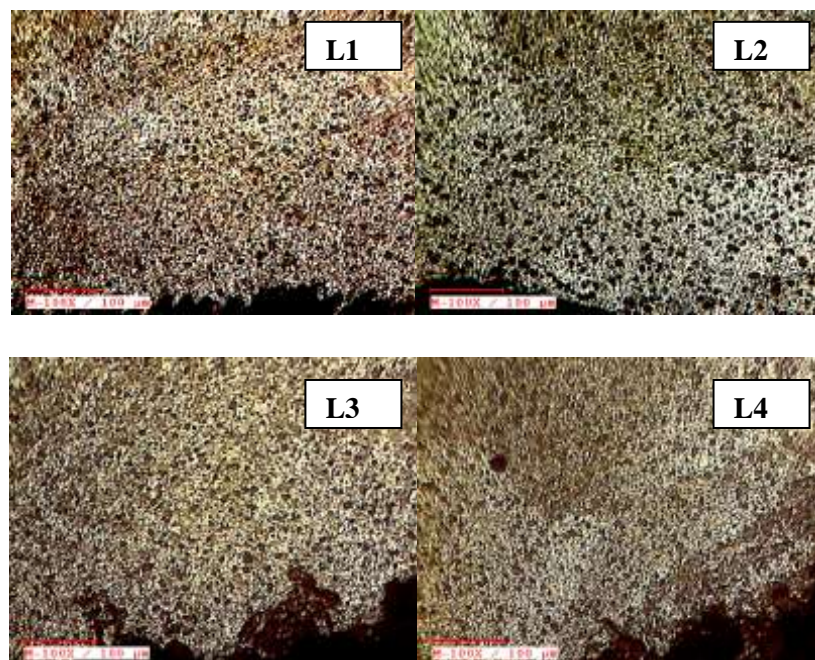
Fig. 3.9.   Optical macrograph Shoulder Zones:
L1- 2 kN, L2- 3 kN, L3- 4 kN, L4- 5 kN

Heat affected zones (Fig. 3.10) were characterized with grains finer than the base metal due to the heat. The grains show some disorientation in case of L1, L3 and L4, indicating stronger joint. However the images are not sufficient to establish the pin effect.
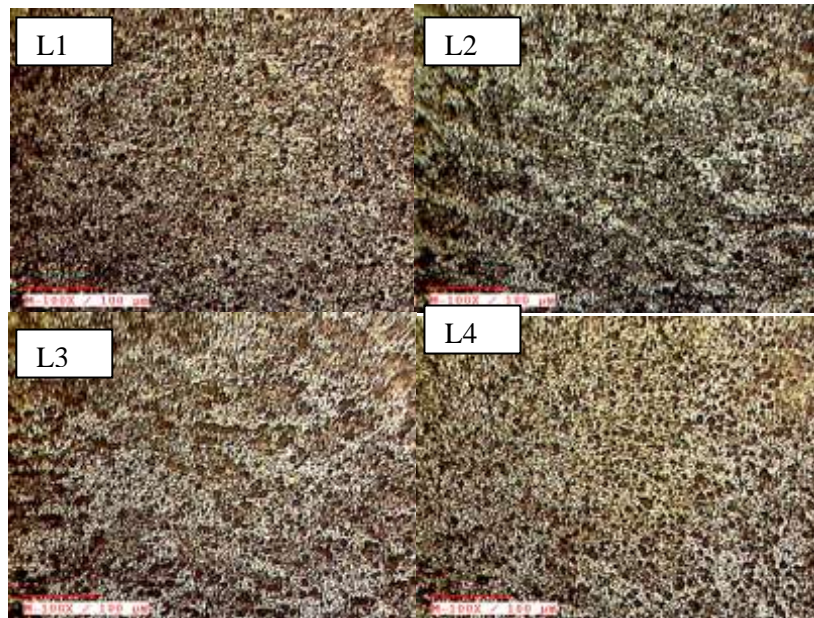
Fig. 3.10 . Optical macrograph : Heat affected zones:
L1- 2 kN, L2- 3 kN, L3- 4 kN, L4- 5 kN.

At the TMAZ region (Fig. 3.11), the material is subjected to intense mechanical deformation and heat. For all the welds, the chosen parameters were apparently sufficient to deform the grains thermally and mechanically to transform the material layers in to onion rings at a micro level.

The microstructure in NZ (Fig. 3.12) was apparently subjected to dynamic recrystallization, and showed dissolution of eutectic particles. Presence of fine and fragmented particles of Mg_2Si was detected in this region.
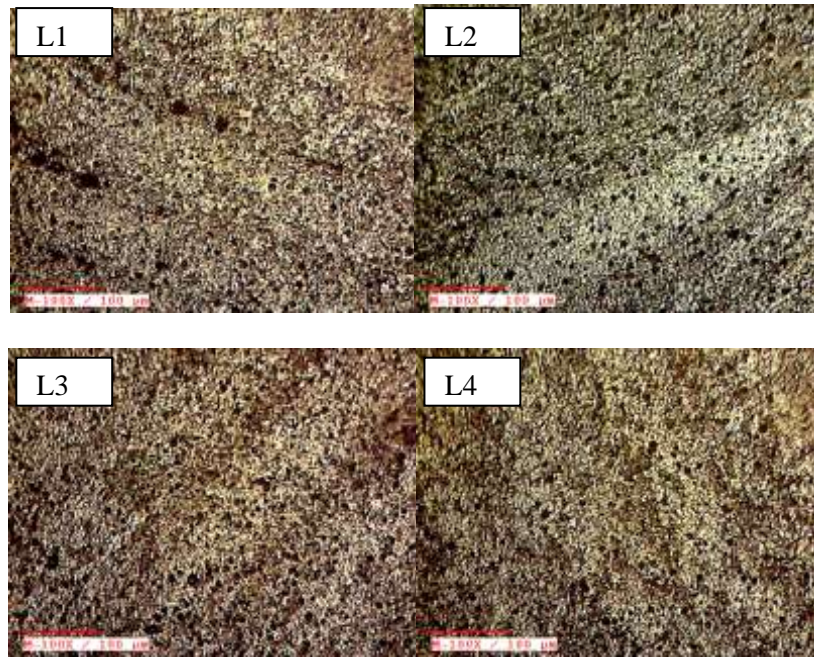
Fig. 3.11. Optical macrograph TMAZ: L1 - 2 kN,
L2 - 3 kN, L3 - 4 kN, L4 - 5 kN.

During FSW the downward force keeps the shoulder in contact with the material. The downward force enhances the friction and keeps the stirred material in the weld region. The downward force increases the plastic flow of material during the welding process. An optimum combination of axial force and welding temperature results in consistent filling of welding cavity through consolidating the pin driven and shoulder driven material with the base material. However the increase in down ward force beyond a limit increases subsurface material flow which hampers the effective filling of welding cavity. Hence, increased downward force affects the tensile properties. Welding speed and tool rotational speeds are the predominant factors for the welding temperature. In the present study, as these parameters were kept constant, the welding temperature was not affected significantly. The microstructure analysis underlies this effect. Therefore the varying axial forces influence the material flow. The variation in tensile strength which appears to have a maximum value at 4 kN and a trend of decrease and the macrostructure indicate that the optimum value for the axial force is 4 kN, for the given parameters.
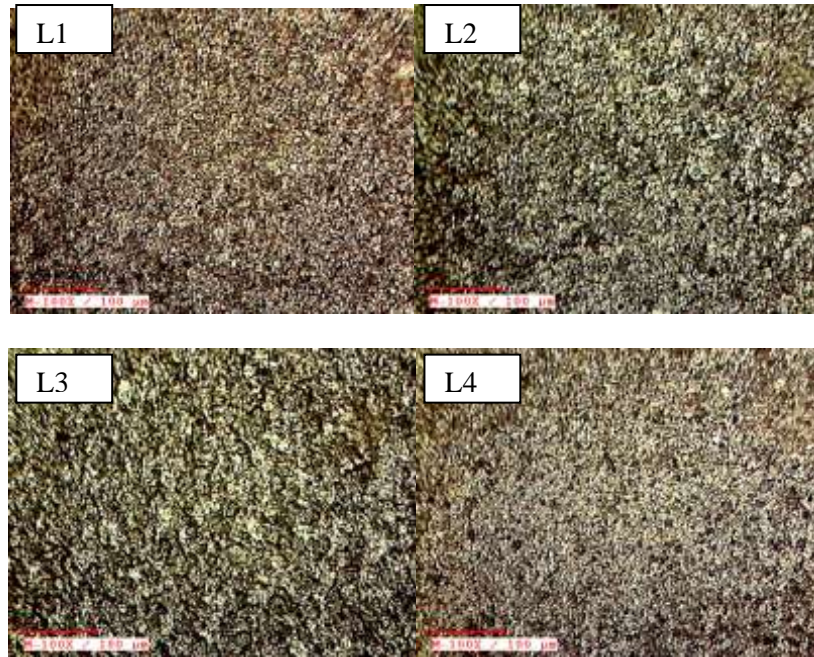
Figure 3.12. Optical micrograph of centre of NZ:

L1 - 2 kN, L2 - 3 kN, L3 - 4 kN, L4 - 5 kN

The macrostructure and microstructure of the welds indicated the variation in weld properties. L1, L3 and L4 were sound in microstructure by virtue of the grain disorientation. However, the macrostructure of the weld indicated presence of crack defect extended to the NZ in the specimen L1. The nugget collapse of the weld in the tensile test specimen for L1 was attributed to the presence of the crack defect. The onion ring formation in the NZ is an index for the material flow. Periodic and consistent material flow filling the weld cavity is indicated by the onion string structure. The NZ of the specimen L2 apparently fail in keeping the desired material flow. The flaws in the material flow reduced its ductility in the NZ which lead to the nugget collapse through brittle fracture in the specimen L2 as shown in the fracture location.

3.3.3 Microhardness

The microhardness values for various joints under different axial forces are plotted as shown in Fig. 3.13. All the welds recorded hardness values, slightly higher than the

base metal, at nugget zones. Two low hardness zones were identified both at RHS and LHS, near the TMAZ/HAZ boundary.
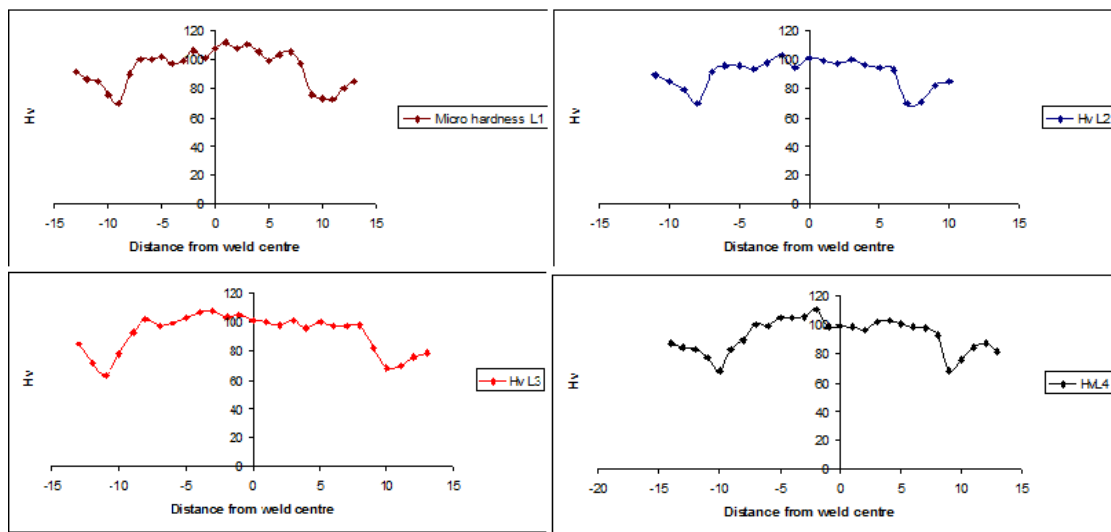
Fig. 3. 13. Microhardness for various joints: L1, L2, L3 & L4

In the case of FSW, the general perception is that the weld region is subjected to softening because of the thermal cycle and plastic deformation associated with the process. However, in case of precipitation hardened alloys like AA 6082 the mechanical properties largely influenced by the coarsening, dissolution and distribution of strengthening precipitates during welding, than by the grain size [103]. The hardness of the stir zone is significantly affected by the precipitation of strengthening particles during the welding after the cooling [83].

It was reported that, in the FSW of precipitation hardened aluminium alloys, coarsening and dissolution of precipitates plays the major role in softening the weld region. In this case, the strain rate and heat input may not vary significantly as the shoulder diameter, pin profile and rotational speeds remain constant for various weld trials [130, 82]. Therefore it is apparent that the inconsistency in mechanical deformation with varying axial force results in the precipitation and/ or dissolution of precipitates. The micro hardness maps for different welds endorsed the causes of

variation in the mode of fracture and weld strength. The micrograph of the NZ of the welds observed the presence of Mg_2Si precipitates and dynamic crystallisation of grains, which contributed the hardness values slightly higher than the base metal. It is widely reported that the FSW of AA 6082 alloys results in the lowering of hardness in the weld region for the selected regime of parameters. In this experiment, the selection of the parameters for the weld trials apparently instigated optimum level of precipitation of the strengthening precipitates to provide the best results for the weld strength. The micrographs of TMAZ showed deformed grains due to intense mechanical and thermal cycle. But the HAZ regions were characterised by elongated grains by thermal cycle. Hence the TMAZ and HAZ boundary becomes weaker than other sections in the weld microstructure. As a common principle, it was reported that the weld tensile specimen failed in this region through ductile fracture, indicating strong joints.

3.4   CONCLUSIONS

FSW of AA 6082 - T6 alloy was carried out by varying the axial force where other parameters were kept constant. Even though other process parameters were selected such that they fall in a 'FSW window' corresponding to good weld formation, axial force was found to influence the mechanical properties of the weld joints significantly. The observations from the experimental trials can be concluded as follows.

- Tensile strength of the welds increased with axial force, reached a local maximum for 4 kN axial force and then exhibited a decreasing trend.
- Microstructure revealed that variation in axial force did not affect the precipitation or distribution of the strengthening precipitates which indicated that variation in axial force did not influence the heat input.

- Microhardness of the nugget was significantly higher than that of the base metal which indicated that variation in axial force did not affect the precipitation or distribution of the strengthening precipitates.

- The variation in tensile properties may be due to the defect formation as revealed by the macro graph of the welds. The maximum tensile strength corresponded to 4 kN axial force which might assure proper material flow along with the combination of the other parameter level considered.

- Axial force had a significant influence on the material flow when shoulder diameter was kept constant. Selection of axial force in FSW is very important in achieving a defect free weld with optimum mechanical properties.

……ജ*ര……

CHAPTER 4

EFFECT OF PROCESS PARAMETERS ON HIGH SPEED
FSW OF AA 2219 ALLOY

4.1 INTRODUCTION

FSW brought a radical change in metal joining processes. Since the inception of this technology, the researchers have mainly focused on consolidating the process parameters for the process feasibility and productivity. Nevertheless, studies to suggest an appropriate combination of process parameters are yet to be concluded. The process parameters apparently affect the thermal cycle and material flow, which in turn determine the weld quality. The thermal cycle brings about the microstructural changes which are to be thoroughly investigated for assessing the weld quality and feasibility of FSW process. Grain structure and the precipitates distribution are the traits of the welds which are to be focussed. In case of precipitation hardenable alloys the changes occur during FSW has more impact on the weld quality. AA 2219 is a precipitation hardenable alloy popular in aerospace applications [131]. As it offers high strength and toughness at low temperatures, AA 2219 is selected for the construction of cryogenic elements. Comparative experimental studies indicated that friction stir welded AA 2219 alloy joints exhibit superior tensile and fatigue properties compared to electron beam welding (EBM) and guided tungsten arc Welding (GTAW) processes [132]. With conventional welding process, AA 2219 exhibited superior weldability, but it recorded poor weld strength. Being a precipitation hardened alloy, the microlevel changes occur to the strengthening precipitates during FSW is crucial for the weld properties of AA 2219 alloy joints [133]. Attallah and Salem, postulated that the static properties of friction stir welded AA 2219 is dependent on the distribution of strengthening precipitates rather than the

grain size [28]. These strengthening precipitates are formed due to the solution treatment and subsequent artificial aging. In FSW there is no melting and hence no dissolution of precipitates in the matrix, but it was reported that during FSW the Al_2Cu particles show clear evidence of agglomeration [80]. These observations are significant in the investigation of effect of process parameters on the strength of FSW of precipitation hardened alloys.

In the reported studies to optimize the process parameters of FSW for AA 2219 alloy, the tool traversal speeds were found to be significantly low. In this report, the effort and results of the experimental analysis to achieve an optimum combination of process parameters of FSW for AA 2219 at higher traversal speed is elaborated.

4.2 MATERIALS AND EXPERIMENTATION:

AA 2219 is an Al - Cu - Mn tertiary alloy with remarkable cryogenic properties. The chemical composition and mechanical properties of base metal are summarized in Tables 4.1 and 4.2. AA 2219 in annealed condition was used as the base metal for the experiments.

Table 4.1. Chemical composition (wt. %) of base metal

Cu	Mn	Zr	V	Ti	Fe	Si	Zn	Mg	Al
6.2	0.3	0.11	0.09	0.06	0.16	0.05	0.01	0.01	93.01

Table 4.2. Mechanical properties of base metal

UTS (MPa)	YS (MPa)	% Elongation(On 50mm GL)
151.2	68	15

The metallic plates of 6 mm thickness were cut in to 150 mm length and 50 mm wide rectangular pieces.. L9 orthogonal array of the Taguchi design method was used as the design matrix. The parameters considered were tool rotational speed, tool traversal speed, axial force and tool pin profile. The various parametric levels and the design of experiment matrix are given as Tables 4.3 and 4.4.

Table 4.3. Factors and levels used in the experiments

Factors	Level 1	Level 2	Level 3
Tool rotational speed, N (rpm)	1200	1400	1600
Tool traversal speed, S (mm/min)	125	151	180
Vertical force F (kN)	11	12.5	14.5
Tool pin profile, D	Taper	Cylindrical	Threaded

Table 4.4. Design matrix for experiments

Expt. No.	N	S	F	D
1	1200	125	11.0	1
2	1200	151	12.5	2
3	1200	180	14.5	3
4	1400	125	12.5	3
5	1400	151	14.5	1
6	1400	180	11.0	2
7	1600	125	14.5	2
8	1600	151	11.0	3
9	1600	180	12.5	1

The effect of tool action was analysed by varying the pin of the cylindrical tools. Three types of tools with different pin profiles viz. cylindrical pin, tapered pin and threaded pin were used for the experiment as shown in Fig. 4.1.

Fig. 4.1. Tool pin profliles

Tools were fabricated from H 13 tool steel and heat treated. As a thumb rule the tool pin diameter were suggested as equal to the base metal thickness and the shoulder diameter was suggested as equal to three times that of the pin diameter. Accordingly, tool shoulder diameter was kept constant at 18 mm and pin diameter was fixed at 6 mm. Pin length was fixed as 5.8 mm to ensure sufficient plunge depth and the prevention of any damage to the pin by striking on the backing plate. The experiments were carried out on a 11kV/1440 RPM/440 V (AC) direct FSW machine.

Tensile tests were carried out on the specimen cut perpendicular to the weld seam and prepared in accordance to ASTM E8M - 04 standards. Specimens were cut in a milling machine. Micro structural analysis was carried out using a Trinocular metallurgical microscope (TMM) and specimen were etched with Keller's reagent.

4.3   RESULTS AND DISCUSSION

In all cases of experiments, flashes were found on the weld indicating that the shoulder was unable to trap the material beneath it (Fig. 4.2). Researchers have

reasonably explained this phenomenon as due to the excessive axial force which caused the material to extrude out and the shoulder size was not enough to trap the extruded material. Another possibility for this phenomenon is the excessive stirring of the material due to high temperature and consequently excessive softening of the material [134]. All the welds showed a smooth surface which indicated that the weld was formed in cold condition wherein the temperature is not too high [135].

The strength of the welds was assessed by measuring the ultimate tensile strength (UTS). The value of UTS for the joints fabricated at various parametric levels is given in Table 4.5. Ultimate tensile strength was found to be the maximum for the joint fabricated with a threaded pin profile at 1200 rpm, 180 mm/min, and under an axial load of 14.5 kN.
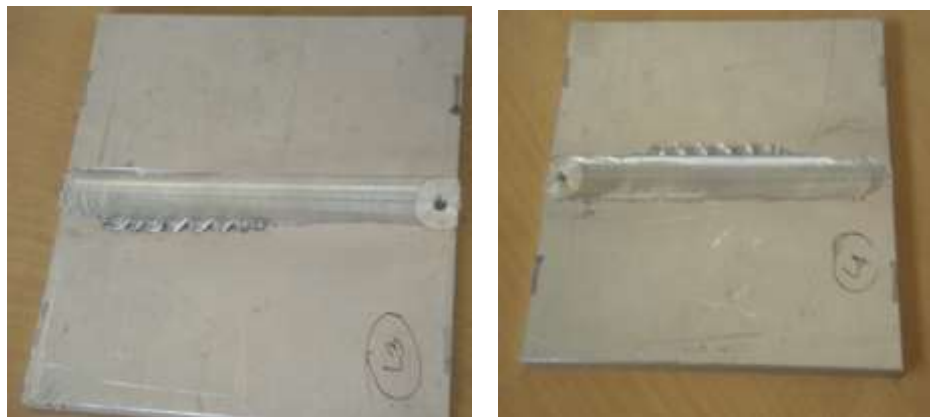
Fig. 4. 2 Flashes on the weld surface

Table. 4.5. Process parameters and ultimate tensile strength.

Expt. No	N	S	F	D	UTS (MPa)
1	1200	125	11.0	1	50.654
2	1200	151	12.5	2	58.652
3	1200	180	14.5	3	109.360
4	1400	125	12.5	3	90.644
5	1400	151	14.5	1	30.980
6	1400	180	11.0	2	66.650
7	1600	125	14.5	2	61.318
8	1600	151	11.0	3	87.000
9	1600	180	12.5	1	58.652

4.3.1 Taguchi optimization

The effect of process parameters on the strength and efficiency of the weld joints were analysed using Taguchi optimisation. The Taguchi method employs a special design of orthogonal array (OA) to analyse the output characteristics, thereby reducing the number of experimental trials. In Taguchi analysis, two types of factors are proposed which affect the functional characteristics of a product or process: control factors and noise factors. Control factors are those factors which can easily be controlled; on the other hand noise factors are those which are difficult or too expensive to control. Taguchi method uses signal to noise (S/N) ratio to assess, how the output varies relative to the target value under different noise conditions. The S/N ratio is calculated under three criteria, namely, 'smaller the better', 'larger the better' and 'nominal the better' depending upon the desired output. In this case, Maximum value for UTS was considered as the desired condition. Hence Taguchi analysis was carried out with a

criterion of 'larger the better', using equation 4.1 for deriving the process combination for maximum tensile strength.

$$SN_L = -10\log\left(\frac{1}{n}\sum_{i=1}^{n}\frac{1}{y_i^{\,2}}\right)$$ (4.1)

The analysis was carried out using MINITAB software. The effect of each factor level on the response characteristic was displayed in the response tables and main effect plots. The degree of response to the S/N ratio gave the most influential parameter. From the mean plots of S/N ratio and mean response tables the factor and factor levels which have the maximum effect on the response characteristic and the optimum levels for the parameters were identified.

The response table for S/N ratio is given in the Table 4.6 and that for means is shown as Table 4.7. Main effect plots for S/N ratio and means are shown as Figs. 4.3 and 4.4.

Table. 4.6. Response table for signal to noise ratios

Level	N	S	F	D
1	36.75	36.33	36.45	33.09
2	35.15	34.66	36.63	35.86
3	36.64	37.54	35.45	39.57
Delta	1.60	2.88	1.18	6.48
Rank	3	2	4	1

Table. 4.7 Response table for means

Level	N	S	F	D
1	72.89	67.54	68.10	46.76
2	62.76	58.88	69.32	62.21
3	68.99	78.22	67.22	95.67
Delta	10.13	19.34	2.10	48.91
Rank	3	2	4	1

The response tables for S/N ratio and means depicted the ranks of each factor based on the delta statistics, which compared the relative magnitudes of the effect on the output characteristic. From Tables 4.6, 4.7 and main effect plots (Figs. 4.3 and 4.4) it can be confirmed that the tool pin profile have the greatest effect on the tensile strength followed by feed, rpm and axial force.
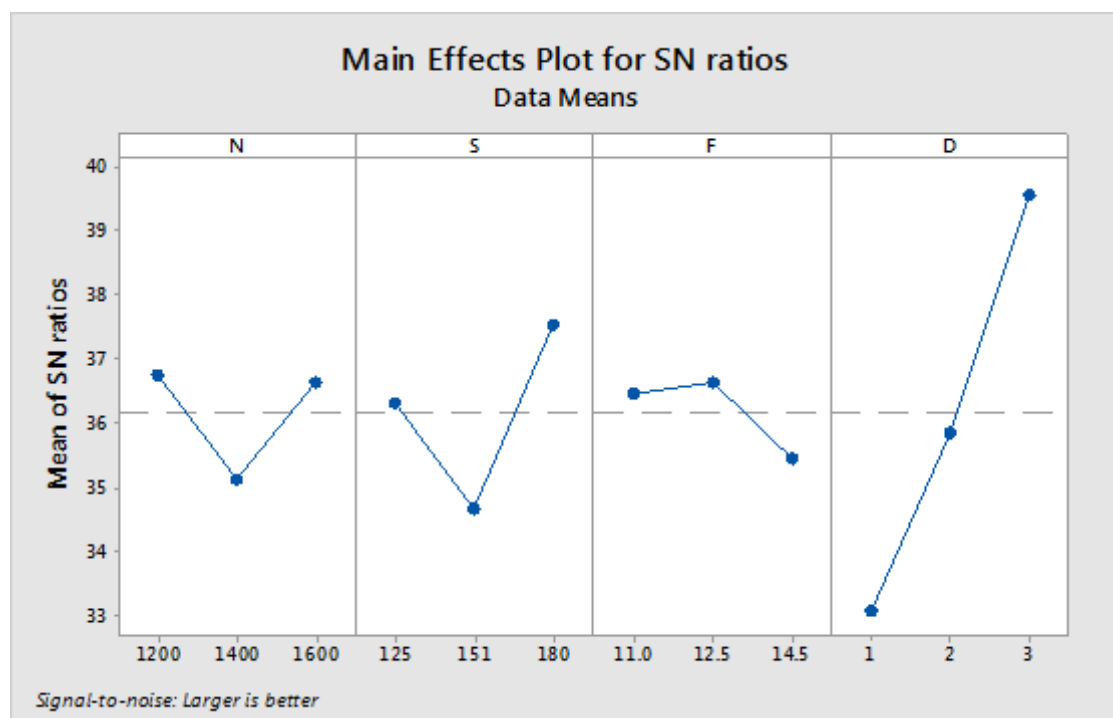
Fig. 4.3 Main effects plot for S/N ratio

Fig. 4.4 Main effect plot for means.

4.3.2 Optimium combination of parameters:

Optimum combination of the parameters was identified by choosing the factor levels which have the highest effect on the S/N ratio. Then expected response corresponding to this factor setting was obtained. The value of tensile strength so obtained was compared with the result of experiment conducted with the same factor levels. Optimum values for process parameters, predicted value of corresponding weld strength in terms of UTS and the experimental result of strength for the same parametric combinations are given in Table 4.8.

Table. 4.8. Optimum parametric combination

Tool rotational speed (RPM)	Tool traversal speed (mm/min)	Axial force (kN)	Tool pin profile	UTS Predicted (MPa)	UTS Experimental (MPa)
1200	180	12.5	Threaded pin	111.5	109.8

4.3.3 Microstructure

Microstructure of the base material showed matrix of uniform eutectic grains of Cu-Al_2 in aluminium solid solution. Some lumps of free copper were also observed. The nature of the precipitates showed that the material is in annealed condition as shown in Fig. 4.5.
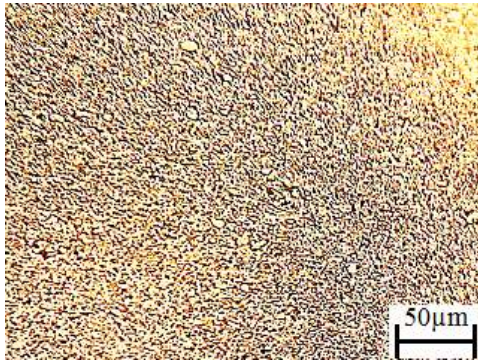
Fig. 4.5 Optical micrograph for base metal
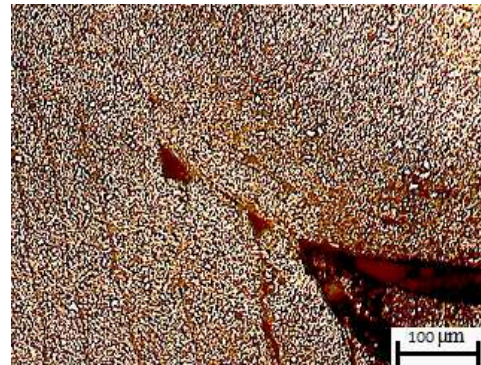
Fig. 4.6 Nugget below the tapered pin ; N = 1200, S = 125, F = 11

It was observed for taperted pin profile and for N = 1200, S = 125, F = 11, the nugget zone below the pin showed the three distct zones tend to separate and giving origin for a tunnel defect as shown in Fig. 4.8. This could be due to inadequate stirring and mixing of material resulted from lower heat input as rteported in some studies [156, 158, 81]. In all these cases a deviation from an optimum cobination of speed and rpm of tool can be seen as a common cause for this defect.
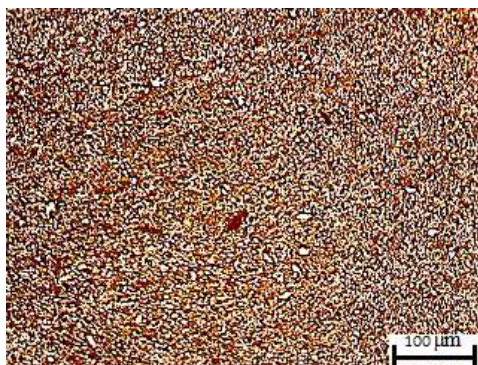
Fig. 4.7 Nugget zone - Tapered pin profile
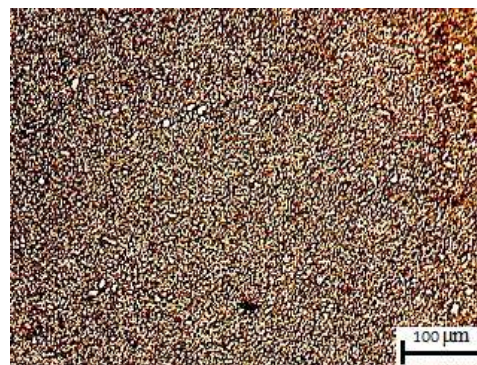
Fig. 4.8 Nugget zone - cylindrical pin
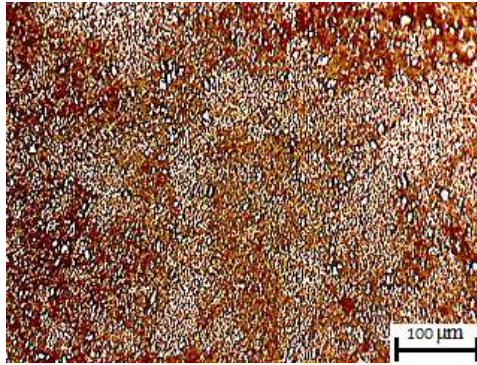
Fig. 4. 9 Nugget zone – Threaded pin profile

The nugget zone exhibited fine recrystallised grains (Figs. 4.7, 4.8 and 4.9). Tapered cylindrical pin caused fine fragmented particles of Al_2Cu in Al solid solution. Nugget zone for cylindrical and threaded pin profile tools showed finer and partially dissolved particles of Al_2Cu (Figs. 4.8 and 4.9). Presence of fine and undissolved precipitates has contributed to the higher tensile strength of the weldments in case of these profiles.

4.4   CONCLUSIONS

The objective of this study was to examine the feasibility of FSW of AA2219 at higher translational speeds and to determine which process parameter has the highest effect on the weld strength. Taguchi method was used to analyze the experimental results to achieve this goal. From the experimental investigation it can be concluded that:

- Friction stir welding of AA 2219 at higher translational speed is feasible by the appropriate selection of process parameters.

- The tool pin profile is the most influential process parameter in deciding the weld strength followed by tool traversal speed, tool rotational speed and axial force.

- From the experimental results an optimum combination of process parameters

has been derived as 1200 rpm for tool rotation, 180 mm/min for tool traversal speed, 12.5 kN for axial force, threaded pin profile for tool and the corresponding tensile strength has been computed as 111.5 N/mm^2. The results have been validated experimentally.

- The structural observations indicated that better strength of the weld while using a threaded pin profile tool was attributed to the presence of fine and undissolved particles of Al$_2$Cu in the nugget zone.

……୪*ଛ……

CHAPTER 5

EFFECT OF PROCESS PARAMETERS ON HIGH SPEED

FSW OF AA 6082 - T6 ALUMINIUM ALLOY

5.1 INTRODUCTION

Selection of the process parameters is very crucial in achieving good weld joint in the FSW. Different materials and joint configurations demand different parametric combinations. Tool rotational speed, tool traversal speed, tool shoulder geometry, pin geometry, axial force and tool tilt angle were identified as the process parameters which have effect on heat generation and material flow. In most of the analysis of the FSW, the selection of the parameters was limited to rotational speed, transversal speed, tool geometry and axial force. The role and effect of tool tilt angle were not clearly established.

It was reported that as the tool was tilted in the trailing direction, tensile strength and microhardness of the weld joint increases for dissimilar joint of aluminium and copper [78]. Researches on the FSW of dissimilar joints of aluminium and steel indicated that an increase in tool tilt angle influences the tensile strength of the welded joint [137]. Tool tilt angle of 1.5^0 or 2^0 was found to provide good results for aluminium welded joints [80, 11]. Certain studies stipulated that the surface defects can be eliminated by effective filling by tilting the tool for the FSW of aluminium alloys [138]. These reported results of the effect of tool tilt angle, were pertaining to lower welding speeds. Ana et al. [82] suggested an optimum condition for FSW of 6082 - T6 alloy with good strength at a speed of 360 mm/min. The study considered welding speed, tool rotating speed, axial force and tool tilt angle as the process parameters; nevertheless the effect of tool tilt on the weld strength was not

established. Rodrigues et al. [139] proposed that FSW at higher traverse speeds were strongly dependent on the base material characteristics and plate thickness. Good welds were up to a speed of 350 mm/min for 6 mm thick base metal. The experimental trials were performed under a wide range of process parameters including tool tilt angle. However, it was not asserted that whether the tool tilt influenced the weld quality.

Extensive researches have established the feasibility of FSW and it is commercially applied for joining aluminium alloys. However, low welding speed impedes the productivity of FSW. Hence the second phase of research in FSW needs exploring the possibility of FSW at higher welding speed.

The researches in FSW were conducted at lower or medium range of welding speeds. It is noteworthy that commercialization of FSW is retarded by lower welding speeds. The issues in high speed welding of FSW were not yet explored adequately. Efforts to identify a combination of parameters which offers welding at higher linear speeds with acceptable quality of welds are in demand by the industry. Reported efforts for the process optimization of FSW of aluminium alloys were performed at lower welding speeds [58, 70]. Table 5.1 illustrates the earlier studies focused on FSW of 6XXX series aluminium alloys to highlight the thickness, welding speed, other process parameters, weld quality and mechanical properties.

Reghubabu et al. [75] examined the effect of tool rotational speed and welding speeds on mechanical and microstructural properties of friction stir welded 6082 - T6 alloy. They carried out the experiments at the highest welding speed of 585 mm/min and suggested an optimum condition for welding with a speed of 170 mm/min.

Table 5.1 Summary of previous studies on FSW of 6XXX series alloys

Base metal	Tool geometry	Process parameters	Recommended parameters	Tensile strength	Ref:
6082 - T6 Thickness 1.5 mm	Shoulder With Scroll, Shallow cavity, Flat face. Cylindrical pin	N - 1810, S - 460	Shoulder with scroll	77%	[140]
6082 - T6 Thickness 6 mm	Shoulder surface with scroll and fillet, fillet and cavity, fillet. Non Threaded pin	N - 1810, S - 460	Shoulder with fillet and cavity	80%	[141]
6082 - T6 Thickness 2 mm	Flat shoulder Cylindrical pin	N - 1500 , S - 400	-	80%	[142]
6082- T6 Thickness 5 mm	Flat shoulder Threaded Pin	N - 215- 1700, S – 115 - 585	-	65%	[77]
6082 - O Thickness 5 mm	Flat shoulder, Taper screw thread pin, Triflute pin	N - 1200, S - 60, 70, 75, 85	Taper screw thread pin, 1200, 70	92%	[76]
6082 - T6 Thickness 6 mm, 4mm	Conical shoulder Cylindrical pin	N - 300,400, 500 S - 200,273, 350 F - 10, 15, 20 Tool tilt- 0, $1^0,2^0,3^0$	400 rpm, 200 m/mn 500 rpm, 350 mm/mn	-	[143]
6061 - T6 Thickness 6.3 mm	Raised and recessed fan , Ramp shoulder Straight cylindrical pin	N - 1200, S - 810	Raised fan shoulder	67%	[144]

Table 5.1 Continued

Base metal	Tool geometry	Process parameters	Recommended parameters	Tensile strength	Ref:
6061 Thickness 6 mm	Flat shoulder Straight, Taper, Threaded, Square, and Triangular pin profiles	N - 1200, S - 75, F - 6,7,8	Square pin profile, 7 kN force	65%	[62]
6082- T651 Thickness 6 mm	Flat shoulder, tapered cylindrical	N - 300,400, 500,600,700 S - 15, 20, 25, 30, 35 F- 4, 5, 6, 7, 8	530 rpm,28mm/mn, 7 kN, pin dia 7mm	84.5%	[144]
AA 6351 Thickness 6 mm	Flat shoulder Square pin	N - 600, 782, 1050, 1317, 1500 S -27, 51, 72, 120, 144 F- 1.2, 2	N- 1050 rpm, 85.2 mm/mn, F 1.45	70%	[146]

N - Rotational speed (rpm), S - Welding speed (mm/min), F - Axial force (kN)

Patil et al. [76] investigated the effect of welding speed and tool pin profile on the weld quality of AA6082 - O aluminium alloy. The study used taper screw thread and tri- flute pin profiles. They proposed a condition for high strength weld in terms of these parameters; however the maximum value of the welding speed was limited to 80 mm/min. Adamowski et al. [77] analysed the effect of welding speed and rotational speed on the FSW of 6082 - T6 alloy with the highest speed of 585mm/min with a threaded pin tool. The defects associated with welds which were made at the higher range of tool linear speeds are caused by insufficient material flow. The void defect formation, widely reported in such cases was resulted from the ineffectiveness of tool action to consolidate the material flow to form a defect free joint. Material flow within the weld depends on the tool interaction with the work material which in turn depends on the tool rotational speed, welding speed and axial force exerted on the tool [147].

The material properties of the parent metal control the tool interaction during the welding process. However, for a given material the tool action is optimized by adjusting the various process parameters. The good weld condition - with sufficient strength and without defect depends on adequate softening and the flow of material during the process. The velocity of the tool traversal plays a crucial role in determining the good weld condition. Certain studies reported the feasibility of FSW at higher welding speeds by providing different shapes for the tool shoulder [148]. But such approaches enhanced the operational cost and complexity of tool fabrication. Hence, it may be appreciable if welds can be made at higher traverse speeds by adjusting the process parameters.

Higher tool travel speeds lessen the heating of base material and hence retard the material flow. The failure to make weld joint is attributed to deceleration of plastic flow of weld metal. A tool tilt accelerates the material stirring and hence the metal

flow. Moreover the pressing of tool shoulder resulting from the tool tilt may enhance the friction and therefore increase the frictional heat.

In this chapter, the results of the experiments to investigate the effect of tool tilt angle on the quality of weld joint and to achieve an optimum combination of process parameters including tool tilt angle for the FSW of AA 6082 T - 6 at highest possible traversal speeds is discussed. Simple tool shapes were adopted with a view of better productivity and reliability. Experimental design and analysis were carried out based on Taguchi method.

5.2   MATERIALS AND EXPERIMENTATION

The base metal used in the experiments was AA 6082 T - 6 aluminum alloy. The mechanical properties of the base metal are summarized in Table. 5.2. The base metal was in rolled condition and in the form of metallic plates of 6 mm thickness. The plates were cut in to 100 mm length and 50 mm wide rectangular pieces to make the butt joints. The faying surfaces were prepared by milling.

Table. 5.2. Mechanical properties of base metal

UTS (MPa)	YS (MPa)	% Elongation(On	Hardness, Hv,
300	245	9	110

The following process parameters were considered for the FSW; tool rotational speed (N), tool traversal speed (S), axial force (F) and tool tilt angle. The various parameters and levels are given in the Table 5.3

Table. 5.3. Process parameters and levels

Factors	Level 1	Level 2
Tool rotational speed,N (rpm)	1080	1260
Tool traversal speed, S (mm/min)	600	700
Vertical force F (kN)	10	15
Tool tilt angle, D (Degree)	0	1.5

The FSW tool was fabricated from H13 tool steel and was oil hardened. The cylindrical pin was provided with right hand threads (Fig. 5.1). Simple tool shoulder with a flat face was provided. Other tool parameters viz. shoulder and pin diameters were kept constant to focus the effect of tool tilt on weld formation. As a thumb rule, the tool pin diameter was suggested as equal to the thickness of the parent metal and the shoulder diameter as three times as that of the pin diameter. Accordingly shoulder diameter and pin diameter were fixed at 18 mm and 6 mm respectively.
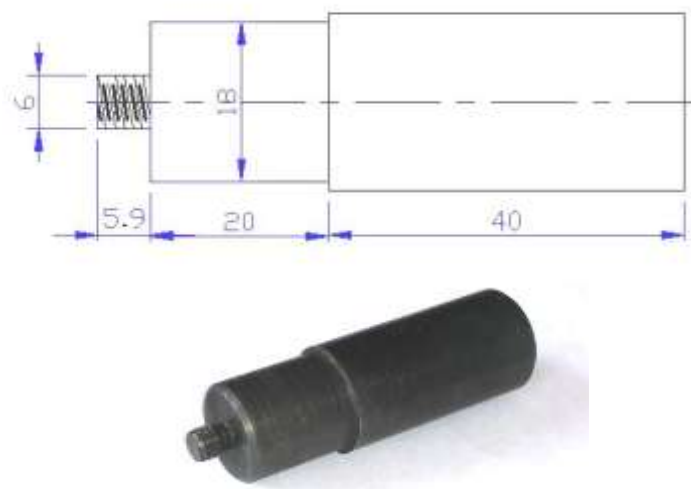
Fig. 5.1. FSW tool.

The experimental matrix was prepared according to the Taguchi L8 orthogonal array. FSW was carried out on a 11kV/440 V (AC) direct FSW machine.

Table 5.4. displays the experimental design matrix which is an orthogonal array with two levels of parameters. The weld samples were subjected to 100% destructive post weld examination. Three specimens were cut transverse to the weld seam from each sample, in a milling machine. Specimens were prepared in conformance with American Society for Testing and Materials (ASTM) standard E8M- 04 for the tensile tests. The average value of the tensile strength was considered for each sample. For micro structural analysis samples were cut thwart wise to the weld line. The specimens were grounded, polished and etched with Keller's reagent. A Trinocular metallurgical microscope (TMM) was used to examine the microstructure of the weld.
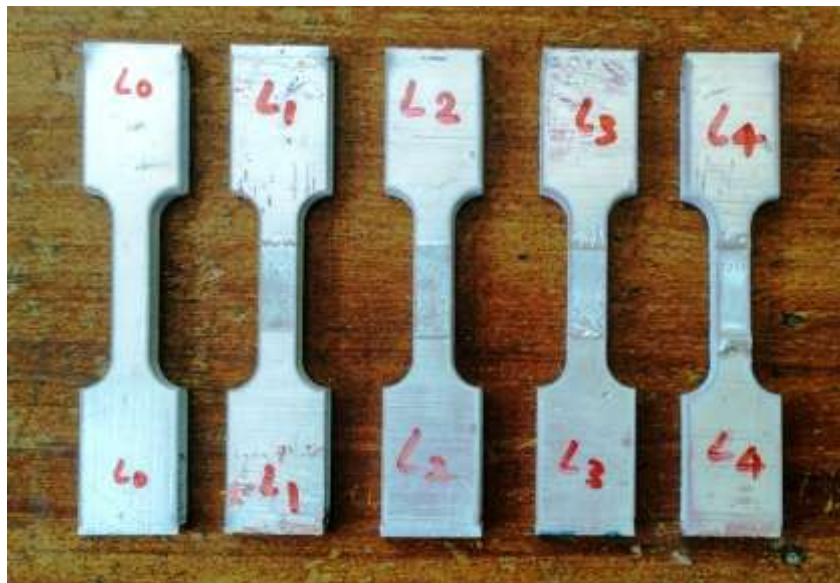
Fig. 5.2. Tensile test specimen.

The disparateness in mechanical properties of the weld joints was examined through hardness measurements across the transverse cross section of the weld. Measurements were taken by a Vicker's hardness tester at 0.5 kgf load with a dwell time of 10 Sec. Readings were taken 1.5 mm below from nugget zone and at an interval of 1 mm.

Table. 5.4 Experimental matrix with parameters and levels.

Trial No	Tool tilt angle(^{0})	S (mm/min)	N (rpm)	F (kN)
1	0	600	1080	10
2	0	600	1260	15
3	0	700	1080	15
4	0	700	1260	10
5	1.5	600	1080	15
6	1.5	600	1260	10
7	1.5	700	1080	10
8	1.5	700	1260	15

5.3   RESULTS AND DISCUSSION

5.3.1 Visual inspection

All welds were visually checked to verify the presence of possible external defects such as flashes and surface tunnel. Welded joints were visibly free of defects and showed smooth surfaces. In the case of weld joints formed at higher temperatures, the weld surface was characterised by the roughness and the presence of small aluminium particles giving an abrasive paper like appearance. On the other hand, cold welds were seen to have smooth surfaces on visual examination. Fig. 5.3 indicated that, in this case the welds were formed at cold weld condition.

Fig. 5.3. FSW joint.

5.3.2 Tensile strength

The variation of ultimate tensile strength (UTS) for the joints fabricated at various parametric levels is displayed in Fig. 5.4. The results show that tensile strength registered a significant descent as the tool was tilted by an angle of 1.5^0. Maximum tensile strength was reported for a tool tilt of 0^0 even at a higher tool travel speed of 600 mm/min. This travel speed is one of the highest values ever reported for AA6082 - T6 alloy for the thickness of 6 mm.
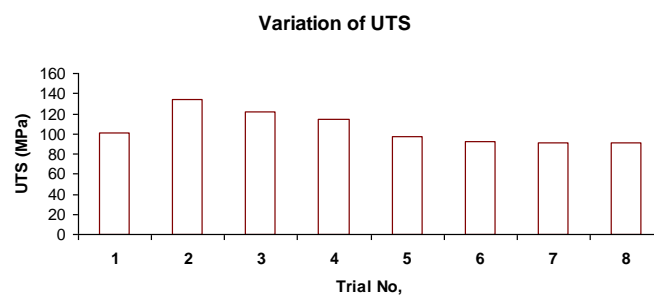
Fig. 5.4 Variation of ultimate tensile strength.

The effect of process parameters on the strength of the weld joints were analysed based on the criterion of 'larger the better' for predicting the process combination for maximum tensile strength. The response tables for 'signal to noise' (S/N) ratio and means illustrated the ranks of each factor based on the delta statistics, which compared the relative magnitudes of the effect on the output characteristic.

Optimum combination of the parameters was identified by choosing the factor levels which have the highest effect on the S/N ratio. Afterwards expected response corresponding to this factor setting was obtained. The effect of process parameters on the strength and of the weld joints were summarised as response tables. From the mean plots of S/N ratio and the mean responses the optimum parametric levels were identified. The response tables for S/N ratio are given in the Tables 5.5 and 5.6.

Table. 5.5. Response table for signal to noise ratios

Level	TILT	S	N	F
1	41.37	40.43	40.19	39.94
2	39.36	40.31	40.55	40.80
Delta	2.01	0.12	0.36	0.85
Rank	1	4	3	2

Table. 5.6. Response table for means

Level	TILT	S	N	F
1	117.77	106.20	102.79	99.73
2	92.97	104.54	107.95	111.02
Delta	24.80	1.66	5.16	11.30
Rank	1	4	3	2

From Tables 5.5 and 5.6, it can be inferred that the tool tilt angle has the highest effect on the tensile strength followed by force, tool rotational speed and welding speed. The effect of parameters is illustrated by the main effect plots as shown in Fig. 5.5.

Based on the response tables optimum values for process parameters were suggested as 0^0 tool tilt angle, 600 mm/min travel speed, 1260 rpm and a vertical force of 15 kN.
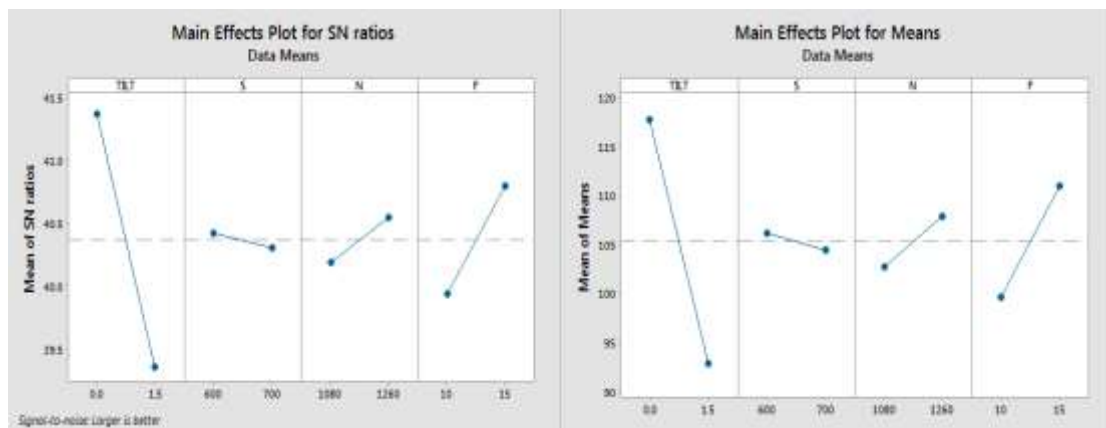
Fig. 5.5. Main effect plots for SN ratio and means

5.3.3 Microhardness

The variation in microhardness for two cases; one with a tilt angle of 0^0, 700 mm/min, 1080 rpm and other with 1.5^0, 600 mm/min, 1080 rpm are shown in Fig. 5.6 as a representative example. The microhardness distribution exemplified the effect of tool tilt angle distinctively. Welds obtained with 1.5^0 tilt angles showed lower values for hardness. Hardness shows a higher value in the advancing side as reported in various studies [149, 150]. It is observed that micro hardness of the welds is about 70 leading to a softening up to 63% relative to the base-material hardness in case of 0^0 tool tilt angle, whereas the microstructure hardness value is reduced to 45 in case of 1.5^0 tool tilt angle.
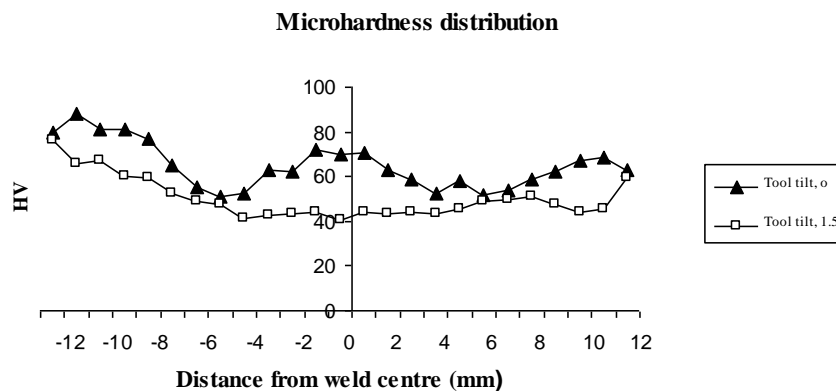
Fig. 5.6 Variation in microhardness

Variation in ultimate tensile strength and micro hardness characterizes the change in mechanical properties of the welds with variation in process parameters. Tensile strength recorded a notable descent for welds produced with tool tilted at an angle of 1.5^0. Similar result was reported for the FSW of polyethylene [151]. However the general observation is that a tool tilt favors higher strength for FSW joints of aluminium alloys. Micro structural characterization of friction stir welded steel joints concluded that tool tilt is the most influential parameter for the tensile strength of the weld joints and a tool tilt enhances the tensile strength of the welds [152].

Experimental analyses have been reported endorsing the postulate that a tool tilt favors mixing and periodical filling of material in the weld joint and the confinement of extruded material in the weld line by the tool shoulder [153]. But the fall in the weld strength registered in this experiment indicated that a tilted tool at higher speeds may not be effective in achieving confinement and mixing of extruded material. The variation in UTS and microhardness is examined based on the microstructure, in the later part of this chapter.

5.3.4   Microstructure

Fig. 5.7. Macrostructure of weld generated at 0^0 tool tilt angle, 600 mm/min, 1260 rpm
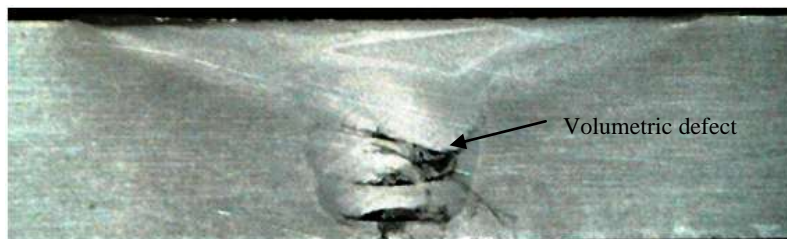
Fig. 5.8 Macrostructure of weld generated at 1.5^0 tool tilt angle, 700 mm/min, 1260 rpm
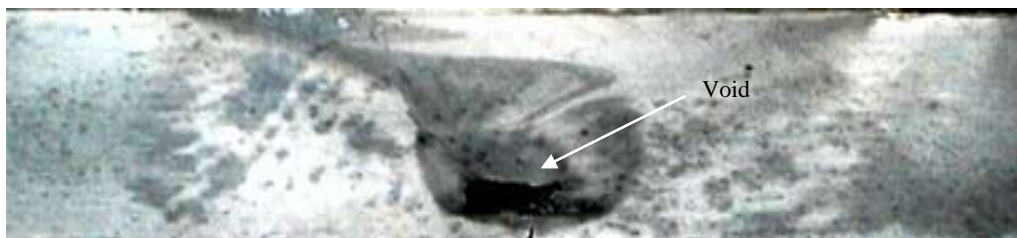
Fig. 5.9 : Macrostructure of weld generated at 1.5^0 tool tilt angle, 700 mm/min, 1080 rpm

The microstructure indicated that the base metal was in solution treated and precipitation hardened condition. Presence of fine uniform precipitated Mg_2Si eutectic particles in primary aluminium solid solution, were evident as seen in Fig. 5.10. The Grain orientation shows that the material was subjected to rolling process. The grains orientation could be seen along the direction with parallel lines. The micrograph also shows some insoluble inter metallic compound Al_6 (Fe Mn) in base metal matrix.

As a representative example the microstructure of the different zones of the weld generated with 0^0 and 1.5^0 tool tilt are illustrated.

Fig. 5.10 Microstructure of the base metal.
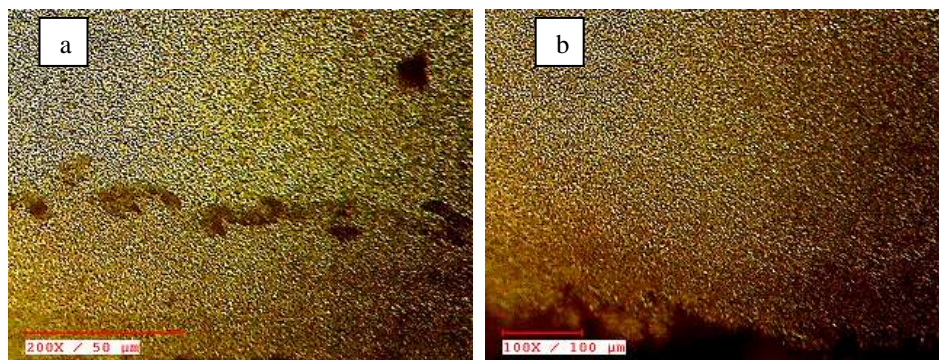
Fig. 5.11.   Shoulder zone: (a) 0^0 tilt angle (b) 1.5^0 tilt angle.

In both the cases fragmentation of the eutectic particles occurred at the shoulder zone (SZ) due to the pressure of the rotating shoulder. The insoluble inter metallic compounds have formed a cluster at the shoulder zone as seen in Fig. 5.11. (a) & (b).
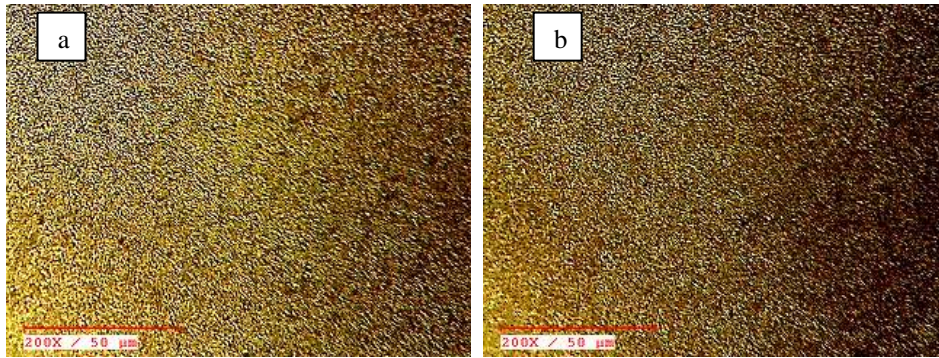
Fig. 5.12. Microstructure of the NZ (a) 0 tilt angle (b) 1.5 tilt angle

The nugget zones (NZ) of both cases show no difference in optical micrograph. The nugget zones show fragmented particles of eutectic Mg_2Si which have undergone dynamic recrystallization as can be seen in Fig. 5.12. (a) & (b). The evidence of recrystallization is seen as due to the absence of grain orientation, which was present in the parent metal. The stirring stress and the thermal effect would have caused the dissolution and rapid re-precipitation of the eutectic particles.

The microstructure reveals no significant difference for various welds generated under various parameters. Hence it is logical to assume that heat input was comparable for all the welds. The defect formation in certain welds may therefore be attributed to the insufficiency in material flow. The macrostructure of the welds under various parameters supports this observation.

Joining mechanism in FSW can be comprehended to extrusion and forging of materials. As the pin rotates the material got softened due to frictional heating and extruded around the pin and subsequently forged by the shoulder action. The appropriate combination of the rotational and transversal speed is to be achieved for the effectiveness of this action. Heat input is critical to soften the material to facilitate proper mixing of the extruded material. Low heat input was reported to be the main cause of tunnel defect or kissing bond [154].

A steady and continuous FW is performed under partial sticky and sliding, interface contact conditions except for the tool plunge phase [155]. Nevertheless, at higher speed, sticky contact conditions dominate the process. Hence at higher speeds tool torque will be high. Various studies have suggested that, except in the cases of overheating, tool torque has a strong inverse linear relation with nugget hardness, yield strength and ultimate tensile strength [156]. As the welding speed increases, heat input decreases, power consumed increases, because of the reduced time for material deformation and processing. Moreover, at higher welding speeds, the material ahead of the pin gets little time to preheat the material in the surrounding and this retards the material softening for the welding process, which requires higher tool torque. In such a condition, the heat input relies largely on the plastic deformation of the surrounding bulk material. In FSW, the input power is converted into plastic deformation energy, which is partially stored in the microstructure and partially converted into heat. The results of numerical simulations reveal that the heat energy so obtained from plastic deformation varies from 2 to 20% [157]. These observations substantiate low heat input at higher welding speeds. The general trend of low UTS in all welds was indicative of low heat input in the selected range of welding speed.

Macrostructure of the weld generated at 0^0 tilt angle is shown in Fig. 5.7. The macrostructure indicates that the weld obtained was free from major defects. The NZ is relatively larger than other types of welds. It was reported that in FSW, the rotating pin deforms the material immediately in the vicinity of the tool surface and is referred as the rotating shear material (RSM). When a threaded pin profile is provided with the tool, the heavily deformed material from the tool pin thread surface drags the surrounding material by the pin action, and this surrounding flow, RSM and the shoulder driven material periodically fills the cavity formed by the tool advancement

to avoid the formation of volumetric defects [158]. Larger NZ indicates sufficient rounding flow and shoulder driven flow. Hence the size of the NZ is emblematic of better material flow and corresponding mechanical properties. The material flow in the macrostructure indicated onion ring formation. The better mechanical properties of this weld may be attributed to the better material transfer and consolidation when compared to other welds.

Macrostructure of the welds generated at 1.5^0 tool tilt angle shows insufficient material flow leading to defects of inadequate filling seen as in Figs. 5.8 & 5.9. Shoulder driven material must be adequately merged with the pin driven material to avoid defect formation [159]. Temperature and axial force play a significant role in this mechanism of material flow. Since the tool tilt influences the shoulder driven material flow and hydrostatic pressure, it may be logical to conclude that tilt angle of the tool, at the higher traversal speed adversely affects the material flow and merging of layered material during welding and causes defect formation. FSW of AA 6082 is reportedly sensitive to the shoulder driven material flow [160]. When tool is tilted, the vertical force acting on the weld line is altered. This may affect the material drawn by the shoulder and heat generated. This effect may assume relevance at higher speeds. This may be a possible reason for the generation of defects when the tool is tilted as shown in the macrograph in Fig. 5.8.

The shoulder action generates most of the heat in FSW and the axial pressure exerted by the shoulder on plasticized material influences the material flow as well. The pin action controls the material consolidation and periodic filling of the joint by transferring material. In the advancing side the material is pushed downwards and in the retreating side the material is moved upwards [161]. Material ahead of the pin is moved upwards and the tool threads pulls the material downwards [162]. The tool tilt

favours the upward movement of the material ahead of the pin. However the consolidation through periodic transfer of the material is influenced by other parameters viz. axial force, rotational speed and welding speed. Even if the modes of shoulder driven flow and pin driven flow are unaffected, the individual flow volume and hence the total stir zone is a function of welding speed [163]. Hence the material flow can presumably be affected more, by the welding speed.

Material flow of the tool action in FSW is complex. Guerra et al. [164] suggested a division of the material processing zone in to rotation zone and transition zone. Rotation zone is located immediately in the tool pin surface where the material flow is a combination of transverse, longitudinal and angular with respect to the tool axis. The shear layer of material located between the rotational zone and material matrix was identified as the transition zone. The overall friction stir volume is a function of heat input.

In FSW the weld formation proceeds through a time delay in material filling. Effective combination of parameters overshadows this time delay by filling the material cavities periodically to ensure a defect free weld. The formation of tunnel defects has resulted from this time delay when the cavities are not compensated by the effective material flow. Based on the material flow, weld zone can be divided into shoulder affected zone (SAZ), pin affected zone (PAZ), and weld bottom zone (WBZ) (Fig. 5.13). Time delay for material filling in the PAZ is viewed as the source of tunnel defect. If the material flow from retreating side to the advancing side is not sufficient, and, or the axial force is not sufficient, then the downward material flow in the SAZ is reduced and as a result, defects are generated. It was reported that in the SAZ, the material flow is continuous because the material in contact with the shoulder rotates with the same velocity as that of the tool. In the PAZ, the material flows in the

direction of tool rotation and also in the vertically downward direction. Hence, in the PAZ the material flow is non-continuous. The flow velocity of material in the WBZ which is located between the tool tip and the bottom surface of the parent metal is relatively small. The filling of material in the WBZ occurs during the linear movement of the tool. At any instant, at any point on the weld line, WBZ is filled when tool passes that point. Therefore in the WBZ, the weld formation required more time [165].
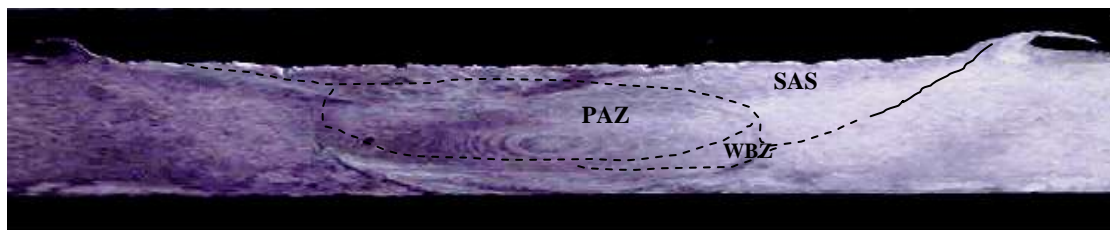
Fig. 5.13. Weld zones based on material flow.

The time delay in material flow forms different deposition patterns in the weld nugget zone. In PAZ material is driven by the pin rotation to the trailing side and the cavities are filled periodically. At higher welding speeds, the material in the PAZ will not get enough time to rotate with the pin for one whole round. So the material flow may be terminated at some point leaving a gap between the PAZ and shearing edge in the material matrix. This delay in material flow leads to the volumetric defects [166].

Macrostructure of the weld shown in Fig. 5.9 indicates a considerably large area of void at the bottom of the pin. Insufficient heat input leading to a cold weld condition has resulted in such defects [167]. Higher welding speed might have stimulated this condition and conversion of the void in to a tunnel or worm hole defect. In FSW pin slithers the material around it and in addition the material flows vertically in almost circular pattern in layers [168]. Fig. 5.8 indicates ineffective mixing of material in different tiers of the process. Ineffective material flow around the pin and lack of

sufficient forging action by the shoulder may be the reason behind it. The tool tilt at higher speeds might not be able to use the geometrical features of the threaded pin in achieving the appropriate material flow. It might have lead to the internal folding defects as shown in Fig. 5.8.

The macrostructure of the welds prepared with a tool tilt explain the possible effect of tool tilt on defect formation. Zhang et al. [169] proposed a criterion for the formation of defect free welds in FSW, which was represented as follows.

$$\frac{P.\omega}{v} \geq \frac{V}{k(r_{sh} - r_p)} \tag{5.1}$$

where P is the pressure, ω, and v are the rotary and linear speeds of the tool respectively, V is the volume of the defect, r_{sh}, r_p are the radii of the tool and k is the constant of proportionality. According to this criterion, they suggested that the pressure should be larger than a limiting value. It can be observed that tool tilt reduces the pressure vertically applied on the weld surface. From the relation 5.1, According to the above relation it can be seen that the low pressure increases the volume of defect, especially at the higher range of the welding speeds. Hence, it can be concluded that tool tilt at higher welding speeds adversely affect the weld quality, which substantiates the experimental results of this work.

The microhardness values show a clear distinction with the change in tool tilt as shown in Fig. 5.6. But NZs in these cases appear with little difference, even though the distribution of hardening precipitates is not clear. In FSW, dissolution of hardening precipitates lessens the microhardness. The variation in microhardness for the weld with zero tool tilt angle submitted in the present study is comparable with the available results in various studies. The microhardness behavior is underlined by the presence of dynamically recrystallised precipitates as shown in the NZ microstructure as in the Fig. 5.12. But for the weld produced by tilting the tool to 1.5^0 the micro

hardness values were dramatically reduced even though the rotational speed remained the same. The tool tilt angle is reported to be an influential parameter along with rotational speed, for the heat input. Hence it can be concluded that at higher tilt angle the heat input may not be optimum to ensure the re precipitation of the strengthening particles, which causes the fall in hardness.

5.4. CONCLUSIONS

The effect of tool tilt angle on the high speed FSW of 6082 - T6 aluminium alloy was studied along with other process parameters and an optimum combination of process parameters were suggested. The experimental results indicated that:

- Tool tilt angle is the most influential parameter which affects the weld strength and it was found that tool tilt angle adversely affects the weld strength at higher speeds of tool travel.

- The welds performed at higher speeds are visually defect free, but it was observed that the weld strength is relatively low, especially, with a tool tilt.

- Microhardness of the welds was found to be lowered with the tool tilt.

- The UTS values and macrostructure hints higher tool torque conditions for the weld. The macrostructure of the weld formed with a tool tilt indicates that the material flow was not synchronized and periodic in nature.

- With a tool tilt, weld pressure is reduced and the reduced pressure is possibly below the limiting value which is required to avoid volumetric defects. The reduced pressure at higher welding speed might have affected the material flow and caused the defect formation.

……ഛ*ര……

CHAPTER 6

EFFECT OF PROCESS PARAMETERS ON MICROSTRUCTURAL AND MECHANICAL PROPERTIES OF FRICTION STIR WELDED AA 2219 ALUMINIUM ALLOYS

6.1 INTRODUCTION

In FSW, the friction between the plates and tool increases the temperature and generates the metal flow. The frictional heat together with the heat of plastic deformation softens the material at the joint. The plasticized material is extruded by the tool action to form   the joint [170]. Metallic joint is achieved through viscoplastic deformation and consequent heat dissipation occurring much below the melting point of the base metal. The heating cycle below the melting point results in complex microstructural changes in the base metal and reportedly affects the grain refinement and orientation [28]. For precipitation hardened alloys, the dissolution, re precipitation and/or agglomeration of the strengthening particles during hot working dominates the properties of the base metal. However, studies in this direction are scarcely reported in the case of FSW.

Malarvizhi et al. [171] promulgated that during fusion welding, strengthening precipitates dissolved in the metal matrix and the material behaved like cast metal with solute segregate and columnar grains. Various studies suggested that the size and distribution of Al_2Cu particles play a major role in deciding the tensile properties and hardness of the heat treated alloys [172, 173]. Attallah and Salem [28] observed that the static properties of friction stir welded AA 2219 is dependent on the distribution of strengthening precipitates rather than the grain size. These strengthening precipitates were formed due to the solution treatment and subsequent artificial aging. In FSW there is no melting and hence, theoretically no dissolution of precipitates

occurs in the matrix, but it was reported by Cao and Kou [80] that during FSW the Al$_2$Cu particles showed clear evidence of agglomeration. Biswal et al. [174] examined the effect of varying tool geometry on the FSW of Al - Si alloy. They reported that the grain size was found to be maximum in the nugget zone for the joints made by tapered cylindrical pin profile. These observations were significant in the investigation of effect of process parameters on the strength of FSW. Nonetheless, any influence of the process parameters on the alteration of strengthening precipitates has not been clearly established in these studies. Moreover, these reports have not explicitly correlated the effect of process parameters on the microstructure of the welds as well.

The effect of process parameters on the weld quality and strength in FSW have been extensively studied by many researchers [175 - 177]. These experimental studies or simulation analyses were concentrated on the optimum parametric combination for desirable results for welds, or figuring out the most influential parameter for obtaining good welds. But studies on the effect of parameters on correlating the weld quality with the microstructural changes were very little. Age hardened or precipitation hardened alloys are highly sensitive to the heating cycle in case of FSW. Perhaps, the behavior or changes in the strengthening precipitates is the most crucial factor in determining the weld strength, in case of FSW of these alloys. In this context it can be assumed that the change in micro structural characteristics and thereby the mechanical properties in FSW, under varying process parameters needs further study.

In this chapter efforts to correlate the effect of most influential parameter on the strength of friction stir welds, with the microstructural changes is discussed. Experiments and analysis were conducted with AA 2219 as a representative alloy, for precipitation hardened or age hardened group of aluminium alloys.

6.2 MATERIALS AND METHODS

AA 2219 is an Al - Cu - Mn ternary alloy which can be approximated to Al - Cu binary alloy for analysis (Fig. 6.4). AA 2219 belongs to the group of heat treatable alloys which increases their strength by heat treatment. It assumes higher strength on heat treatment by the presence of fine precipitates, consisting mainly of Al_2Cu particles [178].

The base metal used in the experiments was AA 2219, in annealed condition. The chemical composition and mechanical properties of base metal are summarized in Tables 6.1 and 6.2.

Table.6.1. Chemical composition (wt. %) of base metal

Cu	Mn	Zr	V	Ti	Fe	Si	Zn	Mg	Al
6.2	0.3	0.11	0.09	0.06	0.16	0.05	0.01	0.01	93.01

Table. 6.2. Mechanical properties of base metal

UTS (MPa)	YS (MPa)	% Elongation(on 50 mm GL)
151.2	68	15

The metallic plates of 6 mm thickness were cut into 150 mm x 50 mm rectangular pieces. The parameters considered were tool rotational speed, tool traversal speed, axial force and tool pin profile. The various parametric levels and the experimental matrix are given in Tables 6.3 and 6.4.

Table.6.3. Parameters and levels used in the experiments

Factors	Level 1	Level 2	Level 3
Tool rotational speed, N (rpm)	1200	1400	1600
Tool traversal speed, S (mm/min)	125	151	180
Vertical force, F (kN)	11	12.5	14.5
Tool pin profile, D	TC	SC	THC

Table 6.4 Experimental matrix

Expt. No.	N	S	F	D
1	1200	125	11.0	1
2	1200	151	12.5	2
3	1200	180	14.5	3
4	1400	125	12.5	3
5	1400	151	14.5	1
6	1400	180	11.0	2
7	1600	125	14.5	2
8	1600	151	11.0	3
9	1600	180	12.5	1

Three types of pin profiles viz. straight cylindrical (SC), tapered cylindrical (TC) and threaded cylindrical (THC) were used for the experiments. The three types of tools used for the experiments are shown in Fig. 6.1.

Fig.6.1. FSW tools

Tools were fabricated from H13 tool steel and subjected to heat treatment. They were flame hardened. As per the thumb rule available from the literatures tool pin diameter was selected as equal to the base plate thickness and the shoulder diameter was fixed as three times as that of the pin diameter. Accordingly, tool shoulder diameters were kept constant at 18 mm and pin diameters were fixed at 6 mm. Pin length was fixed at 5.8 mm to ensure sufficient plunge depth and for preventing any damage occurring to the pin by striking on the backing plate. The experiments were carried out on a 11kV/440 V (AC) direct FSW machine.

Tensile test specimens were cut perpendicular to the weld seam from the welded pieces in a milling machine, and prepared in accordance with ASTM E8M - 04 standards.

Microhardness values were measured employing a 402 - MVD vickers hardness testing machine across the weld with a load of 0.5 kg. Micro structural analysis was carried out using a trinocular metallurgical microscope (TMM) and specimen were etched with Keller's reagent.

The combinations of specific precipitates were identified by scanning electron microscope (SEM) and energy dispersive spectroscopy (EDS). SU 6600 variable

pressure field emission scanning electron microscope was used for the examination. Table 6.5 shows the technical details of the SEM.

Table 6.5 Technical features of SEM

Make	Hitachi SU 6600 FESEM
Electron gun	Tungsten schottky emission electron source
Resolution	1.2 nm/30 kV, 3.0 nm/1 kV.
Probe current	1 pA – 200 nA
Specimen size	150 mm x 40 mm
Magnification	500,000 x

6.3   RESULTS AND DISCUSSION

The thermomechanical process in FSW results in different microstructure in various parts of the weld. Typical macroscopic zones pertaining to the friction stir weld are shown in Fig. 6.2.
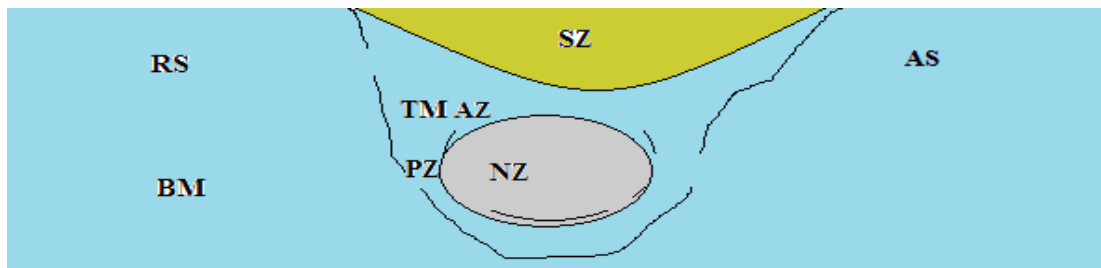
Fig. 6.2 :   Typical macroscopic zones associated with FSW
BM - Base metal; **RS** - Retreating side; **SZ** - Shoulder zone; **TMAZ** - Thermo mechanically affected zone; **PZ** - Pin driven zone; **NZ** - Nugget zone; **AS** - Advancing side

As the rotating tool traverses along the weld line forging action of the tool shoulder triggers softened material flow in the shoulder zone (SZ) continuously in downward direction. The pin initiates the material movement in the pin driven zone (PZ), from retreating side (RS) to advancing side (AS). Accordingly, the material in the PZ will

be subjected to the maximum strain. The strain rate depends upon the process parameters and pin geometry [179].
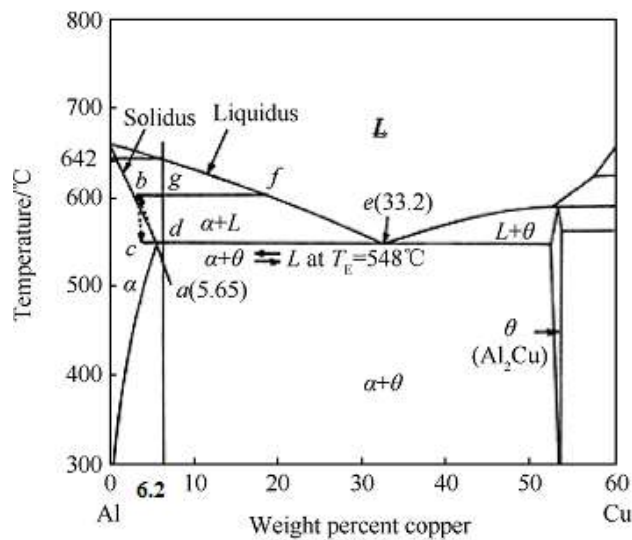
Fig. 6.3. Al - Cu phase diagram [75]

Aluminium rich portion of the phase diagram is shown in Fig. 6.3. The concentration of Cu in AA 2219 alloy is 6.2%, which exceeds the maximum solubility of Cu in aluminium, therefore the base material can be considered to have α, aluminium matrix and additional θ particles which are identified as Al_2Cu [180]. The chemical composition of the constituent elements in the alloy AA2219 allows approximating it as a binary alloy of 6.2 weight percent of Cu.

Optical micrograph of the base material showed matrix of uniform eutectic grains of intermetallic particles in aluminium solid solution. Some lumps of free copper were also observed (Fig. 6.4.a). Nature of the precipitates indicated that the material was in annealed condition.
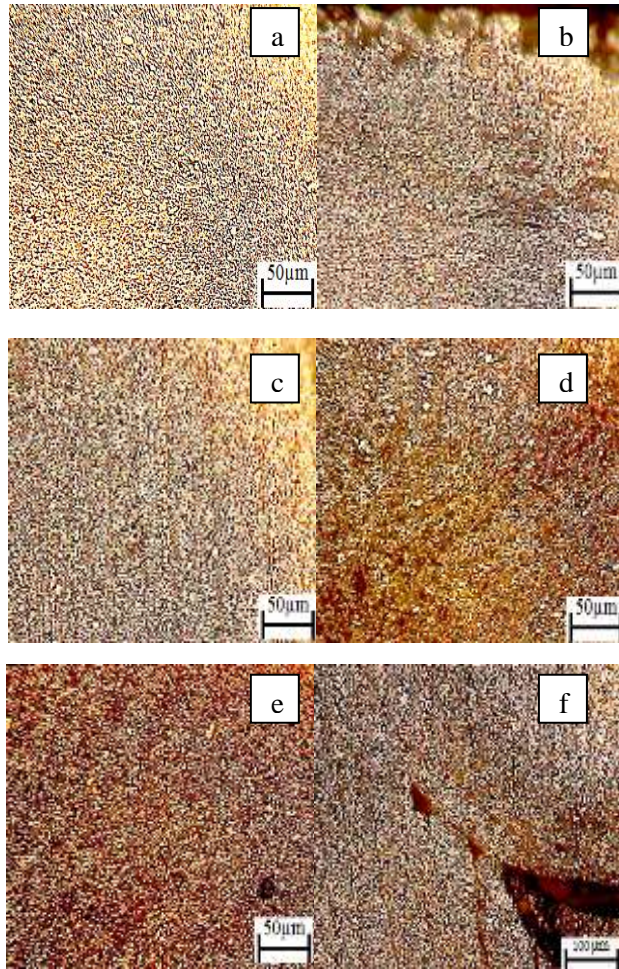
Fig. 6.4 : Optical micrograph of different weld zones.
(a) Base metal (b) SZ- Taper pin profile. (c)
Interface zone, Taper pin profile. (d)
Interface zone, Threaded pin profile. (e)
Interface zone, cylindrical pin profile. (f)
Nugget below the tapered pin

In general, the SZ depicted presence of fragmented particles of Al_2Cu with some
presence of free copper as shown in Fig. 6.4 (b). This is indicative of the fact that the
heat input was low; otherwise more amount of copper would have been dissolved.
The interface zone of TMAZ and NZ showed grains oriented by the effect of stress
and heat. Grains appeared to be finer due to fragmentation. In contrast to taper pin
profile, interface region of TMAZ and NZ of the welds, generated by threaded and
straight cylindrical profile showed disoriented grains even when grains appeared to be
finer due to fragmentation. It was observed for taperted pin profile and for N = 1200
rpm, S = 125 mm/min, F = 11 kN, the nugget zone below the pin showed the three

distict zones which tend to separate and giving origin for a tunnel defect as shown in Fig. 6.4(f). This is due to inadequate stirring and mixing of material resulted from lower heat input. Adamowski and Szkodo, Lakshminarayanan et al., and Reghubabu et al. [135, 181, 75] have reported similar cases for different pin profiles and for different alloys. In all these cases a deviation from an optimum combination of speed and rpm of tool was the reason for this defect.

FSW of high strength aluminium alloys showed soluble and insoluble second phase particles [182]. In case of AA 2219 alloys, Al_2Cu precipitates were identified as the second phase particles in the nugget zone [183]. It was observed that FSW of aluminium alloys with low heat input resulted in refinement of grain structure along with the dissolution of the precipitates [184].

The types of pin profiles have influenced the nugget microstructure significantly. It was reported that the presence of undissolved strengthening precipitates contribute significantly to the ultimate tensile strength of friction stir welded joints of precipitation hardened aluminium alloys [185]. In case of AA 2219 alloy, as the temperature increases, the strengthening precipitates may re-enter the solid solution lowering the hardness. But during the cooling part of the welding thermal cycle, some of them may re precipitate, favouring the total hardness of the weld [186].

In the experiments, the NZs exhibited fine recrystallised grains. Tapered cylindrical pin caused fine fragmented particles of Al_2Cu in Al solid solution. NZ for tapered and threaded pin profile tools showed finer and partially dissolved particles of Al_2Cu. The NZ of the threaded pin profile was characterised by boundary disorientation of grains and finer grains compared to other pin profiles as shown by the optical micrograph in Fig. 6.5 and SEM images in Fig. 6.6.
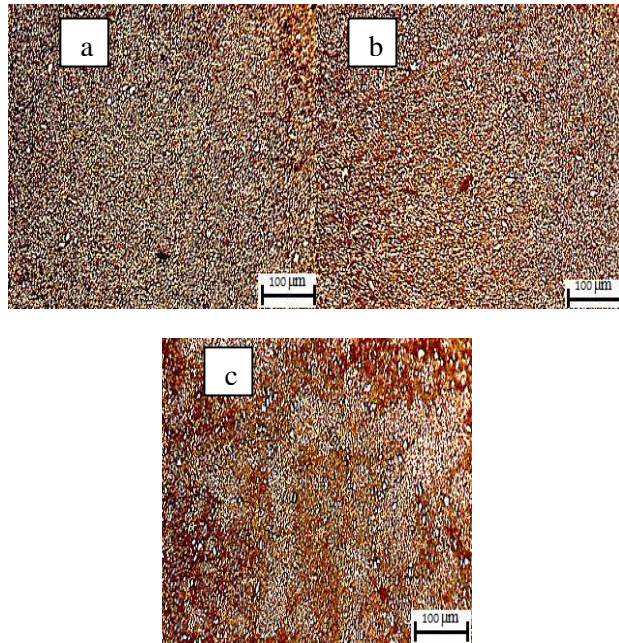
Fig. 6.5 :   Optical micrograph of NZ for different pin profiles.
(a) Tapered pin. (b) Cylindrical pin. (c) Threaded pin.

EDS analysis indicated that Cu and Al are the major components of the intermetallic compounds. The inter-metallic particles were identified as Al_2Cu by EDS spectra as shown in Fig. 6.7. For the straight cylindrical and threaded pin profiles the microstructure indicated that some re precipitation could be expected.
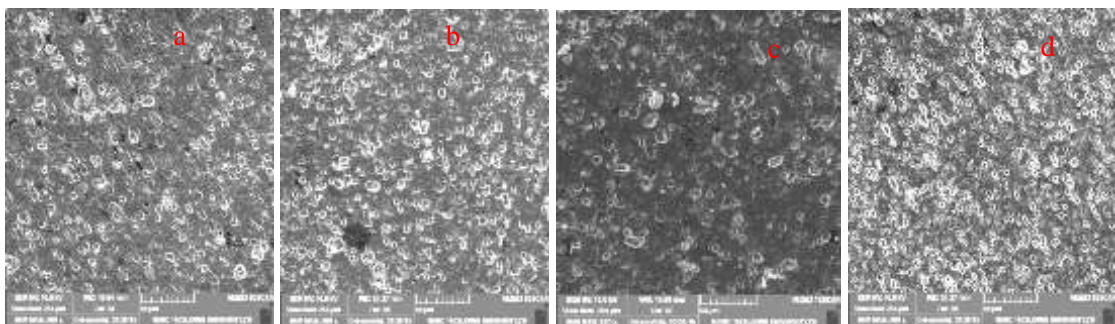
Fig. 6.6 : SEM images of NZ for different pin profiles:
a. Cylindrical. b. Taper. c. Threaded. d. Base metal
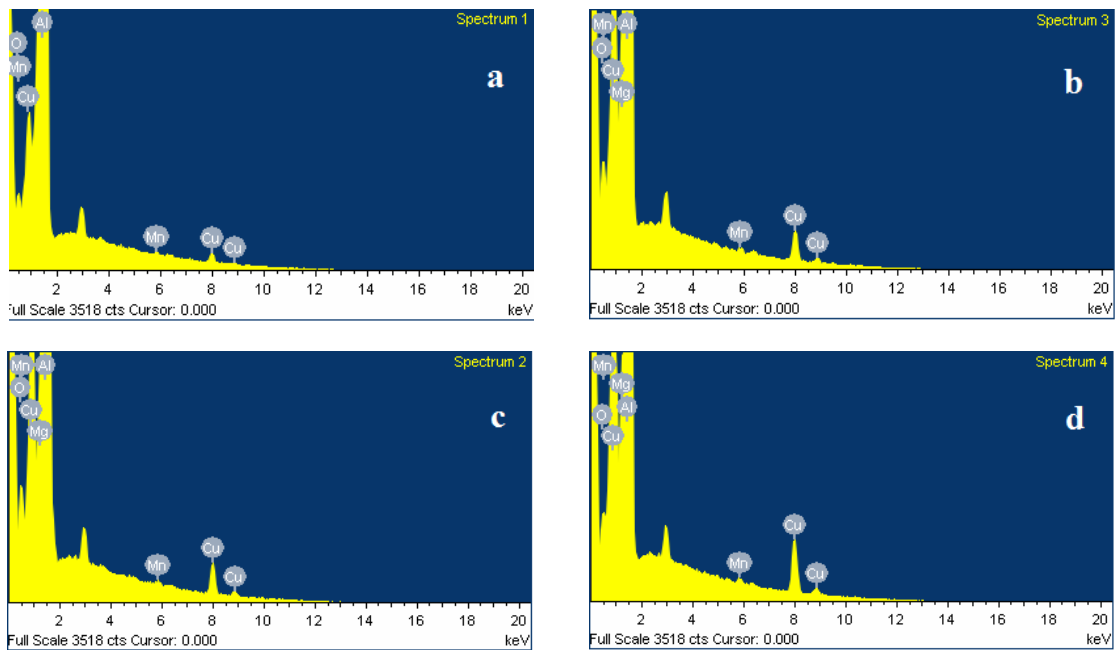
Fig. 6.7 : EDS element spectrum of the weld nugget.
(a) Base metal. (b) Taper pin. (c) Cylindrical pin.(d)
Threaded pin.

The EDS spectra indicated that presence of θ particles were more for threaded pin

profiles, according to Fig. 6.7 and Table. 6.6.

Table 6.6. EDS results: Elemental analysis

Pin Profile	Element	Weight%	Atomic%
Cylindrical pin	Al	86.92	86.53
	Cu	6.34	2.68
Taper pin	Al	87.63	87.91
	Cu	6.49	2.77
Threaded	Al	84.35	87.06
	Cu	10.47	4.59

Fig. 6.8 illustrates the variation in ultimate tensile strength (UTS) for various pin

profiles. The analysis of results showed that the pin profile is the most influential

parameter determining the tensile strength. The maximum tensile strength was

recorded for the welds generated by the threaded pin profile.
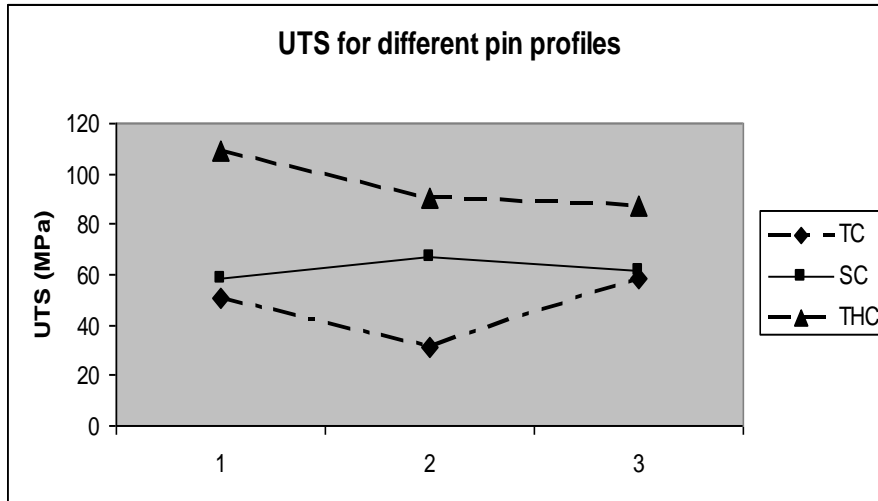
Fig. 6. 8. Variation of UTS for different pin profiles

The microhardness variations across the various regions of the welded plates are shown in Fig. 6.9. The NZ recorded highest hardness for threaded and cylindrical pin profiles. Weld produced using the threaded pin profile exhibited maximum hardness. Hardness variation registered higher values for the advancing side as reported elsewhere [187]. The variation in the microhardness values is expressive of the micro-structural changes. For various pin profiles higher values were registered for hardness in the stir zone than that of TMAZ. Generally, in case of FSW of aluminium alloys strengthening particles were reported to be dissolved by the stirring effect of pin and the frictional heat [188]. But due to the higher strain rate, re-precipitation of the strengthening particles may occur in the case of AA2219 alloy [189]. The higher values of microhardness in the stir zone are attributed to the re-precipitation of the strengthening particles.
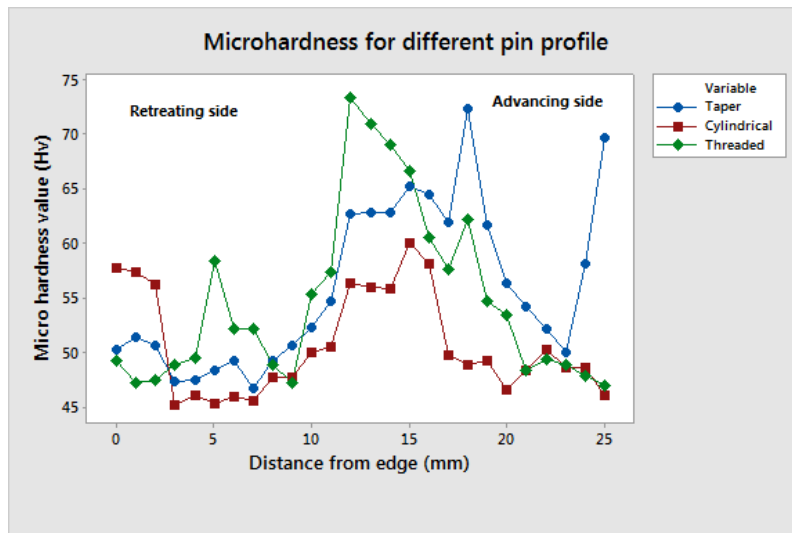
Fig.6.9. Microhardness map for different pin profile

Microhardness variation shows that hardness assumes the highest value for the threaded pin profile. Both grain size and presence of θ particles contributed to the strength of the weld joints. Grain size is determined by the frictional heat generated and the cooling rate. But here tool pin profiles did not have any flat faces and hence the frictional heat generated was not much influenced by the pin profile. The microstructures of the shoulder zones were almost identical as shown in the optical micrographs which indicated nearly identical heat generation. Presence of fine and undissolved precipitates would have contributed to the higher strength and hardness, in case of the welds produced using threaded pin profiles.

6.4   CONCLUSIONS

AA 2219 alloy is a precipitation hardened alloy. Hence the mechanical properties of AA 2219 alloys depend on the distribution and concentration of the strengthening particles. The material phase conditions of AA 2219 result in the presence of α, aluminium matrix and θ particles which are identified as Al_2Cu. Being a thermo - mechanical process FSW brings about significant changes in the presence of Al_2Cu particles. Therefore the effect of process parameters on the mechanical properties of welds in FSW of AA 2219 alloy needs to be studied based on the microstructural

changes containing the dissolution and the precipitation of the θ particles. In FSW tool pin profile takes the major part in heat generation and material flow.

The effect of tool pin profile on the mechanical properties of FSW in relation with the microstructural changes were studied by using three types of simple tool pin profiles. The weld NZs were closely examined, distribution and behavior of strengthening precipitates were identified.

Tensile properties were evaluated and microstructural changes were examined for the behavioral characteristics of the strengthening precipitates. The results of the study can be summarized as follows.

- Welds generated by the threaded pin profile exhibited maximum tensile strength and microhardness.

- Distribution of strengthening precipitates indicated that reprecipitation of the Al_2Cu particles occurred on cooling of the welds.

- SEM and EDS analysis indicated that the precipitation of the Al_2Cu particles was more for the welds generated by the threaded pin profile.

- Presence of fine and undissolved precipitates has contributed to the higher strength and hardness of the welds produced using threaded pin profiles.

……ഊ*ര……

CHAPTER 7

ANALYTICAL MODEL FOR MAXIMUM TEMPERATURE

7.1   INTRODUCTION

In FSW, a rotating tool of complex geometry is inserted at the faying edges of the base metal and traversed to accomplish the joining. The metal joint is accomplished from the thermo mechanical mixing of the base metal below its melting point. As the process temperature is much below the melting point of the base metal, FSW is devoid of the inherent defects of fusion welding. However, the solid state metal joining in FSW is associated with complex thermal cycle and material flow, which makes the analysis of FSW joints clumsy.

FSW technique has been adopted by the industry for joining aluminium alloys. Nevertheless, a considerable part of the basic problems are yet to be solved reliably. Since its inception and development, FSW has been analysed experimentally and by using mathematical models. A generic material theory for understanding the process mechanism is needed to be evolved for joining a variety of alloys. Tool design, selection of parameters is to be optimized based on such a theory, to expand the applications of FSW in the industry. Selection of process parameters to achieve non defective joints with appreciable quality is a critical issue in the FSW process design. Different metal alloys demand different parametric combinations. So far, efforts for parameter optimization, elimination of defects and characterization are mostly confined to experimental analysis. Experimental analyses are met with high cost and are time consuming. Numerical and analytical models can solve these issues conveniently, to certain extent. To ease the efforts for experiments and streamline the process design, various numerical models have been introduced. Most of these models were thermo flow and thermomechanical models [190 - 193].
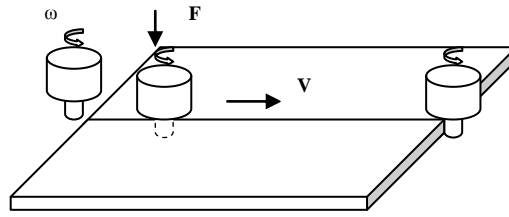
Fig. 7.1. Schematic representation of friction stir welding process

The FSW process consists of three phases; plunging and dwell, traverse and retraction. During the plunge phase the rotating tool is plunged vertically in to the joint line between the mating faces of the work piece. The plunge phase is followed by the dwell period where the rotating tool is held stationary with respect to the base plates. The prerequisite heating for the joining of the base metal is achieved by the friction between the tool and work piece during the dwell period. The mechanical interaction between tool and work piece generates heat by frictional work and material deformation. The heat, thus generated dissipates to the surrounding and the material in the vicinity of the tool softens due to the rise in temperature. During traverse phase the tool moves along the joint line and initiates the actual joint. After covering the weld distance, the tool is retracted which leaves behind a hole in the welded piece. The friction generated between the surfaces of the rotating tool and the base metal is responsible for the metallic joint formation. The heat generation to build up the metallic joint is attributed to mainly the friction and the plastic deformation. Qian et al. [194] proposed an analytical model for optimising the welding speed and tool rotational speed to produce defect free welds. The model is based on a balanced material flow at an optimum temperature. In their model, the optimum temperature range was selected based on a regression analysis of selected data from the previously reported experimental studies. Khandkar et al [195] introduced a torque based model for FSW in which the torque values reported in the previous studies were used to evaluate the heat input. The contact interface interaction is an important aspect of the

FSW process in case of heat input and material flow. The interface contact conditions for tool and material interaction is specified in terms of slip factor. The effectiveness of the metallic joint is governed by the heat generated and the material flow. Hence, any mathematical model of FSW is incomplete if it ignores any of these key components. The material flow and heat generation depend on the tool and material interface contact conditions which are specified as sliding and sticking conditions. Further, the heat generated through friction is governed by the sliding conditions of friction and heat build up by plastic deformation dominates under sticking conditions [196]. Most of the heat generation models suggested by researchers assume 'perfect sliding' as the conditions for tool and work faces interaction [197, 198]. Schmidt et al. [199] proposed an analytical model for heat generation considering various contact conditions for tool and matrix interface viz. slipping and sticking conditions. However, the actual interface contact conditions are determined by the heat generation and proceed through sticking condition and partial sticking and sliding conditions. As the welding speed is a key factor in the heat generation, the interface contact conditions are apparently influenced by the welding speed. In FSW the contact conditions follow a partial sticking and sliding behaviour [200, 201]. However, analytical models based on partial sliding and sticking conditions are scarce. In this study partial sticking and sliding condition for material contact is considered.

An analytical model for tool torque and maximum temperature attained during FSW, based on the contact conditions of tool- material surfaces is elaborated in this study. The model is used to estimate the maximum temperature attained in a realistic contact condition between the tool and matrix interface. The model is assumed to be useful in considering the different interface contact conditions at higher tool speeds. The model proposed is to suggest the process parameters at higher tool linear speeds.

7.2   THEORY AND CALCULATION

Nandan et al. [202] proposed a numerical model for FSW considering the material flow as non Newtonian, incompressible and viscoplastic. In general, the frictional contact between metals can be described by Coulomb friction, and then the shear stress can be calculated as

$$\tau_{contact} = \tau_{friction} = \mu_f \cdot p \tag{7.1}$$

Schmidt et al. and Hasan et al. [203, 204] suggested that the contact conditions are determined by the contact and shear yield stress defined as

$$\tau_{yield} = \frac{\sigma_y}{\sqrt{3}} \tag{7.2}$$

They suggested three conditions for material interface contact in FSW, designated by the slip factor 'δ'

I.   Sliding condition: This condition occurs when the material velocity at the interface is zero and $\delta = 0$

II. Sticking condition: In this condition the material velocity is equal to the tool velocity and $\delta = 1$

III. Partial sticking and sliding condition: Where material velocity is less than the tool velocity and the value of δ varies between 0 and 1.

The coefficient of friction is, in fact, a function of material welded and varies with temperature and the shear stress. With a proposition that shear stress is independent of pressure, a constant shear model is widely accepted for FSW [205]. The mathematical modelling proposed in this study for the torque and, consequently the maximum temperature attained is based on the assumption that coefficient of friction and the shear stress are constants.

7.3   TOTAL TORQUE DEVELOPED

In this model, for the calculation of torque, the coefficient of friction and the shear stress are assumed to be constants.

Measured values of total tool torque recorded a hike at the starting phase of FSW, then a dip and continue to be steady for the rest of the process [206, 207]. It indicates that at the plunge phase sticking friction conditions dominate and then the process goes through partial sticking and sliding conditions.
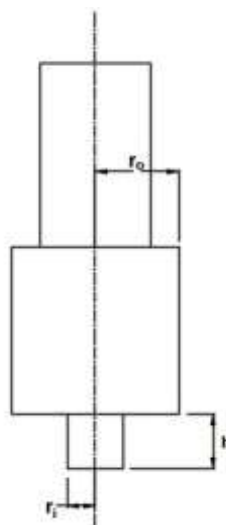
Fig. 7.2. Geometry of FSW tool

Geometry of a typical, cylindrical tool is shown in Fig. 7.2. 'r_o' is the shoulder radius, 'r_i' is the pin radius and 'h' is the height of the pin.

Total torque generated can be considered as equal to the sum of sticking torque and sliding torque [208].

The tool torque is expressed as

$$T_f = r.F \qquad (7.3)$$

Or

$$dT_f = r.\tau.dA \qquad (7.4)$$

Considering the contact conditions [209]

For sliding condition where $\delta = 0$

$$\tau = \mu_f \cdot p \tag{7.5}$$

Where

$$p = F/A \tag{7.6}$$

For sticking condition where $\delta = 1$

$$\tau = \tau_y \tag{7.7}$$

Based on the tool action, total torque can be split into torque generated at the shoulder surface, torque generated at the pin bottom surface and the torque generated at the pin side surface.

a. Torque generated at the shoulder surface:

To calculate the torque generated at the shoulder surface an infinitesimal segment of area dA, at a distance of 'r' from the axis of rotation is considered.

$$dA = r \cdot dr \tag{7.8}$$

Then, torque;

$$dT_f = r \cdot \tau \cdot dA \tag{7.9}$$

From the Fig.7. 2, the shoulder surface r varies from r_i to r_o.

Hence the total shoulder torque,

$$T_{fs} = \int_0^{2\pi} \int_{r_i}^{r_o} r \cdot \tau \cdot r \cdot dr \, d\theta$$

$$= \frac{2}{3} \cdot \pi \cdot \tau \cdot \left(r^3 - r_i^3 \right) \tag{7.10}$$

b. Torque generated at the pin bottom surface:

With the same approach as above torque generated at the pin bottom surface is given by the equation;

$$T_{fb} = T_{fb} \int_0^{2\pi} \int_0^{r_i} r \cdot \tau \cdot r \cdot dr \, d\theta$$

$$= \frac{2}{3} \cdot \pi \cdot \tau \cdot r_i^3 \tag{7.11}$$

c. Torque generated at the pin side surface:

114

Torque is calculated by considering the pin side surface area;

$$T_{fp} = r_i . \tau . 2. \pi . r_i . h$$

$$= 2. \pi . r_i^2 . \tau . h \tag{7.12}$$

Total tool torque is equal to the sum of the torque generated at the shoulder surface, tool bottom surface and pin side surface.

Total torque,

$$T_f = \frac{2}{3} . \pi . \tau . \left(r^3 - r_i^3 \right) + \frac{2}{3} . \pi . \tau . r_i^3 + 2. \pi . r_i^2 . \tau . h$$

$$= 2. \pi . \tau . r_o^2 \left(\frac{r_o}{3} + \frac{r_i^2}{r_o^2} . h \right) \tag{7.13}$$

Equation (7.13) is a general expression for tool torque. Following the equations (7.5) (7.6) and (7.7), for different contact conditions, equations for T_f, can be revised as follows;

For sliding contact conditions, when $\delta = 0$

$$T_{fL} = 2. \pi . \mu . p . r_o^2 \left(\frac{r_o}{3} + \frac{r_i^2}{r_o^2} . h \right) \tag{7.14}$$

But $p = \dfrac{F}{A} = \dfrac{F_N}{\pi . r_o^2}$

Hence $\quad\quad\quad\quad\quad T_{fL} = 2. \mu . F_N . \left(\frac{r_o}{3} + \frac{r_i^2}{r_o^2} . h \right) \tag{7.15}$

For sticking contact conditions, when $\delta = 1$

$$T_{fT} = 2. \pi . \tau_y . r_o^2 \left(\frac{r_o}{3} + \frac{r_i^2}{r_o^2} . h \right) \tag{7.16}$$

Hence for two extreme contact conditions tool torque can be expressed as

115

$$T_{fL} = \mu.F_N.k\ ; \qquad \text{for } \delta = 0 \tag{7.17}$$

$$T_{fT} = \pi.\tau_y.r_o^2.k\ ; \qquad \text{for } \delta = 1 \tag{7.18}$$

From equations (7.17) and (7.18), value of tool torque for partial sticking and sliding condition can be written as follows

$$T_f = \delta.\pi.\tau_y.r_o^2.k + (1-\delta)\mu.F_N.k \tag{7.19}$$

where $\delta = 0$ to 1; and

$$k = 2.\left(\frac{r_o}{3} + \frac{r_i^2}{r_o^2}.h\right)$$

7.4 VARIATION OF SLIP

At the commencement of FSW, during the insertion and dwell phase, tool surface is in close contact with the material. The material layer at the interface gets heated up by the friction and stick to the tool. The material layer rotates with the same velocity as that of the tool. During the traverse phase material softens and slips. Then the material velocity is less than the tool velocity and as an extreme case it can be assumed that the material velocity becomes zero. These contact conditions determine the weld quality and they can be specified by the slip factor. Slip is a spatially varying factor. It depends on the heat input and temperature. It varies along the tool radius. Many researchers have proposed many models and functions for the value for the slip. Certain models calculated slip based on a reference welding condition [209, 210]. But these parameters of reference may vary with alloys. Hamilton et al. [211] expressed slip factor as efficiency of frictional heat transfer based on a concept; maximum effective energy. They have postulated that variation of slip is primarily influenced by the welding energy and zero slip condition is reached when the temperature approaches the solidous temperature of the base metal.

Dependence of process temperature on force and torque is more reasonable, further more; tool action softens the material which in turn dictates the interface contact conditions. As the torque varies from sticking torque T_{fT} to slipping torque T_{fL}, slip factor δ varies from 1 to 0. This variation is gradual and continuous. In this scenario a possible expression for the extend of slip is proposed as follows;

$$\delta = \exp\left(-\frac{T_{fL}}{T_{fT}}\right) \tag{7.20}$$

where T_{fL} is the total torque corresponding to sliding condition and T_{fT} is the torque corresponding to the sticky friction condition.

The equation (7.20) represents slip as a partition of frictional work and work of plastic deformation. For the sliding conditions, where slip factor, $\delta = 0$, plastic deformation alone generates heat. On the other hand, for the sticking conditions where the slip factor is unity friction generates heat. Hence, slip factor has been referred as the partition of heat generated by plastic deformation and heat generated by friction [212]. In equation (7.20), slip is expressed in terms of torque developed under varying contact conditions and it represents the heat transfer effectiveness. Slip has been established as a spatially varying factor. Equation (7.20) retains the spatial dependency of slip. Based on this slip factor total torque is computed.

7.5 MAXIMUM TEMPERATURE

The average power P_a is calculated by multiplying total torque with rotational speed. Then energy per unit length is expressed as the ratio of P_a to the welding velocity.

$$P_a = T_f . \omega \tag{7.21}$$

Energy per unit length,

$$E_l = \frac{P_a}{v} = T_f \frac{\omega}{v} \tag{7.22}$$

117

In order to account the influence of pin length on the welding temperature, the transfer efficiency η is introduced as follows;

$$\eta = \frac{h}{t}$$

Then the effective energy per unit length is

$$\left(E_l\right)_{eff} = E_l.\frac{h}{t} \qquad (7.23)$$

Hamilton et al. [211] introduced an empirical relation for the ratio of maximum temperature to the solidus temperature T_s and the energy per unit length as given below;

$$\frac{T_{max}}{T_s} = 1.5610^{-4}.\left(E_l\right)_{eff} + 0.54 \qquad (7.24)$$

From equations (7.19) – (7.24) maximum temperature can be calculated.

7.6 RESULTS AND DISCUSSION

The analytical model proposed in the previous section accounts for the variation in contact conditions with the tool and material interfaces. This aspect is crucial in FSW as the contact conditions in terms of the slip factor dominate the material flow and bonding. The proposed model was tested for validity against the experimental values of peak temperature attained during FSW with the same parameters, for various aluminium alloys. Table 7.1 lists out the aluminium alloys and the tool parameters considered for validation. Table 7.2 displays the welding parameters and maximum temperature reached in accordance with the model against the experimental values.

Table 7.1. Material properties and tool geometry [210]

Alloy	Ts (K)	r_o (mm)	r_i (mm)	t (mm)	h (mm)
AA 6082 - T6	879	7.5	2.5	6	6
AA 6061 -T651	855	12.7	5	8.13	8
AA 6061 -T6	855	12	9.5	6.4	6
AA 7050 - T7451	761	10.2	3.6	6.4	6.1
AA 7050 - T7451	761	9.5	3.2	19.1	6.4

Table 7. 2: Comparison of experimental values and the calculated values of T_{max}

Alloy	ω (rpm)	v (mm/s)	F (kN)	Tmax Expt. (K) [197]	T_{max} (proposed model)	% age error
AA 6082- T6	1500	5	7	594	604	1.6
		8		548	555.7	1.4
		12		523	528.7	0.9
AA 6061-T6	344	2.2	13	698	724	3.7
AA 6061- T6651	390	2.4	22	739	737.4	0.02
AA 7050- T7451 (1)	360	1.7	24	673	664.06	1.32
	540	2.5	34	663	659.86	0.47
	810	3.8	39	703	652.86	7.1
AA 7050- T7451 (2)	520	1.9	24	448	503	12.3
	700	1	13	533	659.4	19.16
	700	1.9	16	493	539.7	9.5
	700	2.6	18	483	504.06	4.36

Variation of maximum temperature attained in the FSW of various aluminium alloys, recorded through various experiments and those obtained from the mathematical model suggested in this study is shown in Fig. 7.3.
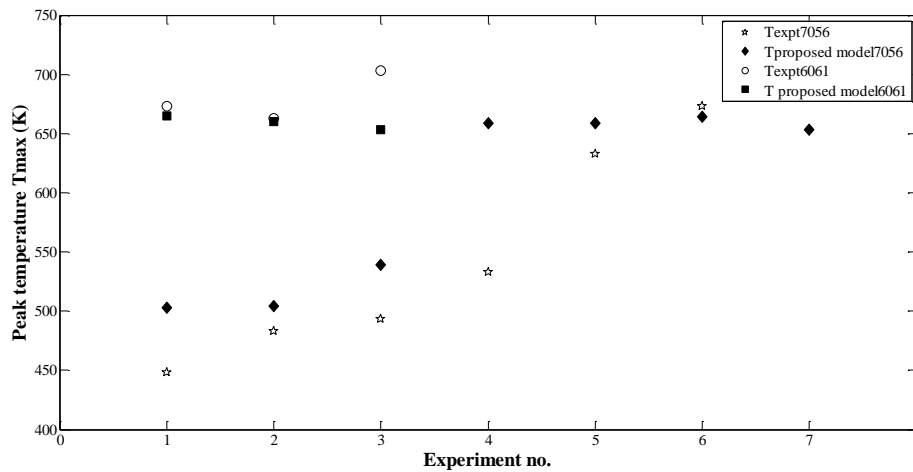
Fig. 7.3   Variation of peak temperature in FSW for various alloys - Experimental value and the proposed model

From the results it can be concluded that the proposed model yields better results which are close to the experimental results for various aluminium alloys. The error percentage of the computed results is minimum, except for alloys with higher thickness. The peak temperature obtained for higher thickness recorded maximum variation. The model may not predict the slip factor values appreciably for higher thickness.

The proposed model is an extension of the existing analytical models for computing the maximum temperature. The maximum temperature attained during the FSW is crucial, as it influences the properties and quality of the weld generated, extensively. The material flow by the tool action is another factor decisive for the weld quality. The proposed analytical model acknowledges the heat input and the material flow in terms of torque and tool matrix interactions.

Table 7.3. Comparison the calculated values of T_{max} in various models

Alloy	Experi - mental Trials	t (mm)	ω (rpm)	v (mm/s)	F (kN)	T_{max} (K) Sameer [198]	T_{max} (K) (Gaddak) [197]	T_{max} (K) (Proposed model)	% age error
AA 6082- T6	1	6	1500	5	7	683	668	604	1.6
	2	6		8		731	731	555.7	1.4
	3	6		12		583	570	528.7	0.9
AA 6061-T6	4	6.4	344	2.2	13	547	534	724	3.7
AA 6061-T651	5	8.13	390	2.4	22	527	514	737.4	0.02
AA 7050- T7451	6	6.4	360	1.7	24	636	661	664.06	1.32
	7	6.4	540	2.5	34	701	773	659.86	0.47
	8	6.4	810	3.8	39	739	821	652.86	7.1
AA 7050- T7451	9	19.1	520	1.9	24	507	517	503	12.3
	10	19.1	700	1	13	529	559	659.4	19.16
	11	19.1	700	1.9	16	497	507	539.7	9.5
	12	19.1	700	2.6	18	490	490	504.06	4.36

Table 7.3 and Fig.7.4 displays a comparison of the peak temperature values attained during experiments, various models, and proposed model.
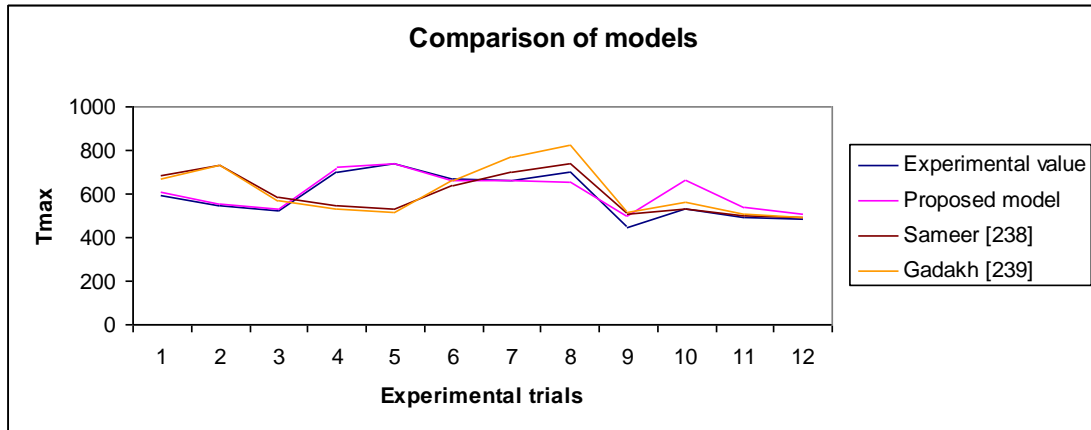
Fig.7.4   Variation of peak temperature for the proposed model, experimental results and other analytical models

These results indicate that the proposed model provides better results which are more close to the experimental values compared to other models, except for the last four cases. These situations are characterised by lower welding speeds (Tables 7.2 and 7.3). Hence it may be observed that the proposed model furnishes better results at higher speeds. The previous analytical models assume 'perfect sliding' as the contact conditions which may not be appropriate for higher welding speeds. At higher welding speeds sticking or partial sticking and sliding condition may dominate the material contact conditions during welding. The proposed model is based on the slip factor which designates the material contact conditions and is therefore able to forecast the maximum temperature more realistically at higher welding speeds.

7.7   CONCLUSIONS

A simple analytical model for FSW of aluminium alloys is suggested in this study. The model calculates the total tool torque taking the slip factor in to account. The model is based on an expression derived for the slip factor in terms of the tool torque. Welding energy per unit length is calculated with reference to the previous research work. An empirical relation already reported is used to calculate the peak temperature attained as a measure of weld efficacy. The calculated results of the model are compared to that of the experimental results available in order to validate the model for a variety of aluminium alloys under different parametric conditions. The results match best with the experimental data, especially at higher welding speeds underlying the relevance of the model.

……ജ*ഝ……

CHAPTER 8

CONCLUSIONS

FSW is a formidable development in material joining process. It is considered as a better option for joining aluminium alloys. In this scenario, two extreme cases can be considered; precipitation hardened alloys and solid solution hardened alloys. Both these are weldable by conventional fusion welding processes. However, precipitation hardened alloy welds were found to be more defective under fusion welding. Hence FSW is a promising technology for these types of aluminium alloys. In this work FSW of precipitation hardened alloys were dealt with by considering AA 2219 O and AA 6082 T6 alloys as representative examples. The effect of various parameters on the strength and microstructure were analysed. The parameters were so chosen that they can be easily adjusted in the dedicated machines presently available. Simple tool geometries with tapered, cylindrical and threaded pin profiles were selected so as to minimize the initial cost. The welding is performed at higher linear speeds to enhance the productivity. Hence the experimental analysis focused on the commercialization and popularisation of the technology.

Effect of axial force on the FSW was explored taking AA 6082 − T6 as the base metal. Experiments were conducted by varying the axial force when other parameters were kept constant. Process parameters considered were tool rotational speed and tool translational or linear speed with a threaded pin profile.

Even for these parameters selected form a 'process window' for good weld conditions as recommended by previous studies, axial force was found to influence the weld properties significantly.

UTS vary with axial force and this variation was attributed to the defect formation. This effect is justifiable as the axial force influences the material flow during welding. The macrographs showed onion ring formation and with surface defects in case of some welds. However 4 kN axial force produced welds with adequate material flow depicted by good onion ring structure and with no defects. This fact was substantiated by the mode and location of the tensile fracture. Welds with low tensile strength due to defects were having a brittle fracture with no neck formation and the fracture occurred at the NZ. In the case of welds formed with 4 kN and 5 kN axial force, the axial force was found to have strong influence in material flow for a given shoulder diameter.

Microhardness of the welds was significantly higher than the base metal. The microstructural characterization revealed that NZ underwent dynamic re crystallization and showed presence of fine fragmented particles of Mg_2Si. This was the possible reason for the enhancement in hardness for all weld specimens. However, the axial force appeared to have no effect on the re-precipitation of the strengthening particles which indicated that the heat flow is least influenced by the variation in axial force. All these factors along with the microstructure of the shoulder zone, pointed out that the axial force was ineffectual to bring about any substantial change in the weld microstructure.

Effect of process parameters on the FSW of AA 2219 - O were analyzed by varying tool rotational speed, tool linear speed, axial force and tool pin profile. The welding was performed at speeds in a range (100 - 150 mm/min.) higher than the generally reported studies. Three types of simple tool pin profiles were used in the experimental campaign namely; tapered, cylindrical and threaded pin profiles.

The selected range of parameters set a hot weld conditions as indicated by the weld appearance and the axial force values were high so that the shoulder couldn't confine the weld material along the weld line as indicated by the flashes associated with most of the welds. But it is noteworthy that the base material AA 2219 - O is a soft alloy in annealed condition.

Taguchi analysis of the experimental results showed that tool pin profile is the most influential process parameter. Threaded pin profile and tapered pin profile provided the best results for the UTS. The microhardness for threaded pin profile and tapered pin profile registered higher values than that of the base metal. Microstructural analysis indicated that threaded pin profile resulted in grain reorientation and re precipitation of Al_2Cu as fine and undissolved particles. For the precipitation hardened alloys, the distribution of strengthening particles determine the strength, rather than the grain size. EDS analysis showed that precipitation of Al_2Cu particles was more for the threaded pin profile. This is the reason for the better strength for the welds produced using threaded pin profile. Higher values of microhardness values welds also substantiated the presence of more precipitates in case of these welds. As the rotational speed and linear speed determine the heat flow and the pin profile influences the material stirring, the impact of pin profile on the degree of precipitation of strengthening particles can be considered as a general characteristic for the precipitation hardened alloys.

FSW of AA 6082 – T6 was performed at the highest linear speed ever reported (600 mm/min, 700 mm/min.) for the considered thickness (6 mm) with a common tool with threaded pin profile to check the feasibility of the process. Apart from the tool rotational speed and linear speed, effect of tool tilt was inquired. A tilt for the tool was recommended for producing good weld was reported in the previous studies. Strength

of the welds were analysed in terms of UTS. Since, welding defects were expected at higher speeds, macrostructure of the weld cross sections were studied. Microstructure evaluation was carried out using microhardness tests and optical micrography.

It was observed that FSW at higher welding speeds was feasible for the given parameters; however the tilted tool produced defective welds. Taguchi analysis of the experimental results proved that the tool tilt was the most influential parameter deciding the weld strength. The weld pressure at higher welding speed was possibly low and the tool tilt caused further depletion in welding pressure. In these cases, the pressure was reduced below a limiting value which was required to avoid volumetric defects. The macrostructure vindicated this fact as it showed that weld material flow for the welds with a tool tilt was not synchronised and periodic. Microhardness of the welds was found to be lower for welds produced with a tool tilt. Hence it can be concluded that tool tilt is detrimental at higher welding speeds or causing a reverse effect at higher welding speeds.

An analytical model was suggested for the FSW of aluminium alloys based on the slip factor with simple tool having cylindrical pin. An expression for slip factor is suggested which represented slip as a partition of frictional work and work of plastic deformation. The slip factor is expressed in terms of the tool torque. It is noticeable that tool torque increases at higher welding speeds. The model enabled computation of maximum temperature in the FSW process. The proposed model has taken partial slipping and partial sticking tool contact conditions in to consideration. That could be the reason that the model displayed errors in the computation of maximum temperature for lower welding speeds. At lower welding speeds slipping contact conditions dominated during welding process. However, at higher welding speeds the model displayed better results for maximum temperature with minimum error when it

is compared with experimental results. The maximum temperature value will be useful in deciding the process parameters if the variation in flow stress of the alloys with temperature is known.

The present experimental work sought the effect of process parameters on FSW of aluminium alloys at higher welding speeds along with the microstructural analysis. Further study is needed to suggest a process window helps to suggest various process parameters with simple tool geometry at higher speeds. This will support the commercialisation of the FSW technology.

……ॐ*ॐ……

REFERENCE:

1. **Thomas, W. M., E. D. Nicholas, J. C. Needham, M. G. Murch, P. Temple-Smith, and C. J. Dawes** (1991) *Friction-stir butt welding. GB Patent No. 9125978.8, International Patent No.PCT/GB92/02203.*

2. **Mishra, R. M. and M. W. Mahoney** *Friction stir welding and processing.* ASM international, 2007.

3. **Ma Yu E and Zhao Zhenqiang** (2013) Structure response in the riveted and friction stir welded stringer panel under the tensile loading *13th international conference on fracture*, Beijing, June, 16 - 21.

4. **Thomas, V. M and E. D. Nicholas** (1997) Friction Stir Welding for the Transportation Industries. *Materials and Design,* **18**, 269 - 273.

5. **Dawes, C. J and W. M. Thomas** (1996) Friction Stir Process Welds Aluminium Alloys. *Welding Journal*, **75**, 41 - 45.

6. **Kallee, S. W., J. Davenport and E. D. Nicholas** (2002) Railway Manufacturers implement friction Stir Welding. *Welding Journal*, **81**, 47 - 50.

7. **Mishra, R. S and Z. Y Ma** (2005) Friction stir welding and processing. *Materials science and engineering*, **R 50**, 1 - 78.

8. **Fujii, H., L. Cui., M. Maeda** and **K. Nogi** (2006) Effect of tool shape on mechanical properties and microstructure of friction stir welded aluminium alloys. *Journal of Materials Science and Engineering A*, **419**, 25- 31.

9. *Welding Handbook, 9th Edition, Volume 3: Welding Process*; American Welding Society, 2007.

10. *Guide for the approval of friction stir welding of Aluminium*, American beauro of shipping, October 2011.

11. **Zhang, Z., B. L. Xiao and Z. Y. Ma** (2012) Effect of welding parameters on microstructure and mechanical properties of friction stir welded 2219 Al- T6 joints. *Journal of Material science*, **47**, 4075 - 4086.

12. **Muruganandan, D** and **Shulil Lal Das** (2011) Friction stir welding process parameters for joining dissimilar aluminium alloys. *International Journal of Mechanical engineering and Technology*, **2 (2)**, 25 - 38.

13. **Cavaliere, P., G. Campanile, F. Panella** and **A. Squillace** (2006) Effect of welding parameters on mechanical and microstructural properties of AA6056 joints produced by friction stir welding. *Journal of Materials Processing Technology*, **180**, 263 -270.

14. **Cavaliere, P., D. A. Santis, F. Panella** and **A. Squillace**, (2008) Effect of anisotropy on fatigue properties of 2198 Al - Li plates joined by friction stir welding. *Engineering Failure Analysis*, **6**, 1856 - 1865.

15. **Surekha, K., B. S. Murthy** and **K. R. Prasad** (2008) Microstructural characterization and corrosion behaviour of multipass friction stir processed AA 2219 aluminium alloy. *Surface & Coating Technology*, **202**, 4057 - 4068.

16. **Oertelt, G., S. S. Babu, S. A. David** and **E. A. Kenik** (2001) Effect of Thermal Cycling on Friction stir welds of 2195 Aluminum alloy. *Welding research*, 71s - 79s.

17. **Aydin, H., A. Bayram, A. Uguz**, and **S. K. Akay** (2009) Tensile properties of friction stir welded joints of 2024 aluminum alloys in different heat treated-state. *Materials and Design*, **30**, 2211 - 2221.

18. **Xu, W., J. Liu., G. Luan** and **C. Dong** (2008) Temperature evolution, microstructure and mechanical properties of friction stir welded thick 2219- O aluminium alloy joints. *Materials and Design*, **30**, 3460 - 3467.

19. **Aydin, H., A. Bayram**, and **I. Durgun**, (2010) The effect of post- weld heat treatment on the mechanical properties of 2024- T4 friction stir- welded joints. *Materials and design*, **31**, 2568 - 2577.

20. **Hatamleh, O** and **A. DeWald** (2009) An investigation of peening effects on the residual stresses in friction stir welded 2195 and 7075 aluminum alloy joints. *Journal of Materials Processing Technology*, **209**, 4822 - 4829.

21. **Su, J. Q, T. W. Nelson, R. Mishra** and **M. Mahoney** (2003) Microstructural investigation of friction stir welded 7050- T651 aluminium. *Acta Materialia*, **51(3)**, 713 - 729.

22. **Rajakumar, S, C. Muralidharan** and **V. Balasubramanian** (2010) Optimization of the friction stir welding process and tool parameters to attain a maximum tensile strength of AA7075-T6 aluminium alloy. Proceedings of the Institution of Mechanical Engineers, Part B: Journal of Engineering Manufacture, **224(8)**, 1175 – 1191.

23. **Kanwar, S, Arora, Sunil Pandey, Michael Schaper** and **Rajneesh Kumar** (2010) Effect of process parameters on friction stir welding of aluminium alloy 2219- T87. *Advanced manufacturing technology*, **50 (9)**, 941 - 952.

24. **Palanivel, R** and **P**. **Koshy Mathews** (2012) Prediction and optimization of process parameter of friction stir welded AA5083-H111 aluminum alloy using response surface methodology. *Journal of central south university*, **19 (1)**, 1 - 8.

25. **Devanathan, C**, **A. Murugan** and **A. Sureshbabu** (2013) Optimization of process parameters in friction stir welding of Al 6063. *International Journal of Design and Manufacturing Technology*, **4 (2)**, 42 - 48.

26. **Jayaraman, M** and **V.Balasubramanian** (2013) Effect of process parameters on tensile strength of friction stir welded cast A356 aluminium alloy joints. *Transactions of nonferrous metals society of China,* **23 (3)**, 605 - 615.

27. **Podrzaj, P, P. Jerman** and **D. Klobcar** (2015) *Welding defects at friction stir welding*. Metalurgija, **54 (2)**, 387 - 389.

28. **Attallah, M. M** and **Hanadi G Salem** (2004), Friction stir welding parameters: a tool for controlling abnormal grain growth during subsequent heat treatment. *Materials Science and Engineering: A*, **391**, 51 - 59.

29. **Malarvizhi, S** and **V. Balasubramanian** (2011) Effect of welding processes on AA2219 aluminium alloy joint properties. *Transactions of Nonferrous Metals Society of China*, **21**, 962 - 973.

30. **Tang, W., X. Guo, J. C. McClure, L. E. Murr** and **Nunes. A** (1988) Heat Input and Temperature Distribution in Friction Stir Welding. *Journal of Materials Processing and Manufacturing Science*, **7 (2)**, 163 - 172.

31.   **McClure, J. C., T. Tang, L. E. Murr, X. Guo** and **Z. Feng**. *A Thermal Model for Friction Stir Welding*. pp. 590 - 595. *In* **J. M. Vitek, S. A. David, J. A. Johnson, H. B. Smart** and **T. Debroy** (eds.) *Trends in Welding Research.* ASM International, Ohio, USA, 1998.

32.   **Yuh. J. Chao, X. Qi** and **W. Tang** (2003) Heat Transfer in Friction Stir Welding- Experimental and Numerical Studies. *Transactions of the ASME*, **125**, 138 - 145.

33.   **Chao, Y. J** and **X. Qi** (1998) Thermal and thermo-mechanical modelling of friction stir welding of aluminium alloy 6061 - T6. *Journal of Material Processing and Manufacturing Science*, **7**, 215 - 233.

34.   **Khandkar, M. Z. H**., **J. A. Khan** and **A. P. Reynolds** (2003) Prediction of temperature distribution and thermal history during friction stir welding: input torque model. *Science and Technology of Welding and Joining*, **8**, 165 - 174.

35.   **Colegrove, P., M. Painter, D. Graham** and **T. Miller** (2000) 3-Dimensional flow and thermal modelling of the friction stir welding process *Proceedings of Second International Symposium on Friction Stir Welding*, Gothenburg, June.

36.   **Russell, M. J** and **H. R. Shercliff** (1999) Analytical modelling of microstructure development in friction stir welding *First International Symposium on Friction Stir Welding*, Thousand Oaks, June.

37.   **Schmidt, H., J. Hattel** and **J. Wert** (2004) An analytical model for the heat generation in friction stir welding. *Modelling and Simulation of Materials Science and Engineering,* **12**, 143 - 157.

38. **Gadakh, V. S** and **K. Kumar Adepu** (2013) Heat generation model for taper cylindrical pin profile in FSW. *Journal of Materials Research and Technology*, **2 (4)**, 370 - 375.

39. **Ahmed Ramadan Shaaban Essa , Mohamed Mohamed Zaky Ahmed, Abdel-Karim Yousif Ahmed Mohamed** and **Ahmed Essa El-Nikhaily** (2016) An analytical model of heat generation for eccentric cylindrical pin in friction stir welding. *Journal of Materials Research and Technology*, **5 (3)**, 234 - 240.

40. **Reynolds, A. P.** (2008) Flow visualization and simulation in FSW. *Scripta Materealia*, **58**, 338 - 342.

41. **Rai, R., A. De, H. K. D. H. Bhadeshia** and **T. DebRoy** (2011) Review: friction stir welding tools. *Science and technology of welding and joining*, **16 (4)**, 325 - 342.

42. **Seidel, T. U** and **A. P. Reynolds** (2001) Visualization of the material flow in AA2195 friction-stir welds using a marker insert technique. *Metallurgical and Materials Transactions A*, **32**, 2879 - 2884.

43. **Schmidt, H. N. B., T. L. Dickerson** and **J. H. Hattel** (2006) Material flow in butt friction stir welds in AA2024-T3. *Acta Materialia*, **54**, 1199 - 1209.

44. **Firouzdor, V** and **S. Kou** (2010) Al-to-Mg friction stir welding: effect of material position, travel speed and rotation speed. *Metallurgical and Materials Transactions* A, **41**, 2914 - 2935.

45.   **Yang, B., J. Yan, M. A. Sutton** and **A. P. Reynolds** (2004) Banded microstructure in AA2024-T351 and AA2524-T351 aluminum friction stir welds: part I. Metallurgical studies. *Materials Science and Engineering* A, **364**, 55 - 65.

46.   **Donatus, U., G. E. Thompson, X. Zhou , J. Wang** and **K. Beamish** (2015) Flow patterns in friction stir welds of AA5083 and AA6082 alloys. *Materials & Design*, **83**, 203 - 213.

47.   **Krishnan, K**. (2002) On the formation of onion rings in friction stir welds. *Materials Science and Engineering* A, **327 (2)**, 246 - 251.

48.   **Sreenivas, P., R. Anil kumar** and **P. S. Sreejith** (2017) Effect of applied axial force on FSW of AA 6082- T6 Aluminium alloys. *International Journal of Mechanical Engineering and Technology*, **8**, 88 - 99.

49.   **W. J. Arbegast**, Modeling friction stir joining as a metal working process, pp 313. *In*: **Z. Jin, A. Beaudoin, T.A. Bieler** and **B. Radhakrishnan** (Eds.), Hot *Deformation of Aluminum Alloys III*, The Minerals, Metals and Materials Society, Warrendale, PA, USA, 2003.

50.   **Gaafer, A. M., T. S. Mahoud** and **E. H. Mansour** (2010) Microstructural and mechanical characteristics of AA 7020- O Al plates joined by friction stir welding. *Materials Science and Engineering* A, **527**, 7424 - 7429.

51.   **Elangovan, K., V. Balasubramanian**, and **S. Babu** (2008) Developing an Empirical Relationship to Predict Tensile Strength of Friction Stir Welded AA2219 Aluminum Alloy. *Journal of Materials Engineering and Performance*, **17**, 820 - 830.

52. **Raza Moshwan, Farazila Yusof , M. A. Hassan and S. M. Rahmat** (2015) Effect of tool rotational speed on force generation, microstructure and mechanical properties of friction stir welded Al – Mg - Cr - Mn (AA 5052-O) alloy. *Materials and design*, **66**, 118 - 128.

53. **Elangovan, K., V. Balasubramanian**, and **S. Babu** (2009) Predicting tensile strength of friction stir welded AA6061 aluminium alloy joints by a mathematical model. *Materials and design*, **30(1)**, 188 - 93.

54. **Tang, W., X, Guo , J. C. McClure, L. E. Murr** and **A. Nunes** (1998) Heat input and temperature distribution in friction stir welding. *Journal of Material Processing and Manufacturing Science*, **7**, 163 - 72.

55. **Hassan Kh, A. A., P. B. Prangnell, A. F. Norman, D. A. Price** and **S. W. Williams** (2003) Effect of welding parameters on nugget zone microstructure and properties in high strength aluminum alloy friction stir welds. *Science and technology of welding and joining*, **8(4)**, 257 - 68.

56. **Lee, W. B., Y. M. Yeon**, and **S. B. Jung** (2003) The Joint Properties of Dissimilar formed aluminium alloys by friction stir welding according to the fixed location of materials. *Scripta Materialia*, **49**, 423 - 428.

57. **Lomolino, S., R. Tovo**, and **J. Dos Santos** (2005) On the fatigue behaviour and design curves of friction stir butt welded Al alloys. *International Journal of Fatigue*, **27**, 305 - 316.

58. **Babu, S., K. Elangovan, V. Balasubramanian**, and **M. Balasubramanian**, (2009) Optimizing Friction Stir Welding Parameters to Maximize Tensile Strength of AA2219 Aluminum Alloy Joints. *Metals and Materials International*, **15 (2)**, 321 - 330.

59. **Elangovan, K., V. Balasubramanian**, and **S. Babu** (2008) Developing an Empirical Relationship to Predict Tensile Strength of Friction Stir Welded AA2219 Aluminum Alloy. *Journal of Materials Engineering and Performance* **17**, 820 - 830.

60. **Fonda, R. W** and **S. G. Lambrakos** (2002) Analysis of friction stir welds using an inverse problem approach. *Science and Technology of Welding and Joining,* **7**,177 - 181.

61. **Kim, Y. G., H. Fujii, T. Tsumura, T. Komazaki** and **K. Nakata** (2006) Three Defects Types in Friction Stir Welding of Aluminium Die Casting Alloy. *Materials Science and Engineering* A, **415**, 250 - 254.

62. **Elangovan, K** and **V. Balasubramanian** (2008) Effect of Tool Pin Profile and Axial Force on the Formation of Friction Stir Processing Zone in AA6061 Aluminium Alloy. *International Journal of Advanced Manufacturing Technology*, **38 (3)**, 285 - 295.

63. **H. A. Rubisoff, J. A. Schneider**, and **A. C. Nunes, Jr**., Control of structure in conventional friction stir welds through a kinematic theory of metal flow. pp 149- 158. *In* **Rajiv, S. Mishra., Murray. W. Mahoney** and **Thomas. J. Lienert** (eds.) *Friction Stir Welding and Processing - V*, The Minerals, Metals & Materials Society*,* Warrendale, USA, 2010.

64. **Ashwani Kumar, Pardeep Kumar** and **Balwinder. S. Sidhu** (2014) Influence of Tool Shoulder Diameter on Mechanical Properties of Friction Stir Welded Dissimilar Aluminium Alloys 2014 and 6082. *International Journal of Surface Engineering & Materials Technology*, **4 (1)**, 5 - 10.

65. **Mohanty, H. K., D. Venkateswarlu, M. M. Mahapatra, Pradeep Kumar** and **N. R. Mandal** (2012) Modeling the Effects of Tool Probe Geometries and Process Parameters on Friction Stirred Aluminium Welds. *Journal of Mechanical Engineering and Automation*, **2(4)**, 74 - 79.

66. **Sung-Wook Kang, Beom-Seon Jang** and **Ha-Cheol Song** (2015) Residual stresses analysis of friction stir welding using one-way FSI simulation. *Journal of Mechanical Science and Technology,* **29(3)**, 1111–1121.

67. **Threadgill, P. L., A. J. Leonard, H. R. Shercliff** and **P. J. Withers** (2009) Friction Stir Welding of Aluminium Alloys. *International Materials Reviews*, **54**, 49 - 93.

68. **Pradeep, A** and **S. Muthukumaran** (2014) Defect Analysis Of Friction Stir Welded Steel Plates On Different Tool Profiles. *International Journal of Mechanical And Production Engineering*, **2 (7)**, 92 - 98.

69. **Amèvi Tongne, Mohammad Jahazi, Eric Feulvarch** and **Christophe Desrayaud** (2015) Banded Structures in Friction Stir Welded Al Alloys. *Journal of materials processing technology*, **221**, 269 - 278.

70. **Rajakumar, S** and **V. Balasubramanian** (2012) Establishing relationships between mechanical properties of aluminium alloys and optimised friction stir welding process parameters. *Materials and Design*, **40**, 17 - 35.

71. **Crawford, R., G. E. Cook, A. M. Strauss, D. A. Hartman**, and **M. A. Stremler** (2006) Experimental Defect Analysis and Force Prediction Simulation of High Weld Pitch Friction Stir Welding. *Science and technology of welding and joining*, **11**, 657 - 665.

72. **Janaki Ramulu, P., R. Ganesh Narayanan, Satish V. Kailas and Jayachandra Reddy** (2013) Internal defect and process parameter analysis during friction stir welding of Al 6061 sheets. *International Journal of Advanced Manufacturing Technology*, **65**, 1515 - 1528.

73. **Scialpi, A., L. A. C. De Filippis** and P. Cavaliere (2007) Influence of shoulder geometry on microstructure and mechanical properties of friction stir welded 6082 aluminium alloy. *Materials and Design*, **28**, 1124 - 1129.

74. **Mohamadreza Nourani, Abbas S Milani** and **Spiro Yannacopoulos** (2011) Taguchi Optimization of Process Parameters in Friction Stir Welding of 6061 Aluminum Alloy: A Review and Case Study. *Engineering,* **3**, 44 - 155.

75. **Reghubabu, G., K. G. K. Murthi** and **G. Ranga Janardhana** (2008) An experimental study of the effect of welding parameters on mechanical and microstructural properties of AA6082 - T6 friction stir welded butt joints. APN *journal of engineering and applied science*, **3 (5)**, 68 - 74.

76. **Patil, H. S** and **S. N. Soman** (2010), Experimental study on the effect of welding speed and tool pin profiles on AA6082-O aluminium friction stir welded butt joints. *International journal of engineering, science and technology*, **2(5)**, 268 - 275.

77. **Adamowski, J., C. Gambaro, E. Lertora, M. Ponte** and **M. Szkodo** (2007) Analysis of FSW welds made of aluminium alloy AW6082-T6. *Archieves of material science and engineering*, **28 (8)**, 453 - 460.

78. **Kush, P, Mehta** and **Vishvesh, J, Badheka** (2016) Effects of tilt angle on the properties of disssimiliar friction stir welding copper to aluminium. *Journal of Materials and Manufacturing Processes,* **31 (3)**, 1 - 9.

79. **Kittipong Kimapong** and **Takehiko Watanab** (2005) Effect of welding process parameters on mechanical property of FSW lap joint between aluminum alloy and steel. *Materials Transactions*, **46 (10)**, 2211 - 2217.

80. **Cao, G** and **S. Kou** (2005) Friction Stir Welding of 2219 Aluminum: Behavior of (Al2Cu) particles. *Welding journal*: 1s - 8s.

81. **Gopala Krishna, G, P. Ram Reddy** and Manzoor Hussain (2014) Effect of tool tilt angle on aluminium 2014 friction stir welds. *Global journal of researches in engineering: J General engineering*, **14 (7)**, 61 - 70.

82. **Ana, C. F, Silva, Daniel, F.O. Braga, M. A. V. De Figueiredo** and **P. M. G. P. Moreira** (2015) Ultimate tensile strength optimization of different FSW aluminium alloy joints. *International Journal of Advanced Manufacturing Technology*, **79**, 805 - 814.

83. **Rodrigues, D. M., C. Leitao, R. Louro, H. Gouveia** and **A. Loureiro** (2010) High speed friction stir welding of aluminium alloys. *Science and Technology of Welding and Joining*, **15(80)**, 676 - 681.

84. **Kanwar, S, Arora., Sunil Pandey, Michael Schaper** and **Rajneesh Kumar** (2010) Effect of process parameters on friction stir welding of aluminium alloy 2219- T87. *Advanced manufacturing technology*, **50 (9)**, 941 - 952.

85.   **Biswas, P., D. A. Kumar** and **N. R. Mandal** (2011) Friction stir welding of aluminium alloy with varying tool geometry and process parameters. *Proceedings of the Institution of Mechanical Engineers, Part B: J. Engineering Manufacture*, **226**, 641 - 648.

86.   **Dude, H., J. Schneider, B. Patton, S. Stafford, T. Waters** and **C. Varner** (2015) Optimizing weld quality of a friction stir welded aluminium alloy. *Journal of materials processing technology*, **222**, 188 - 196.

87.   **Junhui Yan, M. A. Sutton** and **A. P. Reynolds** (2005) Process–structure–property relationships for nugget and heat affected zone regions of AA2524–T351 friction stir welds. *Science and Technology of Welding and Joining*, **10 (6)**, 725 - 736.

88.   **Liu, X. C** and **C. S. Wu** (2015) Elimination of tunnel defect in ultrasonic vibration enhanced friction stir welding friction stir welding. *Journal of materials design*, **90**, 350 - 358.

89.   **Liu, X. C., C. S. Wu** and **G. K. Padhy** (2015) Improved weld macrosection, microstructure and mechanical properties of 2024Al-T4 butt joints in ultrasonic vibration enhanced friction stir welding. *Science and Technology of Welding and Joining*, **20(4)**, 345 - 352.

90.   **Kumar, K** and **S. V. Kailas** (2008) The role of friction stir welding tool on material flow and weld formation. *Materials Science and Engineering A*, **485(1)**, 367 - 374.

91. **Kim, Y. G., H. Fujii, T. Tsumura, T. Komazaki** and **K. Nakata** (2006) Three defect types in friction stir welding of aluminum die casting alloy. *Materials Science and Engineering A*, **415(1)**, 250 - 254.

92. **Chen, H. B., K. Yan, T. Lin, S. B. Chen, C. Y. Jiang** and **Y. Zhao** (2006) The investigation of typical welding defects for 5456 aluminum alloy friction stir welds. *Materials Science and Engineering A*, **433(1)**, 64 - 69.

93. **Ramachandran, K. K., N. Murugan** and **S. Shashi Kumar** (2015) Influence of tool traverse speed on the characteristics of dissimilar friction stir welded aluminium alloy, AA5052 and HSLA steel joints. *Archives of civil and mechanical engineering,* **15**, 822 - 830.

94. **Doude, H., J. Schneider, B. Patton, S. Stafford, T. Waters** and **C. Varner** (2015) Optimizing weld quality of a friction stir welded aluminum alloy. *Journal of Materials Processing Technology*, **222**, 188 - 196.

95. **Tongne, A., M. Jahazi, E. Feulvarch** and **C. Desrayaud** (2015) Banded structures in friction stir welded Al alloys. *Journal of Materials Processing Technology,* **221**, 269 - 278.

96. **Luis Trueba Jr., Georgina Heredia, Daniel Rybicki** and **Lucie B. Johannes** (2015), Effect of tool shoulder features on defects and tensile properties of friction stir welded aluminum 6061-T6. *Journal of Materials Processing Technology,* **219**, 271 - 277.

97. **Trimble, D., G.E. O'Donnell** and **J. Monaghan** (2015) Characterisation of tool shape and rotational speed for increased speed during friction stir welding of AA2024-T3. *Journal of Manufacturing Processes*, **17**, 141 - 150.

98. **Raza Moshwan, Farazila Yusof, M. A. Hassan** and **S. M. Rahmat** (2015) Effect of tool rotational speed on force generation, microstructure and mechanical properties of friction stir welded Al–Mg–Cr–Mn (AA 5052-O) alloy. *Materials and design*, **66**, 118 - 128.

99. **Kumar, K** and **Satish. V. Kailas** (2008) On the role of axial load and the effect of interface position on the tensile strength of a friction stir welded aluminium alloy. *Materials and Design,* **29**, 791 - 797.

100. **Mohiedin Bagheri Hariri, Sajad Gholami Shiri, Yadollah Yaghoubinezhad** and **Masoud Mohammadi Rahvard** (2013) The optimum combination of tool rotation rate and travelling speed for obtaining the preferable corrosion behavior and mechanical properties of friction stir welded AA5052 aluminum alloy. *Materials and design*, **50**, 620 - 634.

101. **De Giorgi, M., A. Scialpi, F.W. Panella** and **L. A. C. De Filippis** (2009) Effect of shoulder geometry on residual stress and fatigue properties of AA6082 fsw joints. *Journal of Mechanical Science and Technology*, **23**, 26 - 35.

102. **Jayaraman, M., R, Sivasubramanian,V. Balasubramanian** and **A. K Lakshminarayanan** (2009) Optimization of process parameters for friction stir welding of cast aluminium alloy A319 by Taguchi method*. Journal of Scientific & Industrial Research*, **68**, 36 - 43.

103. **D.M. Rodrigues, D. M., A. Loureiro , C. Leitao , R. M. Leal, B. M. Chaparro** and **P. Vilaça** (2009) Influence of friction stir welding parameters on the microstructural and mechanical properties of AA 6016-T4 thin welds. *Materials and Design*, **30**, 1913 - 1921.

104. **Rodrigues, D. M., C. Leita , R. Louro, H. Gouveia** and **A. Loureiro** (2010) High speed friction stir welding of aluminium alloys. *Science and Technology of Welding and Joining*, **15 (8)**, 676 - 681.

105. **Barlas, Z** and **U. Ozsarac** (2012) Effects of FSW Parameters on Joint Properties of AlMg3 Alloy. *Welding research*, **91**, 16s - 22s.

106. **Reynolds, A. P., W. Tang, Z. Khandkar, J. A. Khan** and **K. Lindner** (2005) Relationships between weld parameters, hardness distribution and temperature history in alloy7050friction stir welds. *Science and Technology of Welding and Joining,* **10 (2)**, 190 - 199.

107. **Venkata Rao, G. Madhusudhan Reddy** and **K. Srinivasa Rao** (2015) Influence of tool pin profile on microstructure and corrosion behaviour of AA2219 Al - Cu alloy friction stir weld nuggets. *Defence technology*, **11**, 197 - 208.

108. **Mishin,V., A. Godfrey,** and **L. Ostensson,** (2006) Comparative microstructural characterization of a friction – stir - welded aluminium alloy using TEM and SEM-based techniques. *Metallurgical and materials transactions A*, **37A**, 489 - 496.

109. **Kamble, L. V., S. N. Soman** and **P. K. Brahmankar** (2012) Effect of Tool Design and Process VariablesonMechanicalProperties and Microstructure of AA6101-T6 Alloy Welded by Friction Stir Welding. *IOSR Journal of Mechanical and Civil Engineering*, **1 (334)**, 30 - 35.

110. **Singh, R. K. R., Chaitanya Sharma, D. K. Dwivedi, N. K. Mehta** and **P. Kumar** (2011) The microstructure and mechanical properties of friction stir

welded Al - Zn - Mg alloy in as welded and heat treated conditions. *Materials and Design*, **32**, 682 - 687.

111. **Pasquale Cavaliere** (2013) Friction stir welding of Al alloys: analysis of processing parameters affecting mechanical behaviour. *Procedia CIRP*, **11**, 139 - 144.

112. **Palanivel, R** and **P. Koshy Mathews** (2012) Prediction and optimization of process parameter of friction stir welded AA5083-H111 aluminum alloy using response surface methodology. *Journal of central south university*, **19 (1)**, 1 - 8.

113. **Devanathan, C., A. Murugan** and **A. Sureshbabu** (2013) Optimization of process parameters in friction stir welding of Al 6063. *International Journal for Design and Manufacturing Technology*, **4 (2)**, 42 - 48.

114. **Jayaraman, M** and **V. Balasubramanian** (2013) Effect of process parameters on tensile strength of friction stir welded cast A356 aluminium alloy joints. *Transactions of nonferrous metals society of China*, **23 (3)**, 605 - 615.

115. **Zhang, Z., B. L. Xiao** and **Z. Y. Ma** (2012) Effect of welding parameters on microstructure and mechanical properties of friction stir welded 2219Al - T6 joints. *Journal of Materials Science*, **47**, 4075 - 4086.

116. **Kamble, L.V., S. N. Soman** and **P. K. Brahmankar** (2012) Effect of Tool Design and Process Variables on Mechanical Properties and Microstructure of AA6101 -T6 Alloy Welded by Friction Stir Welding. *IOSR Journal of Mechanical and Civil Engineering*, **1 (334)**, 30 - 35.

117. **Weifeng Xu., Jinhe Liu, Guohong Luan** and **Chunlin Dong** (2009) Temperature evolution, microstructure and mechanical properties of friction stir welded thick 2219 - O aluminium alloy joints. *Materials and design*, **30**, 1886 - 1893.

118. **Rodrigues, D. M., A. Loureiro , C. Leitao , R. M. Leal, B. M. Chaparro** and **P. Vilaça** (2009) Influence of friction stir welding parameters on the microstructural and mechanical properties of AA 6016 - T4 thin welds. *Materials and Design*, **30**, 1913 - 1921.

119. **Adamowski, J., C. Gambaro, E. Lertora, M. Ponte** and **M. Szkodo** (2007) Analysis of FSW welds made of aluminium alloy AW6082 - T6. *Archives of Materials Science and Engineering*, **28 (8)**, 435 - 460.

120. **Ana, C. F. Silva., Daniel. F. O. Braga., M. A. V. de. Figueiredo** and **P. M. G. P. Moreira** (2015) Ultimate tensile strength optimization of different FSW aluminium alloy joints. *Advanced manufacturing technology*, **79**, 805 - 814.

121. **Biswas, P., D. A. Kumar** and **N. R. Mandal** (2011) Friction stir welding of aluminum alloy with varying tool geometry and process parameters. *Journal of Engineering Manufacture*, **226**, 641- 648.

122. **Doude, H., J. Schneider, B. Patton, S. Stafford, T. Waters** and **C. Varner** (2015) Optimizing weld quality of a friction stir welded aluminum alloy. *Journal of material processing technology*, **222**, 188 - 196.

123. **Luis Trueba Jr., Georgina Heredia, Daniel Rybicki** and **Lucie, B. Johannes** (2015) Effect of tool shoulder features on defects and tensile properties of friction stir welded aluminium 6061 - T6. *Journal of material processing technology*, **219**, 271 - 277.

124. **Junhui Yan., M. A. Sutton** and **A. P. Reynolds** (2005) Process–structure–property relationships for nugget and heat affected zone regions of AA2524 - T351 friction stir welds. *Science and Technology of Welding and Joining*, **10 (6)**, 725 - 736.

125. **Trimble, D., G. E. O' Donnell** and **J. Monaghan** (2015) Characterisation of tool shape and rotational speed for increased speed during friction stir welding of AA 2024 - T3. *Journal of manufacturing process*, **17**, 141 - 150.

126. **Su, H., C. S. Wu, A. Pittner** and **Rethmeier** (2013) Simultaneous measurement of tool torque, traverse force and axial force in friction stir welding. *Journal of manufacturing process*, **15**, 495 - 500.

127. **Liu, H. J., H. Fujii, M. Maeda** and **K. Nogi** (2003) Tensile properties and fracture locations of friction stir welded joints of 2017- T351 aluminium alloy. *Journal of materials processing technology*, **142 (3)**, 692 - 696.

128. **Liu, H. J., H. Fujii, M. Maeda** and **K. Nogi** (2004) Heterogeneity of mechanical properties of friction stir welded joints of 1050-H24 aluminum Alloy. *Journal of Materials Science Lett*ers, **22**, 441 - 444.

129. **Krishnan, K. N**. (2002) On the formation of onion rings in friction stir welds. *Materials Science and Eng*ineering A, **327**, 246 - 251.

130. **Biswas, P., D. A. Kumar** and **N. R. Mandal** (2012) Friction stir welding of aluminum alloy with varying tool geometry and process parameters. *Proceedings of the Institution of Mechanical Engineers part- B Journal of Engineering Manufacture*, **226 (4)**, 641 - 648.

131. **Srinivasa Rao., K. G. Sivadasan** and **P. K. Basubramanian,** (1996) Structure- property correlation on AA2219 aluminium alloy weldments. *Bulletin of Materials Science*, **19 (3)**, 549 - 557.

132. **Malarvizhi, S** and **V. Balasubramanian**, (2011), Effect of welding processes on AA2219 aluminium joint properties. *Transactions of non ferrous metals society of China,* **21**, 962 - 973.

133. **Malarvizhi, S., K. Raghunadhan** and **N. Viswanadhan** (2008) Effect of post weld aging treatment on tensile properties of electron beam welded AA2219 aluminium alloy. *International Journal of Advanced Manufacturing Technology*, **37(3)**, 294 - 301.

134. **Kumar, K** and **Sathish. V. Kailas** (2008) The role of friction stir welding tool on material flow and weld formation. *Journal of Materials Science and Engineering A*, **485**, 367 - 374.

135. **Adamowski, J** and **M. Szkodo** (2007) Friction stir welds (FSW) of aluminium alloy AW 6082 - T6. *Journal of achievements in materials and manufacturing engineering*, **20**, 403 - 406.

136. **Lakshminarayanan, A, K., S. Malarvizhi** and **V. Balasubramanian** (2011) Developing friction stir welding window for AA 2219 aluminium alloy. *Transactions of non ferrous metals society of China*, **21**, 2339 - 2347.

137. **Kittipong Kimapong** and **Takehiko Watanab** (2005) Effect of welding process parameters on mechanical property of FSW lap joint between aluminum alloy and steel. *Materials Transactions*, **46 (10)**: 2211 - 2217.

138. **Gopala Krishna, G., P. Ram Reddy** and **Manzoor Hussain** (2014) Effect of tool tilt angle on aluminium friction stir welds. *Global journal of researches in engineering: J General engineering*, **14 (7)**, 61 - 70.

139. **Rodrigues, D. M., C. Leita , R. Louro, H. Gouveia** and **A. Loureiro** (2010) High speed friction stir welding of aluminium alloys. *Science and Technology of Welding and Joining*, **15 (8)**, 676 - 681.

140. **De Giorgi, M., A. Scialpi, F.W. Panella** and **L. A. C. De Filippis** (2009) Effect of shoulder geometry on residual stress and fatigue properties of AA6082 fsw joints. *Journal of Mechanical Science and Technology*, **23**: 26 - 35.

141. **Scialpi, A., F. W. Panella** and **L. A. C. De Filippis** and **P. Cavaliere** (2007) Influence of shoulder geometry on microstructure and mechanical properties of friction stir welded 6082 aluminium alloy. *Materials and Design*, **28**, 1124 - 1129.

142. **Walter, V., K. A. Weidenmann** and **V. Schulze** (2014) A comparison of FSW, BHLW, and TIG joints for Al- Si- Mg alloy (EN AW- 6082 T6). *Procedia CIRP*, **18**, 120 - 125.

143. **Rodrigues, D. M, C. Leita, R. Louro, H. Gouveia** and **A. Loureiro** (2010) High speed friction stir welding of aluminium alloys. *Science and Technology of Welding and Joining*, **15 (8)**, 676 - 681.

144. **Luis Trueba Jr., Georgina Heredia, Daniel Rybicki** and **Lucie. B. Johannes** (2015) Effect of tool shoulder features on defects and tensile properties of friction stir welded aluminum 6061 - T6. *Journal of Materials Processing Technology*, **219**, 271 - 277.

145. **Singh, G., K. Singh** and **J. Singh** (2014) Modelling of the Effect of Process Parameters on Tensile Strength of Friction Stir Welded Aluminium Alloy Joints. *Experimental Techniques*, **38**, 63 - 71.

146. **Palanivel, R., P. Koshy Mathews** and **N. Murugan** (2011) Development of mathematical model to predict the mechanical properties of friction stir welded AA6351 aluminum alloy**.** *Journal of Engineering Science and Technology Review*, **4 (1)**, 25 - 31.

147. **Liu, X. C** and **C. S. Wu** (2015) Elimination of tunnel defect in ultrasonic vibration enhanced friction stir welding friction stir welding. Journal of materials design, *Journal of materials design*, **90**, 350 - 358.

148. **Pradeep, A** and **S. Muthukumaran** (2013) An analysis to optimize the process parameters of friction stir welded low alloy steel plates. *International journal of Engineering, Science and technology*, **5**, 25 - 35.

149. **Trimble, D., G. E. O'Donnell** and **J. Monaghan** (2015) Characterisation of tool shape and rotational speed for increased speed during friction stir welding of AA2024 - T3. *Journal of Manufacturing Processes*, **17**, 141 - 150.

150. **Weifeng Xu, Jinhe Liu, Guohong Luan** and **Chunlin Dong** (2009) Temperature evolution, microstructure and mechanical properties of friction stir welded thick 2219 - O aluminum alloy joints. *Materials and Design*, **30**, 1886 - 1893.

151. **Costa, J. D** and **J. A. M. Ferreira** (2011) Influence of spectrum loading on fatigue resistance of AA6082 friction stir welds. *International Journal of Structural Integrity*, **2 (2)**, 122 - 134.

152. **Aziz Armagan Arici** (2007) Effects of tool tilt angle on tensile strength and fracture locations of friction stir welding of polyethylene. *Science and Technology of Welding and Joining*, **12 (6)**, 536 - 539.

153. **Ramanjaneyulu, K., G. Madhusudhan Reddy, A. Venugopal Rao** and **R. Markandeya** (2013) Structure- Property Correlation of AA2014 Friction Stir Welds: Role of Tool Pin Profile. *Journal of Materials Engineering and Performance*, **22 (8)**, 2224 - 2240.

154. **Chen, H. B., K. Yan, T. Lin, S. B. Chen , C. Y. Jiang** and **Y. Zhao** (2006) The investigation of typical welding defects for 5456 aluminium alloy friction stir welds. *Material Science and Engineering A*, **433**, 64 - 69.

155. **Schmidt, H. B** and **J. H. Hattel** (2008) Thermal modelling of friction stir welding. *Scripta Materialia*, **58 (5)**, 332 - 337.

156. **Junhui Yan, M. A. Sutton** and **A. P. Reynolds** (2005) Process - structure - property relationships for nugget and heat affected zone regions of AA2524 - T351 friction stir welds. *Science and Technology of Welding and joining*, **10 (6)**, 725 - 736.

157. **Colegrove, P., M. Painter, D. Graham** and **T. Miller** (2000) 3-Dimensional flow and thermal modeling of the friction stir welding process, Proceedings of *Second International Symposium on Friction Stir Welding*, Gothenburg, Sweden.

158. **Chen, Z. W** and **S. Cui** (2008) Effect of tool speeds and corresponding torque/ energy on stir zone formation during friction stir welding/ processing, Proceedings *of 7th International Symposium on Friction Stir Welding*, Awaji Island, 6 - 9.

159. **Kumar, K** and **Sathish. V. Kailas** (2008) The role of friction stir welding tool on material flow and weld formation. *Materials Science and Engineering A*, **485**, 367 - 374.

160. **Leitao, C., R. Louro** and **D. M. Rodrigues** (2012) Analysis of high temperature plastic behaviour and its relation with weldability in friction stir welding for aluminium alloys AA5083 - H111 and AA6082 - T6. *Materials and Design*, **37**, 402 - 409.

161. **Mishra, R. S** and **Z. Y. Ma** *Friction Stir Welding and Processing: Science and Engineering*. Springer International Publishing, Switzerland, 2014.

162. **London, B., M. Mahoney, W. Bingel, M. Calabrese, R. H. Bossi** and **D. Waldron.** *Material flow in friction stir welding monitored with Al - SiC and Al - W composite markers.* pp 3 - 12. *In*. **K. V. Jatha, M. W. Mahoney, R. S. Mishra, S. L. Semiatin**, and **T. Lienert** (eds.) *Friction Stir Welding and Processing II* , TMS, 2003.

163. **Cui, S** and **Z. W Chen** (2009) Effects of tool speeds and corresponding torque/energy on stir zone formation during friction stir welding/processing. *IOP Conference Series: Materials Science and Engineering*, **4**, 12 - 19.

164. **Guerra, M, C. Schmidt, J. C. McClure, L. E. Murr** and **A. C. Nunes** (2002) Flow patterns during friction stir welding. *Materials Characterization*, **49**, 95 - 101.

165. **Liu, X. C** and **C. S. Wu** (2016) Elimination of tunnel defect in ultrasonic vibration enhanced friction stir welding. *Materials and Design*, **90**, 350 - 358.

166. **Morisada, Y, T. Imaizumi** and **H. Fujii** (2015) Clarification of material flow and defect formation during friction stir welding. *Science and Technology of Welding and Joining*, **20(2)**, 130 - 137.

167. **Gianluca Buffa, Sergio Pellegrino** and **Livan Fatini** (2014) Analytical bonding criteria for joint integrity prediction in friction stir welding of aluminium alloys. *Journal of Materials Processing Technology*, **214**, 2102 - 2111.

168. **Reynolds, A. P., W. D. Lockwood** and **T. U. Seidel** (2000) Processing-property correlation in friction stir welds. *Materials Science Forum*, **331**, 1719 - 1724.

169. **Zhang, H, S. B. Lin, L. Wu, J. C. Feng** and **Ma ShL** (2006) Defects formation procedure and mathematic model for defect free friction stir welding of magnesium alloy. *Materials and Design*, **27**, 805 - 809.

170. **Weifeng Xu, Jinhe Liu, Guohong Luan** and **Chunlin Dong** (2009) Temperature evolution, microstructure and mechanical properties of friction stir welded thick 2219 - O aluminum alloy joints. *Materials and design*, **30**, 1886 - 1893.

171. **Malarvizhi, S., K. Raghunadhan** and **N. Viswanadhan** (2008) Effect of post weld aging treatment on tensile properties of electron beam welded AA2219 aluminium alloy. *International Journal of Advanced Manufacturing Technology*, **37(3)**, 294 - 301.

172. **Chang- Yong Lee, Don- Hyun Choi, Won- Bae Lee, Sun- Kyu Park, Yun- Mo Yeon** and **Seung- Boo Jung** (2008) Microstructures and mechanical properties of double-friction stir welded 2219 Al Alloy. *Materials Transactions*, **49(4)**, 885 - 888 .

173. **Huang, C** and **S. Kou** (2001) Partially melted zone in aluminium welds-planar and cellular solidification. *Welding Journal*, **80(1)**, 46s - 53s.

174. **Biswal, P., D. A. Kumar** and **N. R. Mandal** (2011) Friction stir welding of aluminium alloy with varying tool geometry and process parameters. *Proceedings of the institution of mechanical engineers part B Journal of engineering manufacture*, **226**, 641- 648.

175. **Pasquale Cavaliere** (2013) Friction stir welding of Al alloys: analysis of processing parameters affecting mechanical behaviour. *Procedia CIRP*, **11**, 139 - 144.

176. **Rodrigues, D. M., A. Loureiro , C. Leitao , R. M. Leal, B. M. Chaparro** and **P. Vilaça** (2009) Influence of friction stir welding parameters on the microstructural and mechanical properties of AA 6016-T4 thin welds. *Materials and Design*, **30**, 1913 - 1921.

177. **Mohiedin Bagheri Hariri, Sajad Gholami Shiri, Yadollah Yaghoubinezhad** and **Masoud Mohammadi Rahvard** (2013) The optimum combination of tool rotation rate and travelling speed for obtaining the preferable corrosion behavior and mechanical properties of friction stir welded AA5052 aluminum alloy. *Materials and design*, **50**, 620 - 634.

178. **Ringer, S. P** and **K. Hono** (2000) Microstructural evolution and age hardening in alloys: atom probe field- ion microscopy and transmission electron microscopy studies. *Materials characterization*, **44**,101 - 131.

179. **Liu, X. C** and **C. S. Wu** (2016) Elimination of tunnel defect in ultrasonic vibration enhanced friction stir welding. *Materials and Design*, **90**, 350 - 358.

180. **Venkata Rao, G. Madhusudhan Reddy** and **K. Srinivasa Rao** (2015) Influence of tool pin profile on microstructure and corrosion behaviour of AA 2219 Al Cu alloy friction stir weld nuggets. *Defence technology*, **11 (3)**, 1 - 12.

181. **Lakshminarayanan, A. K., S. Malarvizhi,** and **V. Balasubramanian** (2011) Developing friction stir welding window for AA 2219 aluminium alloy. *Transactions of non ferrous metals society of China*, **21(11)**, 2339 - 2347.

182. **Mahoney, M. W., C. G. Rhodes, J. G. Flintoff, R. A. Spurling** and **W.H. Bingel,** (1998) Properties of friction-stir-welded 7075 T651 aluminum. *Metallurgical and Materials Transactions A: Physical Metallurgy and Materials Science*, **29 (7)**, 1955 - 1964.

183. **Surekha, K., B. S. Murthy** and **K. Prasada Rao** (2008) Microstructural characterization and corrosion behavior of multipass friction stir processed AA2219 aluminium alloy. *Surface & Coatings Technology*, **202**, 4057 - 4068.

184. **Kh .A. A. Hassan, A. F. Norman, D. A. Price** and **P. B. Prangnell** (2003) Stability of Nugget zone grain structures in high strength Al- alloy friction stir welds during solution treatment. *Acta Materialia*, **51**, 1923 - 1936.

185. **Arunkumar, S., P. Rangarajan, K. Devakumaran** and **P. Sathiya** (2015) Comparative study on transverse shrinkage, mechanical and metallurgical properties of AA2219 aluminium weld joints prepared by gas tungsten arc and gas metal arc welding processes. *Defence technology*, **11(3)**, 262 - 268.

186. **Nandan, R., T. DebRoy** and **H. K. D. H. Bhadeshia** (2008) Recent advances in friction stir welding- Process, weldment structure and properties. *Progress in materials science*, **53**, 980 - 1023.

187. **Costa, J. D** and **J. A. M. Ferreira** (2011) Influence of spectrum loading on fatigue resistance of AA6082 friction stir welds. *International Journal of Structural Integrity*, **2 (2)**, 122 - 134.

188. **Yutaka, S, Sato., Hiroyuki Kokawa, Masatoshi Enomoto** and **Shigetoshi Jogan** (1999) Microstructural evolution of 6063 aluminium during friction stir welding. *Metallurgical & Materials Transactions A*, **30(9)**, 2429 - 2437.

189. **Doude, H., J. Schneider, B. Patton, S. Stafford, T. Waters** and **C. Varner** (2015) Optimizing   weld quality of a friction stir welded aluminum alloy. *Journal of Materials Processing Technology*, **222**, 188 - 196.

190. **Song, M** and **R. Kovacevic** (2003) Thermal modelling of friction stir welding in a moving coordinate system and its validation. *International Journal for Machine. Tools and Manufacture*, **43 (6)**, 605 - 615.

191. **Hamilton, C., A. Somme**rs and **S. Dymek** (2009) A thermal model of friction stir welding applied to Sc-modified Al - Zn - Mg - Cu alloy extrusions. *International Journal for Machine. Tools and Manufacture*, **49 (3)**, 230 - 238.

192. **Colegrove, P. A., H. R. Shercliff** and **R. Zettler** (2007) Model for predicting heat generation and temperature in friction stir welding from the material properties. *Science and Technology of Welding and Joining*, **12 (4)**, 284 - 297.

193. **Ulysse, P** (2002) Three-dimensional modeling of the friction stir-welding process. *International Journal for Machine Tools and Manufacture*, **42**, 1549 - 1557.

194. **Jinwen Qian, Jinglong Li, Fu Sun, Jiangtao Xiong, Fusheng Zhang** and **Xin Lina** (2013) An analytical model to optimize rotation speed and travel speed of friction stir welding for defect-free joints. *Scripta materialia*, **68**, 175 - 178.

195. **Khandkar, M. Z. H., J. A. Khan** and **A. P. Reynolds** (2003) Prediction to temperature distribution and thermal history during friction stir welding: input torque based model. *Science and Technology of Welding and Joining*, **8**, 165 - 74.

196. **Arora, A., R. Nandan, A. P. Reynolds** and **T. Debroy** (2009) Torque, power requirement and stir zone geometry in friction stir welding through modelling and experiments. *Scripta Materialia*, **60**, 13 - 16.

197. **Gadakh, V. S** and **K. Adepu** (2013) Heat generation model for taper cylindrical pin profile in FSW. *Journal of Materials Research and Technol*ogy, **2(4)**, 370 - 375.

198. **Sameer. A. Emam** and **Ali El Domiaty** (2009) A refined energy - based model for friction stir welding. *World acdemy of science, engineering and technology,* **9**, 5 - 23.

199. **Schmidt, H., J. Hattel** and **J. Wert** (2004) An analytical model for the heat generation in friction stir welding. *Modelling and Simulation in materials science and engineering,* **12,** 143 - 157.

200. **Neto, D.M** and **P. Neto** (2013) Numerical modelling of friction stir welding process: a literature review. *International Journal of Advanced Manufacturing. Technolog,* **65,** 115 - 126.

201. **Schmidt H. B** and **J. H. Hattel** (2008) Thermal modelling of friction stir welding. *Scripta Materialia,* **58 (5)**, 332 - 337.

202. **Nandan, R., C. G. Roy** and **T. Debroy** (2006) Numerical simulation of three dimensional heat transfer and plastic flow during friction stir welding. *Metallurgical and materials transactions A*, **37 (4)**, 1247 - 1259.

203. **Schimidt, H., J. Hattel** and **J. Wert** (2004) An analytical model for the heat generation in friction stir welding. *Modelling and Simulation in Material Science and Engineering,* **12 (1)**, 143 - 157.

204. **Hasan, A. F., C. J. Bennet**, and **P. H. Shipway** (2015) A numerical comparison of the flow behaviour in Friction Stir Welding (FSW) using unworn and worn tool geometries. *Materials and Design,* **87**, 1037 - 1046.

205. **Mishra, R. S., P. S. De** and **N. Kumar** *Friction stir welding and processing: Science and engineering,* Springer international publishing, Switzerland, 2014.

206. **Trimble, D., G.E. O'Donnell** and **J. Monaghan** (2015) Characterisation of tool shape and rotational speed for increased speed during friction stir welding of AA2024-T3. *Journal of Manufacturing Processes,* **17**, 141–150.

207. **Su, H., C.S. Wu, A. Pittner** and **M. Rethmeier** (2013) Simultaneous measurement of tool torque, traverse force and axial force in friction stir welding. *Journal of Manufacturing Processes*, **15**, 495 - 500.

208. **Arora, A., A. De** and **T. Debroy** (2011) Toward optimum tool shoulder diameter. *Scripta materialia*, **64**, 9 - 12.

209. **Hao Su, Chuan Song Wu, Marcel Bachmann** and **Michael Rethmeier** (2015) Numerical modeling for the effect of pin profiles on thermal and material flow characteristics in friction stir welding. *Materials and Design*, **77**, 114 - 125.

210. **Deng, Z., M. R. Lowell** and **K. A. Tagavi**, Influence of material properties and forming velocity on the interfacial slip characteristics of cross wedge rolling. *Journal Manufacturing Science and Engineering*, **123**, 647 - 653.

211. **Hamilton, C., S. Dymek** and **A. Sommers** (2008) A thermal model of friction stir welding in aluminum alloys. *International Journal of Machine Tools & Manufacture*, **48**, 1120 - 1130.

212. **Nandan, R., G. G. Roy, T. J. Lienert** and **T. Debroy** (2007) Three-dimensional heat and material flow during friction stir welding of mild steel. *Acta Materialia*, **55**, 883 - 895.

……☙*❧……

LIST OF PAPERS

SUBMITTED ON THE BASIS OF THIS THESIS

I **REFEREED JOURNALS**

1. **Sreenivas P, Anil Kumar R and Sreejith P S** (2017) Effect of applied axial force on FSW of AA 6082- T6 Aluminium alloys. *International Journal of Mechanical Engineering and Technology,* **8(1),** 88 - 99. (Scopus indexed).

2. **Sreenivas P and Sreejith P S** (2017) Effect of process parameters on microstructural and mechanical properties of friction stir welded 2219 aluminium alloys, *International Journal of Theoretical and Applied Mechanics (IJTAM),* **12(1),** 135 - 146. (UGC Approved)

II **PRESENTATIONS IN CONFERENCES**

1. **Sreenivas P and Sreejith P S**.(2015) Effect of process parameters on high speed friction stir welding of AA2219 aluminium alloy *IcetIME 15, International Conference on Emerging Trends in Mechanical Engineering,* Cochin University of science& Technology, Kochi, India, Dec. 16 – 17.

2. **Sreenivas P and Sreejith P S**. (2016) Effect of tool tilt angle on high speed friction stir welding of AA6082- T6 aluminium alloy *International Symposium on Green Manufacturing and Applications,* Bali, Indonesia, Korean Society for precision engineering, June 21 – 25.

CURRICULUM VITAE

NAME	: SREENIVAS.P
DATE OF BIRTH	: 29/05/1969

EDUCATIONAL QUALIFICATIONS

1990 **Bachelor of technology (B. Tech)**

Institution	: T. K.M College of Engineering, Quilon (Kerala University).
Specialization	: Mechanical Engineering.

2007 **Master of technology (M.Tech)**

Institution	: School of Engineering, Cochin University of Science and Technology.
Specialization	: Mechanical Engineering- Production Engineering.

EMPLOYMENT DETAILS

1996 - till now

Organisation	: Institute of Human Resources Development (IHRD), Govt. of Kerala.
Designation	: Assistant Professor.

1993 - 1995

Organisation	: Fluid Air India Limited, Bombay, Maharashtra.
Designation	: Site Engineer.

1991 - 1992

Organisation	: Quality Engineering Products, Thane, Maharashtra.
Designation	: Assistant Engineer.